DISSERTATION

THE ONGOING DEVELOPMENT OF THE TECHNIQUE OF TWO-BEAM FLUORESCENCE CROSS-CORRELATION SPECTROSCOPY COUPLED WITH CONTINUOUS-FLOW CAPILLARY ELECTROPHORESIS

Submitted By

Keir Fogarty

Department of Chemistry

In Partial Fulfillment of the Requirement

For the Degree of Doctor of Philosophy

Colorado State University

Fort Collins, CO

Spring, 2008

COLORADO STATE UNIVERSITY

April 7, 2008

WE HEREBY RECOMMEND THAT THE DISSERTATION PREPARED UNDER OUR SUPERVISION BY KEIR H. FOGARTY ENTITLED "THE ONGOING DEVELOPMENT OF THE TECHNIQUE OF TWO-BEAM FLUORESCENCE CROSS-CORRELATION SPECTROSCOPY COUPLED WITH CONTINUOUS-FLOW CAPILLARY ELECTROPHORESIS" BE ACCEPTED AS FULFILLING IN PART REQUIREMENTS FOR THE DEGREE OF DOCTOR OF PHILOSOPHY.

Committee on Graduate Work

B. George Barisas

Nancy E. Levinger

Kevin L. Lear

Advisor: Alan K. Van Orden

Department Head: Anthony K. Rappè

ABSTRACT OF DISSERTATION

THE ONGOING DEVELOPMENT OF THE TECHNIQUE OF TWO-BEAM FLUORESCENCE CROSS-CORRELATION SPECTROSCOPY COUPLED WITH CONTINUOUS-FLOW CAPILLARY ELECTROPHORESIS

This thesis describes work performed in the development and application of the technique of two-beam fluorescence cross-correlation spectroscopy coupled with continuous-flow capillary electrophoresis (2bFCCS-CFCE). In this approach, fluorescently-labeled molecules of interest are monitored as they electrophoretically migrate in continuous solution between two, spatially-separated laser foci. The work presented here illustrates a number of advantages that 2bFCCS-CFCE analysis has over more conventional capillary electrophoresis (CE) techniques. Three sets of experiments were performed that illustrate these advantages. In the first set of experiments, 2bFCCS-CFCE was used to detect and discriminate between three different analyte molecules electrophoretically migrating in opposite directions. The ability of 2bFCCS-CFCE to monitor molecules electrophoretically migrating in opposite directions without the need of sample injection steps or multiple buffers demonstrated a distinct advantage over conventional CE techniques, which require complex buffer conditions, sample injection, and can only analyze species migrating in uniform

direction. The second set of experiments demonstrated 2bFCCS-CFCE on microchip platforms (2bFCCS-CFMCCE). Several design advantages of 2bFCCS-CFMCCE relative to separations-based CE microchip platforms, such as increased miniaturization and simpler fluid handling format, were demonstrated. The third set of experiments demonstrated the ability of 2bFCCS-CFCE to measure the effective charge of a single-stranded DNA (ssDNA) in the presence of magnesium ions. The measurement of effective charge requires analysis of both diffusion and electrophoretic migration simultaneously. Conventional CE experiments are not capable of making this measurement. 2bFCCS-CFCE was used to successfully measure the effective charge, revealing the interesting relationship between ssDNA charge and size.

Keir H. Fogarty

Chemistry Department

Colorado State University

Fort Collins, CO 80523

Spring 2008

ACKNOWLEDGEMENTS

I would like to thank my colleagues in the Van Orden group: Jon Gerding, Jaemyeong Jung, Ming Yu, Vinod Anumareddy, Rajesh Najek, Jeffrey Mcphee, Dale Willard, Tina Mutschler, Douglas Shepherd, Scott Miller, and everybody else who were such supporting compatriots during my time at Colorado State

I would like to thank Katherine Schmitz for being my moral support and optimistic counselor during the difficult times

I would like to thank my parents and sister for their moral support and financial support during my graduate career

I would like to thank my committee for their support

Thanks go to the National Institutes of Health for providing the bulk of funding for the projects presented in this dissertation

I would like to thank all the support staff of the CSU Chemistry Department who made my life more bearable in numerable ways

Finally, I would like to thank my advisor, Alan Van Orden, for the opportunities and guidance he gave me, as well as all the enlightening conversations through all the years—I couldn't have done it without you!

TABLE OF CONTENTS

Chapter 2. Background and Theory

Chapter 3. 2bFCCS-CFCE for Simultaneous Analysis of Positive and Negative Ions

LIST OF FIGURES

LIST OF TABLES

LIST OF ACRONYMS

2bFCCS	Two-Beam Fluorescence Cross-Correlation Spectroscopy
2bFCCS-CFCE	Two-Beam Fluorescence Cross-Correlation Spectroscopy Coupled with Continuous-Flow Capillary Electrophoresis
2bFCCS-CFMCCE	Two-Beam Fluorescence Cross-Correlation Spectroscopy Coupled with Continuous-Flow Microchip Capillary Electrophoresis
BSA	Bovine Serum Albumin
CCD	Charge-Coupled Device
CE	Capillary Electrophoresis
CFCE	Continuous-Flow Capillary Electrophoresis
CZE	Capillary Zone Electrophoresis
DLS	Dynamic Light Scattering
DLS-CFCE	Dynamic Light Scattering Coupled with Continuous-Flow Capillary Electrophoresis
DNA	Deoxyribonucleic Acid
EOF	Electroosmotic Flow
FCS	Fluorescence Correlation Spectroscopy
FCS-CFCE	Fluorescence Correlation Spectroscopy Coupled with Continuous-Flow Capillary Electrophoresis
LIF	Laser-Induced Fluorescence
MCCE	Microchip Capillary Electrophoresis
NA	Numerical Aperture
PCH	Photon Counting Histogram

PDMS	Poly(dimethylsiloxane)
PMMA	Poly(methyl methacrylate)
Polybrene	Hexadimethrine Bromide
PVA	Poly(vinyl alcohol)
PVP	Poly(vinylpyrrolidone)
R6G	Rhodamine 6G
R6G-dCTP	Rhodamine 6G-Labeled Deoxycytosine Triphosphate
R6G-ssDNA	Rhodamine 6G-Labeled Single-Stranded DNA
RNA	Ribonucleic Acid
S/N	Signal-to-Noise Ratio
ssDNA	Single-Stranded DNA
SME	Single Molecule Electrophoresis
SMIE	Single Molecule Imaging Electrophoresis
SSB	Single-Stranded Binding Protein
TAMRA	Tetramethyl-6-Carboxyrhodamine/5-Carboxy-Tetramethylrhodamine
TAMRA-ssDNA	Tetramethyl-6-Carboxyrhodamine-Labeled Single-Stranded DNA
UV	Ultraviolet

Chapter 1: Introduction

1.1 Introduction:

In the early 1980's Jorgenson and Lukacs revolutionized the field of analytical chemistry by effectively introducing the world to capillary electrophoresis (CE)[1-3]. Previous examples of free zone electrophoresis had been demonstrated[4-7], but Jorgenson and Lukacs were the first to achieve incredibly efficient separations in relatively easy to make fused silica capillaries with narrow inner diameters (<100μm). The separations achieved in their CE experiments were so efficient (~10^5 theoretical plates m^{-1}) that they were an order of magnitude more efficient than those commonly demonstrated by other separations techniques such as liquid chromatography[1-3, 8]. Jorgenson and Lukacs created the huge leap in separation efficiency through the use of fused silica capillaries, which offered an advantage over previous free zone electrophoresis techniques by allowing for more efficient heat dissipation due to the high surface area of the capillary. This overcame a significant problem for free zone electrophoresis, which was the convective and diffusive effects that heat had on samples migrating in free solution. In addition, CE offered many

advantages to gel electrophoresis, the prevailing electrophoretic method of the time. Gel electrophoresis typically requires much larger samples than CE, is much more labor intensive, and has lower separation efficiency.

Another advantage of the CE technique introduced by Jorgenson and Lukacs is its relatively simple instrumental requirements. A schematic for a basic CE experiment similar to the one performed by Jorgenson and Lukacs is shown in Figure 1.1. Every CE experiment has 5 basic requirements: 1) a capillary of narrow inner diameter, typically made from fused silica, 2) a high voltage power source, 3) a method of detection of the analytes, 4) the sample solution containing the analytes of interest, and 5) reservoirs of run buffer, typically having the same composition as the sample solution minus the species of interest. In a typical CE experiment, a small amount of the sample, a "plug" typically on the order of 0.1-10 nL, is introduced on one end of a capillary that is pre-filled with run buffer. After sample introduction, the ends of the capillary are submerged in reservoirs filled with the run buffer, and a high voltage, commonly 20,000 to 60,000 V, is applied across the capillary. The electric field causes ions in the sample to migrate towards the anode or cathode. The rate of ion migration, V_x, depends on the charge to size ratio of the ionic species:

$$V_x = \mu E = \frac{qE}{6\pi\eta r} \tag{1.1}$$

Where μ is electrophoretic mobility, q is the charge on the species, η is the solution viscosity, E is the electric field strength, and r is the hydrodynamic radius, or size, of the species[9].

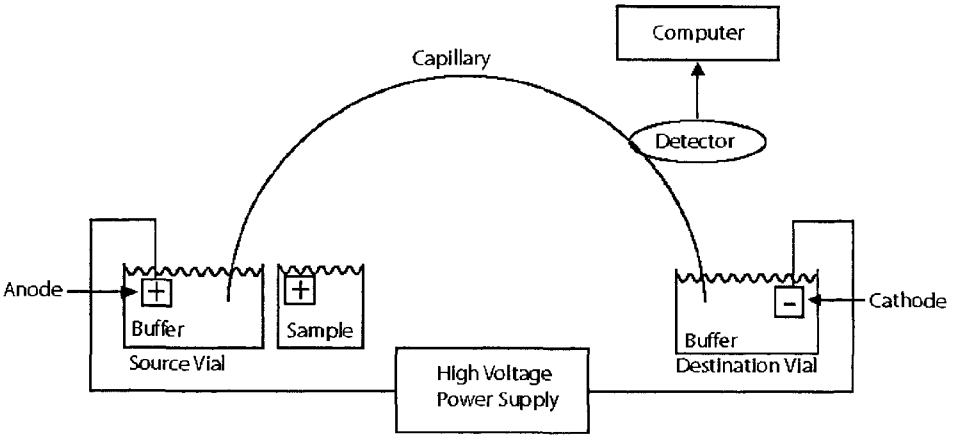

Figure 1.1: Schematic of a typical capillary electrophoresis experiment.

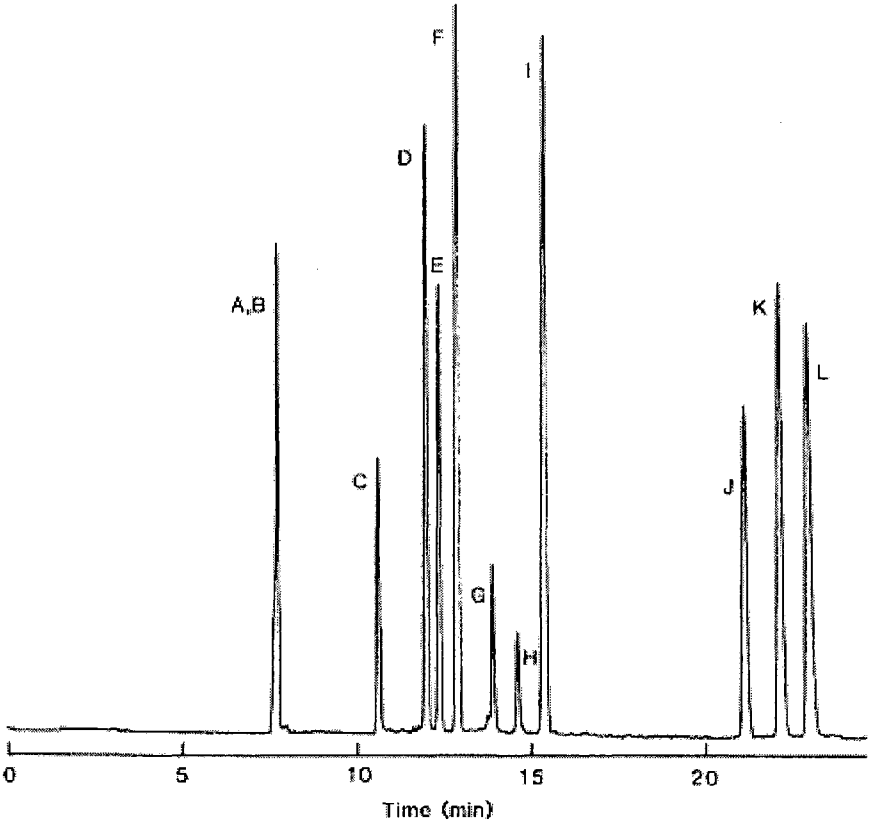

Figure 1.2[2]: An electropherogram obtained from the analysis of an amino acid mixture. The amino acids were fluorescently labeled and detected by laser-induced fluorescence methods.

Smaller, more highly charged ions tend to migrate faster than larger ions of lower charge. The difference in migration rates between the different species causes the sample to separate into bands of like species within in the background run buffer[10]. In conventional CE, a detector is located at the end of the capillary opposite that of the sample injection. As the bands of sample reach the detection area and pass through it, an electropherogram similar to Figure 1.2 is produced[2]. The data of a typical electropherogram manifests as a series of peaks, each peak corresponding to a specific analyte with a unique charge to size ratio. The peaks represent the concentration profile response over time of the detector. In the case of Figure 1.2, fluorescently labeled amino acids of different charge to size ratios separated into bands, and as each band migrated past the laser based fluorescence detection window, it generated a peak in detected fluorescence[2]. The height of the peaks are proportional to the concentration of the analyte, and the width and general shape of the peaks are related to a number of factors, such as the diffusion of the analyte and the injection technique used to introduce the analyte to the capillary[10].

An important aspect of CE that has not yet been discussed is the phenomenon of electroosmotic flow (EOF). Electroosmotic flow is the bulk solvent flow in an electric field that occurs when a high voltage is applied across a capillary with charged walls containing a buffer solution. Figure 1.3 shows a diagram illustrating electroosmotic flow and flow profile of a) pressure driven flow, or laminar flow, and b) electroosmotic flow induced by an electric field. In fused silica capillaries above

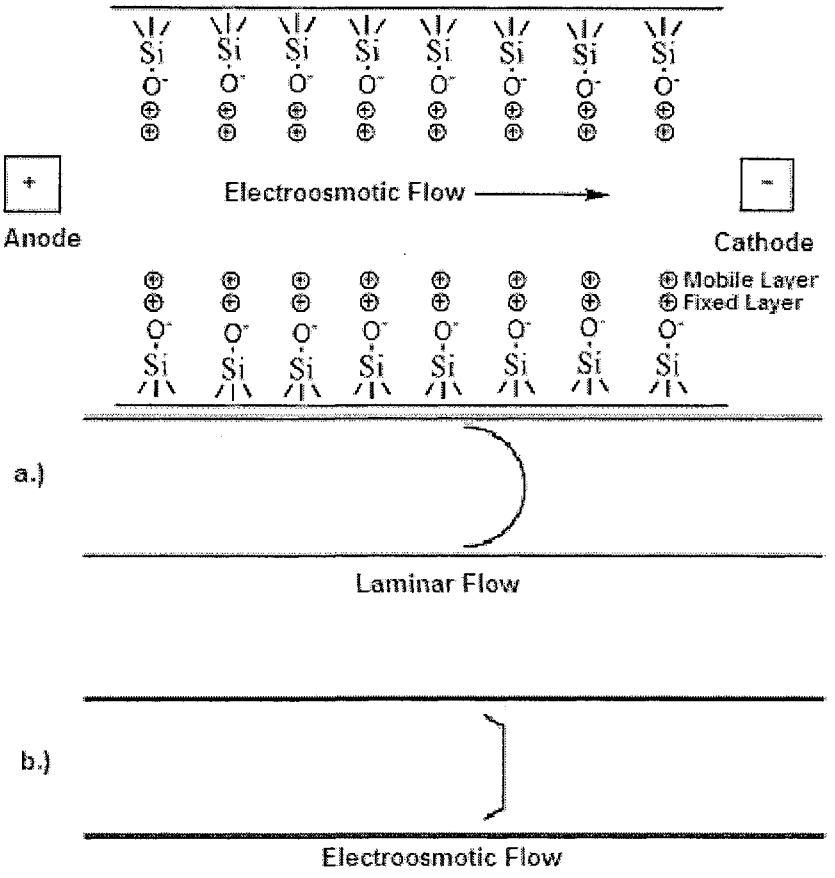

Figure 1.3: *top:* diagram of the inside of a fused silica capillary illustrating the concept of electroosmotic flow. The charged silanol groups of the capillary surface are shown with the electrical double layer formed by buffer cations interacting with the negatively charged groups. The cations drag the surrounding solvent toward the cathode. *Bottom:* flow profiles of the solvent undergoing a) pressure driven flow, and b) Electroosmotic flow driven by an electric field.

pH 3, the silanol chemical groups of the glass have an overall negative charge. Cations in the bulk solvent are attracted to these negatively charged groups at the walls, forming an "electric double layer" at the walls. Cations immediately adjacent to the walls interact strongly with the negatively charged groups, and thus are somewhat immobile. A short distance out, however, there is still a higher concentration of cations relative to the bulk buffer solution due to the effects of the negatively charged walls, but these cations are relatively mobile, and when an electric field is applied, they migrate toward the cathode, or negatively charged electrode. This "sleeve" of cations near the capillary walls migrate towards the cathode pulling the rest of the bulk solvent with it, inducing electroosmotic flow. It is important to realize that the profile of electroosmotic flow, as can be seen at the bottom of Figure 1.3, is piston-like, compared to the parabolic flow profile of pressure driven flow in a capillary. This is an important distinction, because the piston-like flow profile does not contribute to spread of migrating sample zones, and thus does not negatively affect the experiment's resolution. Because the parabolic flow profile contributes to band spreading, CE has an advantage over liquid chromatography, which uses pressure driven flow to separate analytes. It should be noted that if the walls of the capillary were positively charged, the bulk solvent flow would be towards the anode, and if the walls were neutral, there would be no electroosmotic flow at all.

When Jorgenson and Lukacs published their seminal papers on CE in the early 1980's, they used laser-induced fluorescence (LIF) for detection. LIF is an excellent detection method for CE because fluorescent labeling of species of

interest was relatively easy, and the limits of detection are extremely small, something that is necessary when trying to detect the nL volume sample bands of a typical CE experiment[1, 2]. Since the early 1980's, the number of different methods used for detection in CE has exploded as more sensitive methods with lower limits of detection are developed. Some of the more common methods used for detection in CE include: a)LIF, b) absorbance methods, c) mass spectrometric methods (where the CE capillary is coupled with a mass spectrometer), d) monitoring refractive index changes between background run buffer and sample component bands, e) conductivity and amperometric detection (based on the fact that the samples separated consist of ionic species), and f) radioactivity-based detection[10, 11].

The simplicity of CE instrumentation and detection methodology has made it a very valuable and flexible tool for the analytical scientist. CE, however, is not free from limitations, and throughout the period since its inception scientists have devised many methods to overcome some of these limitations. The subject of this dissertation is the application of a technique, two-beam cross-correlation spectroscopy coupled with continuous-flow capillary electrophoresis (2bFCCS-CFCE), which overcomes some of the inherent limitations in CE. In the next section, the limitations of conventional CE that inspired the development of the 2bFCCS-CFCE technique will be discussed, along with other techniques that have been developed to address them.

1.2 Experimental Limitations of CE:

As discussed in the previous section, CE is a separations and analysis technique of unparalleled efficiency. Its simple design allows for great flexibility in its application. CE, however, is not without its limitations. These limitations manifest in two distinct areas; the complexity of factors affecting data output in CE, and the inherent design limits of CE. In the following section, the limitations inherent to CE will be discussed, first, by exploring the data output issues, and second, by investigating inherent design limitations of CE.

In an ideal world, the peaks produced by a CE experiment would be Gaussian, because the only factor affecting their width would be the diffusion of the analytes. The Gaussian peak width is related to the standard deviation, σ. This is often expressed to the second power as variance, σ^2, which for the case of diffusion is:

$$\sigma_{diff}^2 = 2Dt \tag{1.2}$$

where D is the diffusion constant of the species, and t is the timescale of the experiment. The molecules of respective analytes should all migrate with the same velocity down the capillary, but as they migrate, the analyte molecules diffuse, and thus increase the migration band/peak width. If diffusion were the only factor affecting peak width, it would be possible to analyze the peak width using equation 1.2 to obtain the diffusion constant, and thus, the size of the analytes concerned. The knowledge of analyte size would also allow the analytical scientist to interrogate the effective charge of the analyte through the

use of equation 1.1. Being able to discriminate between the effective charge and size of analytes is important when the analyte species are unknown, especially when they are unknown biological molecules like proteins, where independent size and charge information is crucial to identification[9]. Unfortunately, the total variance of CE peak data, σ_{tot}^2, which is a measure of peak width is dependent on multiple factors :

$$\sigma_{tot}^2 = \sigma_{diff}^2 + \sigma_{inj}^2 + \sigma_{wall}^2 + \sigma_{JH}^2 + \sigma_{\det}^2 + \sigma_{em}^2 + \sigma_{flo}^2 \tag{1.3}$$

where σ_{inj}^2 is the variance due to sample injection, σ_{wall}^2 is the variance due to wall effects, σ_{JH}^2 is the variance due to joule heating effects, $\sigma_{\det}^2$ is the variance due to the size of the detection region, σ_{em}^2 is the variance due to electromigration dispersion, and σ_{flo}^2 is the variance due to nonuniform velocity flow profile[9, 12-16]. The equation relating the total variance, σ_{tot}^2, to the peak width is:

$$\sigma_{tot}^2 = \frac{1}{8\ln 2}\left(\frac{w_h L}{t}\right)^2 \tag{1.4}$$

where w_h is the peak width at half-height, L is the migration distance, and t is the migration time of the peak-producing sample band[12]. As can be seen in equation 1.3, there are a multitude of factors affecting the peak width in a typical electropherogram. A comprehensive analysis of peak width would require accounting for and quantifying every source of variance. Unfortunately, almost every form of variance has random and unpredictable aspects that negatively effect analysis of peak shape in CE.

1.2.1 Sample Injection:

The contribution of sample injection to peak width in CE can be attributed to two factors: the length of the injection plug, and non-ideal plug geometries/compositions. If the variance of injection were solely attributable to sample plug length, the variance would be solvable as:

$$\sigma_{inj}^{\ 2} = l_{inj}^{\ 2} / 12 \tag{1.5}$$

where l_{inj} is the length of the injected plug, assuming the plug is rectangular in shape[9]. It is obvious that an ideal injection would minimize l_{inj}, but due to the fact that the sample injection length must be nonzero, variance introduced by sample injection is unavoidable. The two most common methods for sample injection in CE are hydrodynamic and electrokinetic, both contributing to the variance in characteristic ways. In hydrodynamic injection, the capillary is first filled with the run buffer, and then one end of the capillary is introduced into the sample buffer. The sample is then injected into the capillary in one of three ways: 1) raising of the sample buffer level a fixed height over the level of the run buffer at the opposite end of the capillary, creating hydrostatic pressure which injects the sample, 2) exerting positive pressure on the sample buffer container, which causes sample to be pushed into the capillary, and 3) applying a vacuum at the opposite end of the capillary, pulling sample buffer into the capillary. In electrokinetic injection, the initial steps are the same as hydrodynamic injection, but instead of using pressure to introduce a sample plug to the capillary, a

voltage is applied which induces migration of the sample into the capillary. There are two forces which induce the sample migration into the capillary: electrophoretic migration of the components of the sample, and electroosmotic flow[17, 18].

Both of the above methods for injection have unique contributions to the peak variance of CE electropherograms, but do share some common sources of error. In a traditional CE experiment, one can imagine a starting condition where the capillary has been rinsed and filled with the run buffer, and sits with both ends submerged in respective run buffer reservoirs. In order to perform sample injection, one end of the capillary must be removed from its run buffer reservoir and transferred to the sample buffer reservoir. The sample is then injected, and the capillary end must then be removed from the sample and returned to the run buffer in order to start the experiment. This injection procedure inevitably leads to nonreproducible error. First of all, removal of capillary ends from the buffer solution can cause several negative effects. When one capillary end is being transferred from run to sample buffer, or vice versa, the fluid inside the capillary can experience variable hydrodynamic forces due to a variety of factors. Firstly, when one end of the capillary is in air and the other is submerged, evaporation can cause the fluid to retreat past the end of the capillary, so that when it is re-submerged, an air bubble is introduced in the capillary. Evaporation can also cause concentration gradients as solvent is removed but solute remains. In addition, the sample or run buffer can form droplets that adhere to the capillary end as it is transferred from solution to solution. This can cause cross-

contamination and uncontrollable additional injection of unwanted sample. Finally as the capillary end is pushed into or pulled out of buffer, the motion induces pressure gradients that can push buffer into, or pull buffer out of the capillary, altering injection amounts nonreproducably[14, 17-19]. Techniques have been developed which eliminate the need for capillary transfer in sample injection, but suffer from more complex instrumentation requirements that have limited their application[19-22].

As noted above, the length of the injected sample plug contributes to the variance caused by sample injection. The contribution of plug length could theoretically be accounted for by equation 1.5, but, as is often the case, the reality of sample plug injection often deviates from theoretical approximations used to derive equation 1.5. In an ideal world, the plug would be a perfect cylinder or rectangle, with precisely defined length and geometry, unfortunately, this is nearly impossible. The beginning and endpoint of the plug is universally ambiguous, because of unintentional injection discussed in the previous paragraph, and because of sample diffusion into and out of the capillary during the "dead time" immediately before and after sample injection[23, 24].

The hydrodynamic injection technique introduces additional plug length variance because it is a pressure flow technique. As stated previously, pressure flow is parabolic. This creates boundaries to the sample plug that are difficult to analyze geometrically, especially when one considers that diffusion would quickly disturb the parabolic profile into an even less theoretically accessible profile. In addition it is nearly impossible to perform pressure injection without ill-defined

pressure gradients. If one performs injection by changing the respective buffer heights of the capillary at either end, the process of raising and lowering the levels to and from the injection heights results in inconsistent pressure gradients. If one uses applied pressure or vacuum injection, there is a finite time required to reach the desired pressures, which results in poorly defined pressure gradients, and thus sample plug lengths[17, 25]. Another possible source of ill-defined sample plugs is in differences of viscosity between sample buffer and run buffer, which can introduce non-ideal plug geometries and diffusion effects[14]. This problem can be accounted for by ensuring the sample and run buffer have similar viscosities, but it is another issue that adds to the complexity of sample injection in CE.

Electrokinetic injection is the other major method for sample plug injection in CE, and it too is not without its weaknesses. The rectangular flow profile more closely resembles the assumed ideal plug of equation 1.5 than does the parabolic flow profile of hydrodynamic injection, but electrokinetic injection introduces many factors that affect the reproducibility of the sample plug that hydrodynamic injection does not suffer from. Perhaps the most important is the issue of nonuniform component injection. Individual components of the sample, including background electrolyte species, will be injected into the capillary at different rates, depending on the speed with which they migrate in an electric field. This might cause overloading of one component in comparison with another, resulting in imprecise representation of relative concentrations of components in the sample. In addition, concentration gradients are introduced

as one end of the plug will be composed predominately of the more highly mobile species, while the other end of the plug will be composed of the less mobile species. These concentration gradients can change the conductivity of different regions of the sample plug, altering the electric field that different components experience, which leads, in turn, to greater peak variance that is difficult to analyze.

Another factor that affects the rate at which sample is introduced is the electroosmotic flow. The amount of electroosmotic flow is extremely dependent on the surface conditions of the walls of the capillary, and unfortunately this can change significantly from capillary to capillary and over time in the same capillary. Ions in the solvent can absorb and desorb from the surface of the capillary over time, and alter the surface charge density of the walls, changing the electroosmotic flow[14, 17, 24-26]. One other important factor effecting electrokinetic injection is the profile of the capillary end in which sample is to be injected. If the end of the capillary is not smooth cut, the jagged shape produces distorted electroosmotic flow profiles which cause non-reproducible sample plug shapes[26, 27]. To ensure reproducibility of electroosmotic flow during injection, care must be taken to cut capillaries smoothly, and it is wise to perform buffer rinsing steps to try to minimize differences in the surface charge density of the capillary walls from run to run[17, 26, 27]. It should be noted that hydrodynamic injection is widely considered to be the most reliable method, as its inconsistencies are more predictable than electrokinetic injection[14, 17].

1.2.2 Wall Effects:

The inner walls of the fused silica capillaries typically used in CE experiments contribute to the total peak variance through two of the terms in equation 1.3; σ^2_{wall} and σ^2_{flo}. σ^2_{wall} represents the variance caused by the interaction of analyte molecules with the capillary walls. σ^2_{flo} represents disturbances in the flow profile of a sample band due to variability of the inner capillary wall's surface charge density.

Analyte molecules that find themselves near the wall of a capillary during the course of the experiment have the opportunity to interact with whatever chemical groups are bound to the surface. In fused silica capillaries, the predominate stationary chemical groups on capillary surfaces are silanol groups. Though fused silica capillaries are popular because of their cost-effectiveness and adaptability, a drawback that comes from their use is the typically strong interactions that many analyte molecules have with silica surfaces. This is especially true of many biological macromolecules, which are, perhaps, the most studied analytes of CE[28]. Analyte-wall interactions can be represented by the following reversible chemical reaction equation:

$$A + Wall \underset{k_d}{\overset{k_a}{\leftrightarrows}} A \cdot Wall \qquad (1.6)$$

where A is the analyte species, $Wall$ is a binding site on the capillary wall, $A \cdot Wall$ represents the analyte bound to the wall, and k_a and k_d are the

association and dissociation rate constants, respectively[9, 29]. Analyte molecules interacting with the walls of a capillary during CE have slower migration times than non-interacting analytes due to the fact that when analyte molecules associate with the wall, they stop migrating, and only resume migration upon dissociation. Electropherograms produced by CE experiments in which wall adsorption is a significant problem typically exhibit "tailing," an example of which can be seen in Figure 1.4 A[30].

In order to try to address the contribution to the variance of wall adsorption, equation 1.6 has served as the starting point of several theoretical approaches[28, 29, 31-33]. It must be understood that equation 1.6 represents the interaction of one analyte species with one binding site on the capillary wall. In reality there is a multitude of possible binding sites on capillary walls, all with potentially different adsorption/desorption kinetics. Theoretical treatments that start with equation 1.6 must first estimate the relative abundance of binding sites on the capillary walls, and must make the critical assumption that they all exhibit adsorption/desorption kinetics in a close enough range that average rate constants can be used to model the system. In addition, if one is performing an analysis using buffers containing multiple species, as is most commonly the case in CE, it would be necessary to model each species' unique interaction with the walls to arrive at a complete picture of wall adsorption phenomena, as each species' interaction with the walls would influence the availability of binding sites for other species.

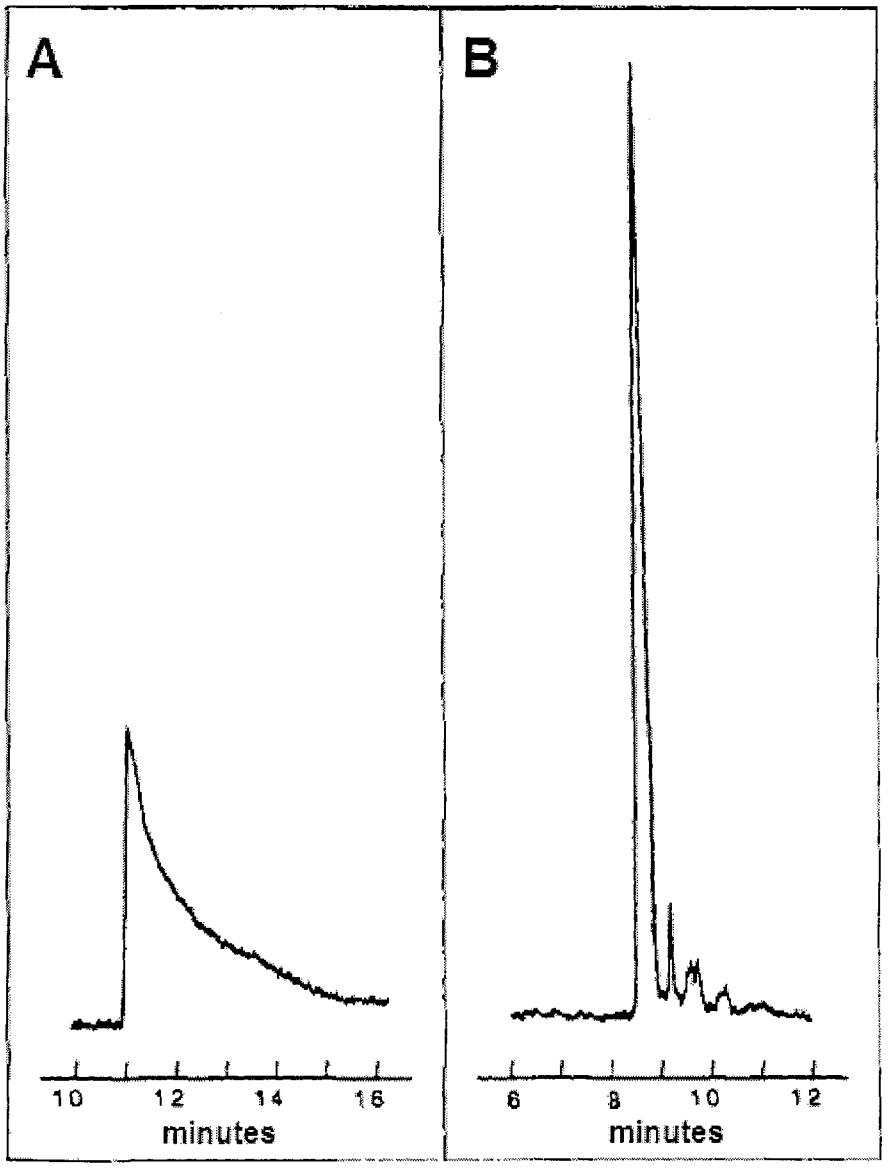

Figure 1.4[30]**:** A) An electropherogram peak produced by the protein cytochrome c in an untreated capillary clearly showing tailing indicative of wall interactions. B) An electropherogram produced by cytochrome c in coated capillaries in which the tailing has been eliminated by reducing wall interactions.

The complex nature of this problem has made it difficult to accurately calculate peak variance contributions from wall adsorption experimentally. By far the most common method to account for wall interactions in CE is to try to eliminate them entirely through the modification of the chemistry of the capillary walls. By tailoring the wall chemistry of a capillary to be repulsive of analyte molecules, one should, in theory, be able to eliminate their interaction. This can be accomplished a number of ways[34-36]. Perhaps the most common method for the elimination of wall interactions is the application of polymer coatings to the inner walls of the capillary. Polymer coatings effectively replace the silanol chemical groups of the silica surface with polymer chemical groups best tailored to avoid interaction with the analytes being studied[34-36]. Another method for eliminating wall interactions in CE is by using additives in the run and sample buffers that outcompete analyte molecules for the wall binding sites on the surface of the capillary. The use of detergents and high ionic strength buffers are the most common methods to achieve this[34-36]. In Figure 1.4, a polycation was used as an additive to reduce the effect of wall interactions seen in Figure 1.4 A, the treatment was effective in eliminating the peak tailing, as can be seen in Figure 1.4 B[30]. Finally, the pH chemistry of silanol groups can be used to eliminate wall interactions. pH can be adjusted to either completely protonate or deprotonate the silanol groups, resulting in neutral or negatively charged surfaces, respectively. The problem with the attempt to eliminate wall interactions entirely is that it is very nearly impossible. In fact, it has been

demonstrated that, no matter the wall conditions, there are always wall interactions to varying degrees[9, 37].

When considering the wall effects on CE experiments, one must note the impact of wall chemistry on electroosmotic flow. If the walls of the capillary are uniformly charged throughout, then the electroosmotic flow should be uniform and should not affect the peak width adversely. Unfortunately, as described in the previous paragraph, species in the run and sample buffers inevitably adsorb to the capillary walls. This not only can effect the surface roughness of the capillary, but also the effective surface charge density. Both of these factors can lead to different rates of electroosmotic flow in different regions of the capillary, which can lead to distortions in the flow profiles of sample bands[32, 34, 38]. Creating conditions in which both the surface charge density of the capillary walls is uniform and the walls are free from adsorbed species that alter the surface roughness would solve the problem of nonuniform EOF, but as said before, eliminating the adsorption of species is impossible, and this will inevitably change both surface roughness and charge density. Coatings and buffer conditions can significantly diminish the surface charge variability which can impact EOF, but ultimately the unpredictability of wall effects will negatively affect any attempts to comprehensively analyze the peak width of electropherograms.

1.2.3 Joule Heating:

When a voltage is applied across a capillary in a CE experiment, heat is produced according to the equation[39]:

$$Q = \frac{VI}{\pi r^2 L} \tag{1.7}$$

where Q is the rate of heat generation in watts per unit volume, V is the applied voltage in the CE experiment, I is the current in amperes, and the expression $\pi r^2 L$ corresponds to the internal volume of the capillary (which is assumed to be cylindrical). As one can see from equation 1.7, the generation of heat, or joule heating, is an intrinsic property of capillary electrophoresis. Unfortunately, joule heating contributes to the dispersion of peaks in CE through a number of means. Heat lowers the viscosity of the buffers used in CE, and it also increases the diffusion of ionic species. In addition, because heat is dissipated from the capillary walls to the surrounding environment, the temperature profile across a capillary varies from higher temperatures at the center to lower temperatures at the walls. The combination of these factors results in a flow profile much like that seen in laminar flow conditions (Figure 1.3). The higher diffusion and lower viscosity caused by joule heating at the center of the capillary allows for greater ion mobility compared to that at the walls, resulting in a parabolic flow profile. The higher ion mobility also results in increased current, which further exacerbates the joule heating according to equation 1.7, creating a kind of feedback loop[28, 39, 40].

There are two ways to account for joule heating's impact on peaks in CE; attempting to minimize the impact of joule heating on peak dispersion through tailoring experimental conditions or specific calculation of the variance contribution due to joule heating through the use of theoretical models. The simplest way to address the influence of joule heat on experiment reproducibility is to minimize the variables in equation 1.7 that contribute to heating. Careful selection of buffers and applied voltages can minimize the current that flows in a CE experiment, which reduces the joule heating. In addition, minimizing the diameter of capillaries used in the experiment can further reduce the joule heating[34]. Optimizing the heat transfer from the capillary to the surrounding environment through forced air or fluid convection can dissipate the joule heat quickly to minimize its impact[34]. Because the flow profile induced by joule heating is parabolic, it has been suggested that the dispersion due to joule heating can be counteracted through application of pressure driven flow in the opposite direction. This method showed some promise in wider bore (400 μm) capillaries[40].

The drawbacks to the manipulation of experimental conditions in CE to minimize joule heating is that conditions are usually chosen based on the analytes being studied and the equipment on hand. Minimizing current is sometimes impossible due to the buffer conditions necessary for the analysis. Smaller capillaries can reduce the amount of sample in the sample peak to levels that are difficult to detect[40]. In addition, one must consider cost in choosing the capillaries used for the experiment, and specialized capillaries of smaller sizes

may prove to be prohibitively expensive. Many commercial instruments include air or liquid convection to promote capillary cooling, but joule heating was still found to impact experimental results[34]. Finally, selection of pressure flows that cancel the dispersion due to joule heating requires extensive and time consuming control experiments for the experimental conditions used.

If joule heating cannot be eliminated experimentally, it becomes necessary in any analysis of peak variance to account for it analytically. There have been a number of approaches to this problem[39, 41-45]. Analytical treatments have focused on either determining the temperature inside the capillary through measurement, or treating the contribution to variance theoretically. Grushka et al. have theoretically derived an expression for the variance due to joule heating in a typical CE experiment:

$$\sigma_{JH}^2 = \frac{r^6 E^4 C_b^2 B^2 \Lambda^2 t}{1536 D_i k_b^2 T^4} \qquad (1.8)$$

where r is the capillary radius, E is the applied electric field, C_b is the buffer concentration, B is a buffer related viscosity constant, Λ is the equivalent conductance of the electrolyte solution, t is the timescale of the experiment, D_i is the diffusion constant of the peak-producing analyte, k_b is the Boltzmann constant, and T is the absolute temperature[9, 39]. While this expression is useful for experimental design, it is not routinely used for analysis of peak variance due to its numerous assumptions concerning experimental conditions[41]. Davis et al.[41] modified Grushka's treatment by taking into account the fact the diffusion constant of the analyte is not constant as assumed by equation 1.8, but is

temperature dependent, and thus is likely to have different values at different points in the capillary. Despite this treatment, the authors freely admitted that their modified equation still made numerous assumptions that may hinder its application to experimental results[41]. In addition, it has been found that the temperature variation due to joule heating can vary significantly axially as well as radially, a fact which no theoretical treatment of the variance due to joule heating takes into account[45, 46].

A number of control experiments have been developed to directly measure the variance due to joule heating or the increased temperatures due to joule heating. Fluorescent dyes exhibit a temperature dependent quantum efficiency, and experiments have shown that it can be used to measure the temperature inside the capillary during a CE experiment[42, 45]. Macka et al. have also shown that control experiments can be used to monitor the variability of EOF, electrophoretic mobilities, and buffer conductivity at different applied voltages[43, 44]. These control experiments can then be used to adjust for the impact of joule heating on experimental results.

Joule heating is a fairly well understood phenomenon, and a number of methods have been developed to account for or negate its impact on CE experiments. Though many of these techniques show promise, the fact remains that the complexity of joule heating makes it difficult to analytically study its impact on peak variance in CE. Indeed, the assumption most often made with respect to joule heating's impact on peak variance is to assume that it is negligible.

1.2.4 Other Contributions to Peak Variance:

Diffusion, sample injection, wall adsorption, and joule heating are the most commonly referred to sources of peak variance in CE experiments, but some additional sources of variance warrant mentioning. Electromigration dispersion resulting from conductivity differences between sample and run buffers is another source of peak variance that must be accounted for[16, 28, 32, 47]. Due to the fact that the sample zone of a CE experiment has different ionic components than the background run buffer, its conductivity will be different. This difference in conductivity causes ions in the sample buffer region to experience different electrically driven forces than ions in the run buffer. As the experiment progresses the variable forces acting on identical ions in different regions of the sample zone can lead to dispersion of the sample zone, impacting the peak width of the electrophoresis experiment. A common manifestation of this in electropherogram peaks is peak tailing like that seen in figure 1.4[34]. Another phenomenon linked to electromigration dispersion is the existence of system zones in CE experiments[48]. System zones are disturbances in the ion composition of the run buffer caused by the injection of the sample. These disturbances can create conductivity differences in both the run buffer and sample buffer, further exacerbating the problem of electromigration dispersion. The variance contribution of electromigration dispersion can be minimized by carefully choosing buffer conditions that minimize conductivity differences.

Unfortunately, the necessary absence of sample ions in the run buffer means that there will always be some contribution from electromigration dispersion to peak width.

Another possible contribution to peak variance that has not yet been discussed is the phenomenon of buffer depletion[34, 49, 50]. In capillary electrophoresis, the voltage is applied through electrodes which are immersed in buffer reservoirs at either end of the capillary. These electrodes can oxidize or reduce constituents of the run buffer as the experiment progresses. The electrochemical reactions at the electrodes can change the composition and pH of the run buffer, which can cause electromigration dispersion, changes in the capillary surface chemistry and thus EOF, and changes in the net charge of analyte molecules through acid-base equilibra. Use of electrochemically stable buffers and low operating voltages can mitigate these effects, but limit the flexibility of CE.

Finally, it should be noted that sources of peak variance in CE are often interdependent. For example, joule heating can change diffusion and the kinetics and equilibria of wall interactions which can in turn affect the EOF which can then exacerbate the electromigration dispersion[28, 34]. The coupled and unpredictable nature of these different phenomena effectively make comprehensive peak width analysis impractical. Specialized applications of CE are required to study such things as diffusion independently from the other sources of peak variance[12, 51-61]. Now that the limitations inherent to CE data have been discussed, limitations inherent to the instrumentation and design of CE experiments will be discussed.

1.3 Addressing Capillary Electrophoresis Experimental Limitations:

The very nature of how conventional capillary electrophoresis is done limits its application in a few key ways. Because macroscopic separation of the samples is required, conventional CE experiments are limited in miniaturization and speed. In addition, conventional CE is limited by the necessity of multiple buffers and sample injection steps which add to the instrumental complexity. Finally, conventional CE requires that all analyte molecules migrate in the same direction to be detected, limiting the versatility of the technique. Specialized forms of capillary electrophoresis, such as microchip capillary electrophoresis and continuous flow capillary electrophoresis, have been developed to address some of these instrumental limitations. The subject of this dissertation is the continued development of one such technique, two-beam fluorescence cross-correlation spectroscopy coupled with continuous flow capillary electrophoresis (2bFCCS-CFCE).

1.3.1 Microchip Capillary Electrophoresis:

Perhaps the most popular form of specialized CE is the performance of CE on microfabricated devices. In microchip capillary electrophoresis (MCCE), lithographic techniques that evolved in the semiconductor industry are used to

create micron sized fluidic channels in insulating substrates[9]. Commonly used substrates for MCCE include glass, polydimethylsiloxane (PDMS), and poly(methyl methacrylate) (PMMA)[9, 62-65]. MCCE has two distinct advantages over conventional CE: 1) MCCE microchannels are formed in a block of insulating material, which allows for the use of much higher applied electric fields than those used for conventional capillary electrophoresis, and 2) the ability to precisely control the fabrication geometry of microchannels allows for more complex fluid handling than is possible with conventional CE[63-71]. The combination of these two advantages allows for the separation channels used in MCCE to be fabricated on much smaller scales, which, in turn, leads to faster analysis times[9].

Figure 1.5a[72] is a schematic layout of what is perhaps the most popular design for microchip electrophoresis: the cross-T chip. Figure 1.5b[72] shows a cross section of the microchannels pictured in figure 1.5a. Figure 1.5c and d depict the sample injection procedure typically used for MCCE performed on cross-T chips. In figure 1.5a, one can already see the design advantages of performing CE on microdevices; the crossed design of the microchannels is a fluid handling capability not available in conventional CE. The microchannels on the chip also have advantages in joule heat dissipation over the cylindrical fused silica capillaries used in conventional CE. The high aspect ratio (~80 μm wide by 7.6 μm deep, figure 1.5b) allows for more efficient heat dissipation, and thus, higher voltages[72]. The ability to apply higher electric fields allows for the separations to be carried out over 1.65 cm, which is much shorter than the typical

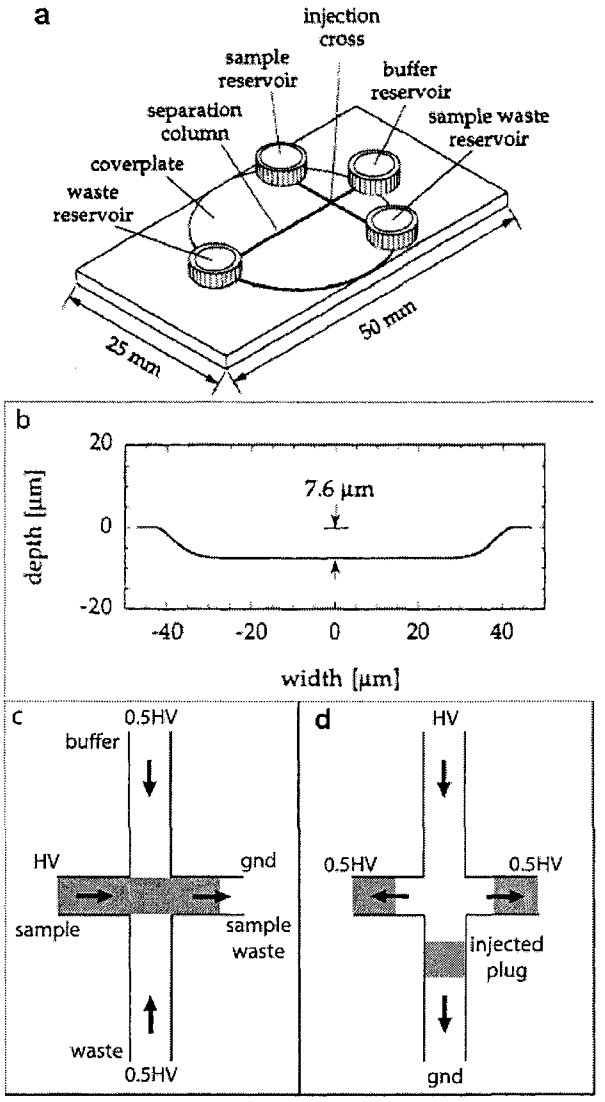

Figure 1.5: a) [72] Schematic of a cross-T chip used in MCCE. The quartz base and quartz cover plate are thermally bonded. The separation column is 1.65 cm in length and ~80 µm in width. **b)** [72] Profile of the separation column on the chip pictured in **a)**. **c)** Step one in a sample injection procedure for a cross-T chip. High voltage is applied to the sample well, and the sample waste well is kept at ground while the buffer and waste are kept at half voltage. This causes sample to migrate from the sample well to the sample waste well, across the intersection of the microchannels. Arrows indicate direction of flow. **d)** Step two in the sample injection procedure. Voltages are switched to high voltage on the buffer well, ground at the waste well, and half voltage at the sample and sample waste wells. This causes a plug of sample to be injected into the separation column. Arrows indicate direction of flow.

separation distance of conventional CE. This shorter distance allows for fast separations on the order of 15s. Compare this to the minute timescales typical for conventional CE[9].

The sample injection procedure used in MCCE also has some advantages over conventional CE. Because of the ability to specially design fluid handling channels, injection can be achieved without the relocation of buffer solutions. Instead, injection can be performed by carefully altering voltages applied to the four wells seen in figure 1.5a. Figure 1.5c shows the first stage of sample injection for MCCE. High voltage is applied to the sample well, and the sample waste well is kept at ground while the buffer and waste are kept at half voltage. This causes sample to migrate from the sample well to the sample waste well, across the intersection of the microchannels. The voltages are then switched to high voltage on the buffer well, ground at the waste well, and half voltage at the sample and sample waste wells, as can be seen in figure 1.5d. This causes the sample in the intersection of the microchannels to be injected and separated on the separations channel, while the rest of the sample in the cross channel is pushed away from the intersection to avoid contamination. This injection procedure leads to fairly reproducible sample injections[73].

The small scale, fast separation times and fluid handling capability of MCCE allows for much more complex instrumental design than possible with conventional CE. Figure 1.6[74] shows an example of the design advantage available to MCCE. The compact microchip pictured in figure 1.6 was used to analyze 96 samples of DNA fragments in ~8 min[74]. The high-throughput

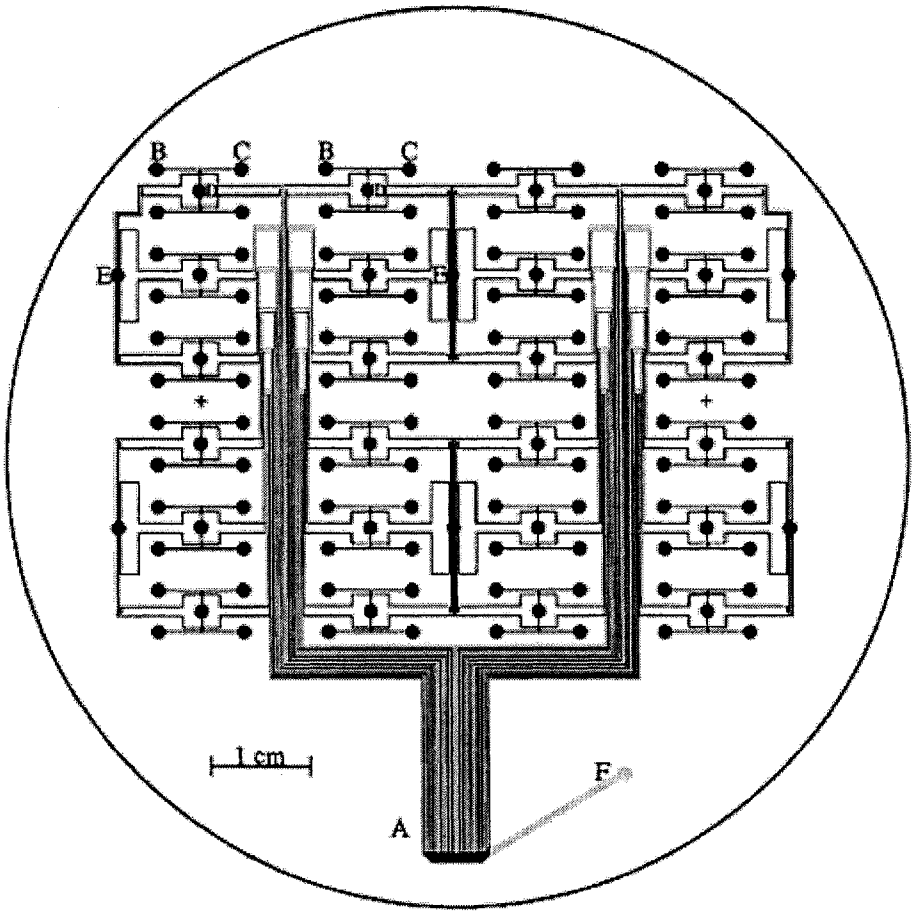

Figure 1.6[74]**:** Schematic of a 96-sample MCCE array. A is the detection region, B and C are sample reservoirs, D are waste reservoirs, E are cathode reservoirs, and F is the anode.

capability offered by this MCCE device is simply not possible with conventional CE.

Despite the obvious advantages of performing CE on microdevices, MCCE is not without its own limitations. First of all, fabrication of microdevices is more expensive and time consuming than using prefabricated fused silica capillaries[9, 62-64, 75]. In addition, the fabrication process of microchip devices for CE creates key differences in the microchip electrophoresis channels versus conventional capillaries. The fused silica capillaries used in conventional capillary electrophoresis have smooth glass walls and a cylindrical shape, which minimizes the wall surface area available to the analyte solution. Microchip electrophoresis channels, however, are fabricated through lithographic methods which can generate far more variable wall surfaces[75-77]. In addition, the high aspect ratio of lithographically formed channels can enhance wall effects experienced by analyte species[75]. The variable surface roughness and enhanced surface absorption of microchannels enhance EOF variability, which leads to increased peak dispersion[75, 77].

The walls of fused silica capillaries used in conventional CE have fairly well understood glass surface chemistry. Microchips constructed of glass have this same chemistry, and so the wall effects in glass MCCE are much the same as those in conventional CE. Microchips constructed with alternative materials, such as PDMS, have different wall chemistries which can completely change the nature of wall adsorption and EOF in MCCE experiments. It has been found, for example, that the wall chemistry of PDMS can be quite variable and the surface

much more porous than glass surfaces. This can have a pronounced and somewhat unpredictable impact on surface adsorption and EOF[76]. In some microchips different materials are used for the base and cover plates, which result in channels with heterogeneous channel surfaces. Different materials have different surface chemistries which result in different rates of EOF, increasing peak dispersion in MCCE[78].

The ability to form complex channel designs on microchips provide several advantages over conventional CE in terms of fluid handling and experimental complexity. Unfortunately, complex fluid handling in MCCE is not without drawbacks. Sample plugs in MCCE devices experience two dispersive effects not present in conventional CE; traversing channel intersections, and negotiating channel turns. The intersections commonly used for injection in MCCE can create complex dispersive effects on the sample plug introduced to the separations channel[77]. In addition, the fluid pressures experienced by sample plugs at intersections are quite a bit more complex than conventional CE, and much harder to control, resulting in possible pressure induced flows which increase dispersion[79]. Finally, many MCCE devices have relatively sharp turns due to size constraints or fluid handling steps. It has been shown that sample plugs negotiating these sharp turns experience dispersive effects[80].

Performing capillary electrophoresis on microchip offers many advantages over conventional CE. Unfortunately it also suffers from disadvantages that conventional CE does not suffer from. Ultimately the decision of whether or not to use MCCE instead of conventional CE depends on the system one wishes to

study. The design advantages of MCCE allow for more complex fluid handling, multifunctional devices, and miniaturization while suffering from some peak dispersion contributions that are not an issue with conventional CE. Analysis of peak width in MCCE still suffers from the contributions of multiple sources of variance which can vary significantly from run to run.

1.3.2 Continuous-Flow Capillary Electrophoresis:

Continuous flow capillary electrophoresis (CFCE) is a technique that monitors the characteristic electrophoretic flow velocities of individual analyte molecules in a homogenous solution as they flow continuously through an electrophoresis flow channel[59-61, 81-94]. No macroscopic separation of the analytes is required. Elimination of the requirement of macroscopic separation gives CFCE multiple advantages over conventional CE. Because of the requirement for macroscopic separation in CE, the separation efficiency and peak variance of CE depend on the separation length (equation 1.4). This limits the potential of miniaturization for CE. CFCE does not require macroscopic separation of components, and therefore has much more potential for miniaturization. For example, it was recently demonstrated that CFCE analysis of DNA fragments could be carried out on a 0.7 mm column with a resolution that was equivalent to that of a CE separation on a 0.4 cm column.[90] Furthermore, the elimination of complex buffer conditions and the injection step necessary for macroscopic separation reduces the complexity of the instrumentation necessary

for CFCE. These improvements also eliminate much of the complexity in CE data that makes comprehensive analysis difficult or impossible. As an example, the diffusion constant is easily attainable using CFCE techniques, and nearly impossible to accurately determine using conventional CE[59, 89, 91]. Finally, the migrating analyte molecules are typically monitored on timescales far shorter than conventional CE, which opens the door for studying phenomena that occur on timescales too fast for monitoring using conventional CE[59-61, 88, 89].

The key to CFCE experiments is the method of detection used. Efficient detection and identification of single analyte molecules is imperative to the successful application of this technique. Detection methods for CFCE include dynamic light scattering[81, 82, 87], sequential single molecule fluorescence detection[83], single molecule fluorescence imaging[84-86], and various incarnations of fluorescence correlation spectroscopy (FCS)[59, 60, 88-98].

Ware and Flygare first demonstrated the concept of CFCE in the early 1970's using dynamic light scattering (DLS) as the detection method[81, 82]. The authors were able to simultaneously obtain the electrophoretic mobility and diffusion coefficient of bovine serum albumin (BSA) molecules[81, 82], BSA dimers[81], and fibrinogen[81]. This was accomplished by measuring the frequency broadening (related to diffusion) and frequency shift (related to the mobility) of Rayleigh scattered laser light[82]. The DLS-CFCE technique showed the promise CFCE had for overcoming some of the limitations of conventional capillary electrophoresis, but suffered from some weaknesses that limited its use. First of all, the capillaries used in the experiments were large in comparison with the

modern fused silica capillaries used in capillary electrophoresis. Convection induced by joule heating was a major concern, and the electric field could only be applied for very short periods in an attempt to limit convection's impact on measured migration velocities. The other, more significant weakness is that the DLS-CFCE technique is only sensitive to macromolecular motions. This severely limits the range of analyte molecules capable of being studied by DLS-CFCE. Ideally, a CFCE technique would be able to monitor both small and large molecules, and for this reason, fluorescence-based CFCE techniques have found the widest acceptance.

The first reported fluorescence-based CFCE analysis technique was the single molecule electrophoresis (SME) experiment of Castro and Shera.[83] SME uses single molecule fluorescence detection to measure the electrophoretic flow velocities of individual molecules as they flow sequentially through two spatially offset excitation laser beams. The focal region of each laser was 10 μm in diameter and the distance between the two was 250 μm. There are several advantages in using the SME technique. SME was sensitive to analyte molecules present in femtomolar concentrations; a level of sensitivity not matched by conventional CE. In addition, the data was collected over a length of 250 μm and a timescale of 100s of ms, indicating the potential of SME in miniaturized high throughput devices, and far outstripping the capabilities of CE.

SME was not without its weaknesses. The picoliter sized focal volumes of the laser produced high levels of background due to Raman scatter, and so analyte molecules required multiple chromaphores to obtain sufficient signal-to-

noise ratios. This limited the technique to larger molecules. More importantly, in order to obtain migration information, molecules had to be detected in both focal regions. This meant that analyte molecules had to traverse the 250 μm distance between the laser beams in a straight line. This is a problem for smaller molecules, as they diffuse rapidly and are likely to migrate out of the path between laser beams, also limiting SME's application to larger analyte molecules. Finally, though more sensitive than CE, SME was limited to analyte concentrations in the femtomolar range due to the requirement that the mean laser occupancy be less than 1 analyte molecule. This severely limits the choice of sample solutions used for the technique. Once again, though SME showed promise as a CFCE technique, it saw limited application due to its stringent requirements of analyte size, brightness, and concentration.

Yeung and coworkers expanded on the concept of SME by introducing the technique of single molecule imaging electrophoresis (SMIE).[84-86] These authors imaged the fluorescence from individual fluorescently labeled DNA fragments in parallel using a CCD camera. Electrophoretic flow velocities were determined by recording multiple image frames and monitoring the change in position of each molecule in successive frames, or by recording a single frame while pulsing the excitation laser, thereby producing a series of spatially offset fluorescence images from each molecule. The temporal resolution of these methods, as determined by the exposure frequency or the laser pulse frequency, was 50-ms. Like SME, SMIE has the advantage of extremely high concentration sensitivity. Typical analyte concentrations ranged from femto- to picomolar. In addition, the

fluorescence imaging technique has the advantage of high throughput, since many molecules can be detected in parallel. Unfortunately, SMIE suffers from some of the same issues that negatively impact SME. The CCD cameras used are only sensitive to species labeled with multiple chromaphores, limiting the application to larger species. The dynamic range of the experiment also limits its use to extremely dilute concentrations that may not be practical for routine use. Though this technique is perhaps the most promising CFCE technique for high-throughput analysis, it has seen limited application due to its experimental constraints.

The most widely reported form of detection for CFCE is fluorescence correlation spectroscopy (FCS), in various forms[59, 60, 88-98]. FCS is a solution-phase optical technique that is used to monitor time-dependent fluctuations in the fluorescence intensity from a small subvolume of the solution, defined by the near diffraction-limited focal region of an excitation laser beam. FCS provides the highest temporal resolution for CFCE analysis because molecular transit times of individual molecules through these small volumes (or between different volumes) are typically tens of microseconds to milliseconds. Hence, confocal microscopy-based FCS is appropriate for characterizing more rapid fluctuation processes than any of the other CFCE techniques reported to date. Although FCS can also be performed on molecules flowing through a stationary interference pattern created by crossed excitation laser beams,[90] these techniques generally have lower temporal resolution (tens of milliseconds) than the confocal microscopy approach. The total duration of FCS experiments is

also much shorter, on average, than conventional CE. Relevant FCS data can often be obtained on timescales of seconds, which is much faster than the minute timescales typical of conventional CE. FCS has also been demonstrated to efficiently detect single chromaphores, which allows FCS-CFCE to be used for a much wider range of fluorescently labeled analyte molecules than the other CFCE techniques discussed. While FCS does not match SME or SMIE's low limits of detection, it has been shown to be responsive to a much greater concentration range[89].

FCS-CFCE was first demonstrated by Keller and Van Orden[89] in an experiment which demonstrated its ability to discriminate diffusion and electrophoretic migration information from a mixture of rhodamine 6G fluorescent dye (R6G) and rhodamine 6g labeled deoxycytosine triphosphate (R6G-dCTP). The experiment was the first to demonstrate CFCE detection of single chromaphores, but suffered from the fact that the data output of single focus FCS-CFCE is a single curve. This means that information pertaining to different analyte molecules can be difficult to extract from the data, much like diffusion is difficult to extract from CE peak width, which is also dependent on multiple factors.

Van Orden and LeCaptain later demonstrated the use of FCS-CFCE to monitor the interaction of fluorescently labeled single-stranded DNA with single-stranded binding protein (SSB). Dissociation constants obtained from their analysis agreed well with values obtained using conventional CE. The advantage of FCS-CFCE analysis over its CE counterparts was the much shorter

required analysis times of FCS-CFCE. The drawback, like that of the earlier FCS-CFCE demonstration by Keller and Van Orden, was that the generation of data in the format of a single curve limited its applicability to simple systems. In addition, single focus FCS-CFCE cannot be used to determine flow direction, which can pose a problem for discriminating between ions flowing in opposite directions at the same speed.

In response to the disadvantages of single focus FCS, Brinkmeier and Rigler introduced the technique of two beam fluorescence cross correlation spectroscopy (2bFCCS)[97] for the investigation of flow in microdevices. Because of its ability to monitor flow, it was soon combined with CFCE to monitor EOF in microdevices[96]. This technique is conceptually similar to the SME technique of Castro and Shera[83] in that molecular transit times between two spatially offset detection volumes are measured to determine the molecular flow velocities. However, 2bFCCS-CFCE uses smaller detection volumes (femtoliters vs. picoliters) that can be positioned much closer together (micrometers vs. hundreds of micrometers), enabling smaller transit times of ~100 μs to ~10 ms to be measured. 2bFCCS-CFCE has been used primarily for characterizing molecular flow profiles in microfluidics devices[92, 94-98]. Van Orden and LeCaptain were the first to demonstrate the use of 2bFCCS-CFCE in the analysis of multicomponent mixtures[60]. The advantage of 2bFCCS-CFCE, relative to single focus FCS-CFCE, is that it resolves the different components of a mixture into separate electropherogram peaks corresponding to the molecular transit times of each species. In addition, Fogarty and Van Orden[59] demonstrated that it could

determine the direction of analyte migration, which allows the simultaneous monitoring of both positive and negative ions migrating in opposite directions. Rädler and Bayer[91] have demonstrated the use of 2bFCCS-CFCE to simultaneously measure the electrophoretic mobility and diffusion constant of double-stranded DNA, a measurement impossible with conventional CE.

The technique of 2bFCCS-CFCE is perhaps the most versatile CFCE technique. This single molecule technique allows for the use of homogeneous buffer systems, which negates many of the problems associated with data analysis in conventional CE. In addition, the measurement is performed over a distance of microns, which shows the potential for miniaturization far beyond that available to other CE related techniques. The ability to simultaneously monitor diffusion and mobility information of singly labeled analyte molecules allows for greater versatility and analytical power than other specialized CE techniques. Finally, the ability to simultaneously monitor ions flowing in opposite directions overcomes another limit to CE's versatility.

1.4 Summary

This dissertation addresses work done to harness the full potential of the promising 2bFCCS-CFCE method. In the next section, the history and theory of 2bFCCS-CFCE will be laid out in more detail. Following that, three experiments that illuminate 2bFCCS-CFCE's potential for expanding the versatility and

analytical capabilities of CE-based methodologies that have been demonstrated, will be described. The first experiment demonstrated for the first time the potential of 2bFCCS-CFCE in the analysis of multicomponent samples containing ions migrating in opposite directions. The second experiment repeated the analysis of the first experiment on microdevices like those of MCCE. The microdevices used had the potential for miniaturization beyond that available to MCCE devices used in separations-based CE. In addition, the fluid handling required for 2bFCCS-CFCE on a microchip is far simpler than that required using conventional MCCE, which allows for more versatility in design. The third experiment demonstrated the ability of 2bFCCS-CFCE to probe the effective charge of DNA in the presence of magnesium counterions; the first demonstration of such a measurement by a CE-based technique. This was possible because of 2bFCCS-CFCE's unique ability to overcome the obstacles that prevent such a measurement using conventional CE. These three experiments showed the promise of 2bFCCS-CFCE to expand the analytical capabilities of CE-based measurements. The final section will look to the future of 2bFCCS-CFCE and highlight some areas where the analytical power of this technique could provide scientific insights and design capabilities unavailable to other CE-based methods.

1. Jorgenson, J. W.; Lukacs, K. D., Zone electrophoresis in open-tubular glass capillaries. *Analytical Chemistry.* **1981,** 53, (8), 1298-302.

2. Jorgenson, J. W.; Lukacs, K. D., Capillary zone electrophoresis. *Science.* **1983,** 222, (4621), 266-72.

3. Jorgenson, J. W.; DeArman Lukacs, K., High-resolution separations based on electrophoresis and electroosmosis. *Journal of Chromatography* **1981,** 218, 209-16.

4. Hjerten, S., Free zone electrophoresis. *Chromatogr Rev* **1967,** 9, (2), 122-219.

5. Virtanen, R., Zone electrophoresis in a narrow-bore tube employing potentiometric detection. Theoretical and experimental study. *Acta Polytech. Scand., Chem. Incl. Metall. Ser.* **1974,** 123, 67 pp.

6. Mikkers, F. E. P.; Everaerts, F. M.; Verheggen, T. P. E. M., Concentration distributions in free zone electrophoresis. *J. Chromatogr.* **1979,** 169, 1-10.

7. Mikkers, F. E. P.; Everaerts, F. M.; Verheggen, T. P. E. M., High-performance zone electrophoresis. *J. Chromatogr.* **1979,** 169, 11-20.

8. Lauer, H. H.; Ooms, J. B., Advances in capillary electrophoresis: the challenges to liquid chromatography and conventional electrophoresis. *Analytica Chimica Acta* **1991,** 250, (1), 45-60.

9. Landers, J. P., Ed., *Handbook of Capillary Electrophoresis.* 2nd ed.; CRC Press: Boca Raton, 1997; p 894.

10. Skoog, D. A.; Holler, F. J.; Nieman, T. A., *Principles of Instrumental Analysis.* 5th ed.; Harcourt Brace College Publishers: Philadelphia, 1998; p 849.

11. Camilleri, P., Ed., *Capillary Electrophoresis: Theory and Practice.*; CRC Press, Inc.: Boca Raton, 1993; p 495.

12. Yao, Y. J.; Li, S. F. Y., Determination of diffusion coefficients by capillary zone electrophoresis. *Journal of Chromatographic Science* **1994,** 32, (4), 117-20.

13. Foret, F.; Deml, M.; Bocek, P., Capillary zone electrophoresis. Quantitative study of the effects of some dispersive processes on the separation efficiency. *Journal of Chromatography* **1988,** 452, 601-13.

14. Ali, I.; Aboul-Enein, H. Y.; Gupta, V. K., Precision in capillary electrophoresis. *Analytical Letters* **2006,** 39, (11), 2345-2357.

15. Huang, X.; Coleman, W. F.; Zare, R. N., Analysis of factors causing peak broadening in capillary zone electrophoresis. *Journal of Chromatography* **1989,** 480, 95-110.

16. Roberts, G. O.; Rhodes, P. H.; Synder, R. S., Dispersion effects in capillary zone electrophoresis. *Journal of Chromatography* **1989,** 480, 35-67.

17. Rose, D. J., Jr.; Jorgenson, J. W., Characterization and automation of sample introduction methods for capillary zone electrophoresis. *Analytical Chemistry.* **1988,** 60, (7), 642-8.

18. Grushka, E.; McCormick, R. M., Zone broadening due to sample injection in capillary zone electrophoresis. *Journal of Chromatography* **1989,** 471, 421-8.

19. Yao, C.; Gao, R.; Yan, C., Quantitative sample injection for capillary electrophoresis. *Journal of Separation Science* **2003,** 26, (1/2), 37-42.

20. Recknor, M. W.; Wolze, D. A. Pressure injection apparatus for capillary electrophoresis apparatus. US Patent No. 96-US15033 9712235. 1997.

21. Zare, R. N.; Tsuda, T. Capillary electrophoresis injection device and method. US Patent No. 90-470883 5141621. 1992.

22. Virtanen, R. Method and apparatus for feeding a sample into a capillary electrophoresis apparatus. US Patent No. 97-FI149 9733166. 1997.

23. Dose, E. V.; Guiochon, G., Problems of quantitative injection in capillary zone electrophoresis. *Analytical Chemistry.* **1992,** 64, (2), 123-8.

24. Dose, E. V.; Guiochon, G. A., Internal standardization technique for capillary zone electrophoresis. *Analytical Chemistry.* **1991,** 63, (11), 1154-8.

25. Albin, M.; Grossman, P. D.; Moring, S. E., Sensitivity enhancement for capillary electrophoresis. *Analytical Chemistry.* **1993,** 65, (10), 489A-97A.

26. Schaeper, J. P.; Sepaniak, M. J., Parameters affecting reproducibility in capillary electrophoresis. *Electrophoresis* **2000,** 21, (7), 1421-1429.

27. Cohen, N.; Grushka, E., Influence of the capillary edge on the separation efficiency in capillary electrophoresis. *Journal of Chromatography, A* **1994,** 684, (2), 323-8.

28. Hjerten, S., Zone broadening in electrophoresis with special reference to high-performance electrophoresis in capillaries: an interplay between theory and practice. *Electrophoresis* **1990,** 11, (9), 665-90.

29. Schure, M. R.; Lenhoff, A. M., Consequences of wall adsorption in capillary electrophoresis: theory and simulation. *Analytical Chemistry.* **1993,** 65, (21), 3024-37.

30. Towns, J. K.; Regnier, F. E., Impact Of Polycation Adsorption On Efficiency And Electroosmotically Driven Transport In Capillary Electrophoresis. *Analytical Chemistry.* **1992,** 64, (21), 2473-2478.

31. Stedry, M.; Gas, B.; Kenndler, E., Dynamics of peak dispersion in capillary zone electrophoresis including wall adsorption: II. Exact analysis of unsteady linear adsorptive dispersion. *Electrophoresis* **1995,** 16, (11), 2027-33.

32. Gas, B.; Stedry, M.; Kenndler, E., Peak broadening in capillary zone electrophoresis. *Electrophoresis* **1997,** 18, (12-13), 2123-2133.

33. Ermakov, S. V.; Zhukov, M. Y.; Capelli, L.; Righetti, P. G., Wall adsorption in capillary electrophoresis. Experimental study and computer simulation. *Journal of Chromatography, A* **1995,** 699, (1 + 2), 297-313.

34. Mayer, B. X., How to increase precision in capillary electrophoresis. *Journal of Chromatography, A* **2001,** 907, (1-2), 21-37.

35. Horvath, J.; Dolnik, V., Polymer wall coatings for capillary electrophoresis. *Electrophoresis* **2001,** 22, (4), 644-655.

36. Kuhr, W. G.; Monnig, C. A., Capillary electrophoresis. *Analytical Chemistry.* **1992,** 64, (12), 389R-407R.

37. McManigill, D.; Swedberg, S. A., Factors affecting plate height in high performance zonal capillary electrophoreses (HPZCE). *Tech. Protein Chem.* **1989**, 468-78.

38. Ghosal, S., The effect of wall interactions in capillary-zone electrophoresis. *Journal Of Fluid Mechanics* **2003,** 491, 285-300.

39. Grushka, E.; McCormick, R. M.; Kirkland, J. J., Effect of temperature gradients on the efficiency of capillary zone electrophoresis separations. *Analytical Chemistry.* **1989,** 61, (3), 241-6.

40. Gobie, W. A.; Ivory, C. F., Thermal-Model Of Capillary Electrophoresis And A Method For Counteracting Thermal Band Broadening. *Journal Of Chromatography* **1990,** 516, (1), 191-210.

41. Davis, J. M., Influence Of Thermal Variation Of Diffusion-Coefficient On Nonequilibrium Plate Height In Capillary Zone Electrophoresis. *Journal Of Chromatography* **1990,** 517, 521-547.

42. Ross, D.; Gaitan, M.; Locascio, L. E., Temperature measurement in microfluidic systems using a temperature-dependent fluorescent dye. *Analytical Chemistry* **2001,** 73, (17), 4117-4123.

43. Evenhuis, C. J.; Hruska, V.; Guijt, R. M.; Macka, M.; Gas, B.; Marriott, P. J.; Haddad, P. R., Reliable eletrophoretic mobilities free from Joule heating effects using CE. *Electrophoresis* **2007,** 28, (20), 3759-3766.

44. Evenhuis, C. J.; Guijt, R. M.; Macka, M.; Marriott, P. J.; Haddad, P. R., Temperature profiles and heat dissipation in capillary electrophoresis. *Analytical Chemistry* **2006,** 78, (8), 2684-2693.

45. Xuan, X. C.; Xu, B.; Sinton, D.; Li, D. Q., Electroosmotic flow with Joule heating effects. *Lab On A Chip* **2004,** 4, (3), 230-236.

46. Gas, B., Axial Temperature Effects In Electromigration. *Journal Of Chromatography* **1993,** 644, (1), 161-174.

47. Gebauer, P.; Bocek, P., Predicting Peak Symmetry in Capillary Zone Electrophoresis: The Concept of the Peak Shape Diagram. *Analytical Chemistry* **1997,** 69, (8), 1557-1563.

48. Gas, B.; Kenndler, E., System zones in capillary zone electrophoresis. *Electrophoresis* **2004,** 25, (23-24), 3901-3912.

49. Kelly, M. A.; Altria, K. D.; Clark, B. J., Approaches used in the reduction of buffer electrolysis effects for routine capillary electrophoresis procedures in pharmaceutical analysis. *Journal Of Chromatography A* **1997,** 768, (1), 73-80.

50. Strege, M. A.; Lagu, A. L., Studies Of Migration Time Reproducibility Of Capillary Electrophoretic Protein Separations. *Journal Of Liquid Chromatography* **1993,** 16, (1), 51-68.

51. Walbroehl, Y.; Jorgenson, J. W., Capillary zone electrophoresis for the determination of electrophoretic mobilities and diffusion coefficients of proteins. *Journal of Microcolumn Separations* **1989,** 1, (1), 41-5.

52. Nkodo, A. E.; Garnier, J. M.; Tinland, B.; Ren, H.; Desruisseaux, C.; McCormick, L. C.; Drouin, G.; Slater, G. W., Diffusion coefficient of DNA molecules during free solution electrophoresis. *Electrophoresis* **2001,** 22, (12), 2424-2432.

53. Kenndler, E.; Schwer, C., Nondependence of diffusion-controlled peak dispersion on diffusion coefficient and ionic mobility in capillary zone electrophoresis without electroosmotic flow. *Analytical Chemistry* **1991,** 63, (21), 2499-502.

54. Maichel, B.; Gas, B.; Kenndler, E., Diffusion coefficient and capacity factor in capillary electrokinetic chromatography with replaceable charged polymeric pseudophase. *Electrophoresis* **2000,** 21, (8), 1505-1512.

55. Stellwagen, N.; Gelfi, C.; Righetti, P. G., The use of gel and capillary electrophoresis to investigate some of the fundamental physical properties of DNA. *Electrophoresis* **2002,** 23, (2), 167-175.

56. Stellwagen, E.; Stellwagen, N. C., Determining the electrophoretic mobility and translational diffusion coefficients of DNA molecules in free solution. *Electrophoresis* **2002,** 23, (16), 2794-2803.

57. Stellwagen, N. C.; Magnusdottir, S.; Gelfi, C.; Righetti, P. G., Measuring the translational diffusion coefficients of small DNA molecules by capillary electrophoresis. *Biopolymers* **2001,** 58, (4), 390-397.

58. Muijselaar, P. G.; van Straten, M. A.; Claessens, H. A.; Cramers, C. A., Determination of diffusion coefficients and separation numbers in micellar electrokinetic chromatography. *Journal of Chromatography, A* **1997,** 766, (1 + 2), 187-195.

59. Fogarty, K.; Van Orden, A., Two-beam fluorescence cross-correlation spectroscopy for simultaneous analysis of positive and negative ions in continuous-flow capillary electrophoresis. *Analytical Chemistry* **2003,** 75, (23), 6634-6641.

60. LeCaptain, D. J.; Van Orden, A., Two-beam fluorescence cross-correlation spectroscopy in an electrophoretic mobility shift assay. *Analytical Chemistry.* **2002,** 74, (5), 1171-1176.

61. LeCaptain, D. J.; Van Orden, A., Single molecule fluorescence correlation spectroscopy in an electrophoretic mobility shift assay. *Trends in Optics and Photonics* **2002,** 69, (Laser Applications to Chemical and Environmental Analysis), ThA2/1-ThA2/3.

62. Landers, J. P., Molecular Diagnostics on Electrophoretic Microchips. *Analytical Chemistry.* **2003,** 75, (12), 2919-2927.

63. Vilkner, T.; Janasek, D.; Manz, A., Micro Total Analysis Systems. Recent Developments. *Analytical Chemistry* **2004,** 76, (12), 3373-3386.

64. Dolnik, V.; Liu, S.; Jovanovich, S., Capillary electrophoresis on microchip. *Electrophoresis* **2000,** 21, (1), 41-54.

65. Effenhauser, C. S.; Bruin, G. J. M.; Paulus, A., Integrated chip-based capillary electrophoresis. *Electrophoresis* **1997,** 18, (12-13), 2203-2213.

66. Manz, A.; Effenhauser, C. S.; Burggraf, N.; Harrison, D. J.; Seiler, K.; Fluri, K., Electroosmotic pumping and electrophoretic separations for miniaturized chemical analysis systems. *J. Micromech. Microeng.* **1994,** 4, (4), 257-65.

67. Seiler, K.; Harrison, D. J.; Manz, A., Planar glass chips for capillary electrophoresis: repetitive sample injection, quantitation, and separation efficiency. *Analytical Chemistry.* **1993,** 65, (10), 1481-8.

68. Harrison, D. J.; Fluri, K.; Seiler, K.; Fan, Z. H.; Effenhauser, C. S.; Manz, A., Micromachining A Miniaturized Capillary Electrophoresis-Based Chemical-Analysis System On A Chip. *Science* **1993,** 261, (5123), 895-897.

69. Effenhauser, C. S.; Manz, A.; Widmer, H. M., Glass chips for high-speed capillary electrophoresis separations with submicrometer plate heights. *Analytical Chemistry.* **1993,** 65, (19), 2637-42.

70. Manz, A.; Harrison, D. J.; Verpoorte, E. M. J.; Fettinger, J. C.; Paulus, A.; Ludi, H.; Widmer, H. M., Planar Chips Technology For Miniaturization And Integration Of Separation Techniques Into Monitoring Systems - Capillary Electrophoresis On A Chip. *Journal Of Chromatography* **1992,** 593, (1-2), 253-258.

71. Harrison, D. J.; Manz, A.; Fan, Z.; Luedi, H.; Widmer, H. M., Capillary electrophoresis and sample injection systems integrated on a planar glass chip. *Analytical Chemistry.* **1992,** 64, (17), 1926-32.

72. Jacobson, S. C.; Moore, A. W.; Ramsey, J. M., Fused Quartz Substrates For Microchip Electrophoresis. *Analytical Chemistry* **1995,** 67, (13), 2059-2063.

73. Jacobson, S. C.; Hergenroder, R.; Koutny, L. B.; Warmack, R. J.; Ramsey, J. M., Effects Of Injection Schemes And Column Geometry On The Performance Of Microchip Electrophoresis Devices. *Analytical Chemistry* **1994,** 66, (7), 1107-1113.

74. Simpson, P. C.; Roach, D.; Woolley, A. T.; Thorsen, T.; Johnston, R.; Sensabaugh, G. F.; Mathies, R. A., High-throughput genetic analysis using microfabricated 96-sample capillary array electrophoresis microplates. *P Natl. Acad. Sci. USA* **1998,** 95, (5), 2256-2261.

75. Haswell, S. J., Development and operating characteristics of micro flow injection analysis systems based on electroosmotic flow - A review. *Analyst* **1997,** 122, (1), R1-R10.

76. Ocvirk, G.; Munroe, M.; Tang, T.; Oleschuk, R.; Westra, K.; Harrison, D. J., Electrokinetic control of fluid flow in native poly(dimethylsiloxane) capillary electrophoresis devices. *Electrophoresis* **2000,** 21, (1), 107-115.

77. Fan, Z. H.; Harrison, D. J., Micromachining Of Capillary Electrophoresis Injectors And Separators On Glass Chips And Evaluation Of Flow At Capillary Intersections. *Analytical Chemistry* **1994,** 66, (1), 177-184.

78. Bousse, L.; Cohen, C.; Nikiforov, T.; Chow, A.; Kopf-Sill, A. R.; Dubrow, R.; Parce, J. W., Electrokinetically controlled microfluidic analysis systems. *Annual Review Of Biophysics And Biomolecular Structure* **2000,** 29, 155-181.

79. Bianchi, F.; Ferrigno, A.; Girault, H. H., Finite element simulation of an electroosmotic-driven flow division at a T-junction of microscale dimensions. *Analytical Chemistry* **2000,** 72, (9), 1987-1993.

80. Zubritsky, E., Taming turns in micro-channels. *Analytical Chemistry* **2000,** 72, (21), 687A-690A.

81. Ware, B. R.; Flygare, W. H., Light scattering in mixtures of BSA [bovine serum albumin], BSA dimers, and fibrinogen under the influence of electric fields. *J. Coll. Interf. Sci.* **1972,** 39, (3), 670-5.

82. Ware, B. R.; Flygare, W. H., Simultaneous measurement of the electrophoretic mobility and diffusion coefficient in bovine serum albumin solutions by light scattering. *Chem. Phys. Letters* **1971,** 12, (1), 81-5.

83. Castro, A.; Shera, E. B., Single-Molecule electrophoresis. *Analytical Chemistry.* **1995,** 67, (18), 3181-6.

84. Lee, J.-y.; Li, H.-W.; Yeung, E. S., Single-molecule spectroscopy for molecular identification in capillary electrophoresis. *Journal of Chromatography, A* **2004,** 1053, (1-2), 173-179.

85. Anazawa, T.; Matsunaga, H.; Yeung, E. S., Electrophoretic quantitation of nucleic acids without amplification by single-molecule imaging. *Analytical Chemistry* **2002,** 74, (19), 5033-5038.

86. Shortreed, M. R.; Li, H.; Huang, W.-H.; Yeung, E. S., High-Throughput Single-Molecule DNA Screening Based on Electrophoresis. *Analytical Chemistry.* **2000,** 72, (13), 2879-2885.

87. Semenov, S. N., Correlation analysis of fluctuations in continuously monitoring electrophoresis. *Russ. J. Phys. Chem.* **1995,** 69, (11), 1884-1886.

88. LeCaptain, D. J.; Michel, M. A.; Van Orden, A., Characterization of DNA-protein complexes by capillary electrophoresis-single molecule fluorescence correlation spectroscopy. *Analyst* **2001,** 126, (8), 1279-1284.

89. Van Orden, A.; Keller, R. A., Fluorescence Correlation Spectroscopy for Rapid Multicomponent Analysis in a Capillary Electrophoresis System. *Analytical Chemistry.* **1998,** 70, (21), 4463-4471.

90. Sonehara, T.; Kojima, K.; Irie, T., Fluorescence Correlation Spectroscopy Excited with a Stationary Interference Pattern for Capillary Electrophoresis. *Analytical Chemistry.* **2002,** 74, (19), 5121-5131.

91. Bayer, J.; Raedler, J. O., DNA microelectrophoresis using double focus fluorescence correlation spectroscopy. *Electrophoresis* **2006,** 27, (20), 3952-3963.

92. Brister, P. C.; Weston, K. D., Evaluation of two-beam fluorescence cross correlation spectroscopy for electrophoretic analysis of protein digests. *Analyst (Cambridge, United Kingdom)* **2006,** 131, (2), 303-310.

93. Schiro, P. G.; Kuyper, C. L.; Chiu, D. T., Continuous-flow single-molecule CE with high detection efficiency. *Electrophoresis* **2007,** 28, (14), 2430-2438.

94. Brinkmeier, M.; Doerre, K.; Stephan, J.; Eigen, M., Two-beam cross-correlation. A method to characterize transport phenomena in micrometer-sized structures. *Analytical Chemistry.* **1999,** 71, (3), 609-616.

95. Brinkmeier, M., Cross-correlated flow analysis in microstructures. In *Fluorescence Correlation Spectroscopy: Theory and Applications*, ed.; Elson, E. S., Eds. Springer: Berlin, 2001; Vol. 65. pp 379-395.

96. Brinkmeier, M.; Dorre, K.; Riebeseel, K.; Rigler, R., Confocal spectroscopy in microstructures. *Biophys. Chem.* **1997,** 66, (2-3), 229-239.

97. Brinkmeier, M.; Rigler, R., Flow analysis by means of fluorescence correlation spectroscopy. *Exp. Techn. Phys.* **1995,** 41, (2), 205-210.

98. Dittrich, P. S.; Schwille, P., Spatial two-photon fluorescence cross-correlation spectroscopy for controlling molecular transport in microfluidic structures. *Analytical Chemistry.* **2002,** 74, 4472-4479.

Chapter 2: Background and Theory

This chapter discusses some of the background and theory behind the 2bFCCS-CFCE technique. It contains aspects of a 2004 review I contributed to in the journal *Applied Spectroscopy*[1].

2.1 Introduction

This dissertation is concerned with work performed in the development of a powerful analytical technique, two-beam fluorescence cross-correlation spectroscopy coupled with continuous-flow capillary electrophoresis (2bFCCS-CFCE). As discussed in the introduction, the importance of this technique lies in its unique method of fluorescence detection and analysis, which allows capillary electrophoresis (CE) experiments to be performed under conditions that expand the analytical capabilities of the technique. This section will discuss the background and theory pertinent to the development and application of this method of fluorescence analysis. In addition, the instrumentation and data collection tools used in the application of the technique will be discussed.

2.1.1 Basic Concepts

A major advance in our ability to measure the diffusion and flow of microscopic and sub-microscopic particles occurred in the late-1960s and early 1970s with the development of dynamic light scattering (DLS)[2, 3]. It is no coincidence that the advent of these methods followed closely behind the invention of the laser. When a laser beam irradiates a suspension of particles, some of the laser light is elastically scattered by the particles at angles other than the angle of incidence. Because laser light is coherent, the scattered light from multiple particles can interfere to produce variations in the scattered light intensity at different scattering angles. Motion of the particles causes local variations in the particle concentration, which gives rise to fluctuations in the intensity distribution of the scattered light intensity profile. In one of its implementations, DLS monitors the intensity fluctuations at a given scattering angle and then uses a statistical analysis technique referred to as *autocorrelation* analysis to characterize the time dependence of these fluctuations.

Beginning in 1972, Elson, Magde, and Webb published a series of papers describing a fluorescence-based analogue of DLS, which they referred to as fluorescence correlation spectroscopy (FCS)[4-7]. FCS, like DLS, uses autocorrelation analysis to monitor intensity fluctuations of light. FCS monitors fluorescence intensity fluctuations, while DLS monitors intensity fluctuations of scattered light. This technique was proposed because analyzing the molecular motion by monitoring the fluorescence signal imparts several advantages over

measurements based on light scattering. Fluorescence is more chemically selective than light scattering, and allows greater flexibility in studying the motion of specific analytes. Also fluorescence can be detected from molecules that are much too small to be detected by DLS, which allows one to characterize the motion of small molecules as well as large macromolecules.

At the time that the concept of FCS was introduced, it was a technique that was exceedingly difficult to implement. In large ensembles of molecules, fluorescence intensity fluctuations average out. For this reason, FCS analysis requires the ability to monitor the fluorescence of single molecules or very small ensembles of molecules. At the time, the optical components available were unable to detect the fluorescence signal from single molecules. Microscope components in the 1970's created detection volumes on the scale of picoliters, compared to the femtoliter detection volumes possible today. The larger focal volumes resulted in the backscattered light intensity exceeding the fluorescence emission of an individual molecule. In addition, the single photon counting detectors critical to modern FCS analysis had yet to be developed, so even if the fluorescent signal from individual molecules exceeded the background, it could not be detected[1]. It was not until the 1990's that crucial advances in optics created renewed interest in FCS analysis.

In 1990, Keller and coworkers successfully demonstrated the detection of single molecules[8]. In the mid 90's, Rigler and coworkers and Zare and coworkers demonstrated that confocal microscopy could be used to directly detect the fluorescence from individual molecules as they diffused through the

solution[9-12]. Confocal microscopes capable of detecting single molecules at high time resolutions generated renewed interest in FCS; made apparent by the dramatic rise in the number of publications that use FCS analysis[13-22].

Confocal microscopy has been an important biological imaging tool for many years[23]. Its intended purpose is to create micrometer resolution fluorescence images of biological specimens and other materials. In fluctuation spectroscopy, the confocal microscope is used more as a chemical analysis tool for analyzing extremely small sub-volumes of dilute solutions, than as an imaging device, although it should be noted that intracellular imaging is another important area where FCS has started making an impact. FCS is normally done by focusing an excitation laser beam to its diffraction limit using a high numerical aperture (NA) microscope objective, positioning the focal region into the analyte solution, and monitoring the fluorescence generated from the focal volume over time. The same objective lens also serves to collect fluorescence from the sample, an arrangement referred to as *epi-illumination*. A small pinhole, positioned at the image plane of the objective (the position where the image comes into focus behind the rear aperture of the objective), acts as a spatial filter to block fluorescence generated outside the focal region from reaching the detector, thus ensuring that only the fluorescence generated within the focal region can be detected.

The spatial distribution of the light intensity within the laser beam focus serves as the detection volume. The size of the detection volume can be estimated by assuming a cylindrically shaped focal volume with radius, ω_0, and

height, $2z_0$, where z_0 is the axial radius of the focal volume. ω_0 and z_0 are related to the NA of the objective, the wavelength of the excitation light, and the index of refraction, n, of the sample medium according to the equations:

$$\omega_0 = \frac{1.22\lambda}{2 \cdot \mathrm{NA}} \qquad z_0 = \frac{2n\lambda}{(\mathrm{NA})^2} \tag{2.1}$$

In an experiment that utilizes a 1.3 NA objective, a 514.5-nm laser beam as the excitation source, and an aqueous medium (n=1.33), the resulting detection volume is ~0.3 femtoliters. This extremely small detection volume is important for several reasons; it suppresses the background noise caused by backscattered laser light, it enables optical excitation of the fluorophores to their saturation point using a modest average laser power (<1-mW), it ensures that the number of fluorophores being probed at any given time is small, and it allows extremely small volume samples (microliters or less) to be analyzed.

Other aspects of confocal microscopy that are important for single molecule detection include the high collection efficiency of the objective lens (~25-% for a 1.3 NA oil-immersion objective), the high transmission efficiency of the optical components in the wavelength range of interest, and an efficient single photon counting detector. Modern single photon counting avalanche photodiode modules are able to detect visible photons with 30- to 70-% quantum efficiency. All-in-all, collection/detection efficiencies of 5- to 10-% are attainable with modern confocal microscope setups. Considering that many fluorophores can emit up to 10^6 to 10^8 photons per second (prior to photobleaching) when pumped near their optical saturation point, this can lead to photodetection rates that exceed 10^5 photons per second per molecule, albeit over brief time periods.

Modern fluorescence fluctuation analysis takes advantage of the fact that dilute solutions (sub-nanomolar to sub-micromolar) of fluorophores exhibit large amplitude fluorescence intensity fluctuations when probed by single molecule confocal microscopy. Large amplitude fluctuations arise because the average number of fluorophores occupying the detection volume (*i.e.* the *occupancy*) is small compared to the *deviation* from the average at any given time. Random diffusion or induced flow of fluorophores into and out of the detection volume ensures that the number of fluorophores being probed is never the same from one moment to the next. Consider, for example, an analyte concentration of 1-nM. At this concentration, the *average* number of fluorophores within a 1-femtoliter detection volume is ~0.6 molecules. This means that, on average, the occupancy fluctuates between zero and one, corresponding to deviations from the mean occupancy of 0.6 and 0.4, respectively. If the microscope is properly configured for single molecule detection, then the fluorescence signal will be characterized by "quiet" periods, during which only background noise is observed, punctuated by brief, intense "bursts" of signal, due to the passage of a single molecule through the detection volume. The durations of the bursts are characteristic of the diffusion or flow rate of the molecules, with average burst durations typically ranging from a few tens of microseconds to a few milliseconds, depending on the molecule's diffusion rate and migration velocity.

At fluorophore concentrations between ~10- and 100-nM, the number of molecules occupying the detection volume varies about a certain mean value. The fluorescence data collected under these conditions is still representative of

individual molecule transits even though more than one molecule is being probed at a time. As the concentration is increased above ~100-nM, two things happen. The deviation in the occupancy becomes small compared to the average fluorescence signal, and the detector starts to reach its saturation point. This requires lowering the laser power, thus reducing the molecular brightness of the fluorophores. These two affects place an upper limit on the fluorophore concentration in FCS analysis. At the lower end of the concentration scale, the lengthy time interval between detected molecules becomes a limiting factor, as does the presence of fluorescent impurities. In general, fluctuation analysis is useful for analyte concentrations in the range of ~0.1-nM to ~100-nM.

2.1.2 Theory

As a starting point for the discussion of theory, the autocorrelation function derived from fluctuations of fluorescent intensity due to diffusion in a single excitation region will be examined. The discussion will then move on to two focus excitation cross-correlation analysis which requires the addition of a uniform flow in concert with diffusion. In the case of 2bFCCS-CFCE, the source of uniform flow is the applied electric field which causes analyte migration dependent on size and charge.

2.1.2.1 Autocorrelation

In autocorrelation analysis the intensity fluctuations that are measured in a single laser excitation region are caused by concentration fluctuations of the

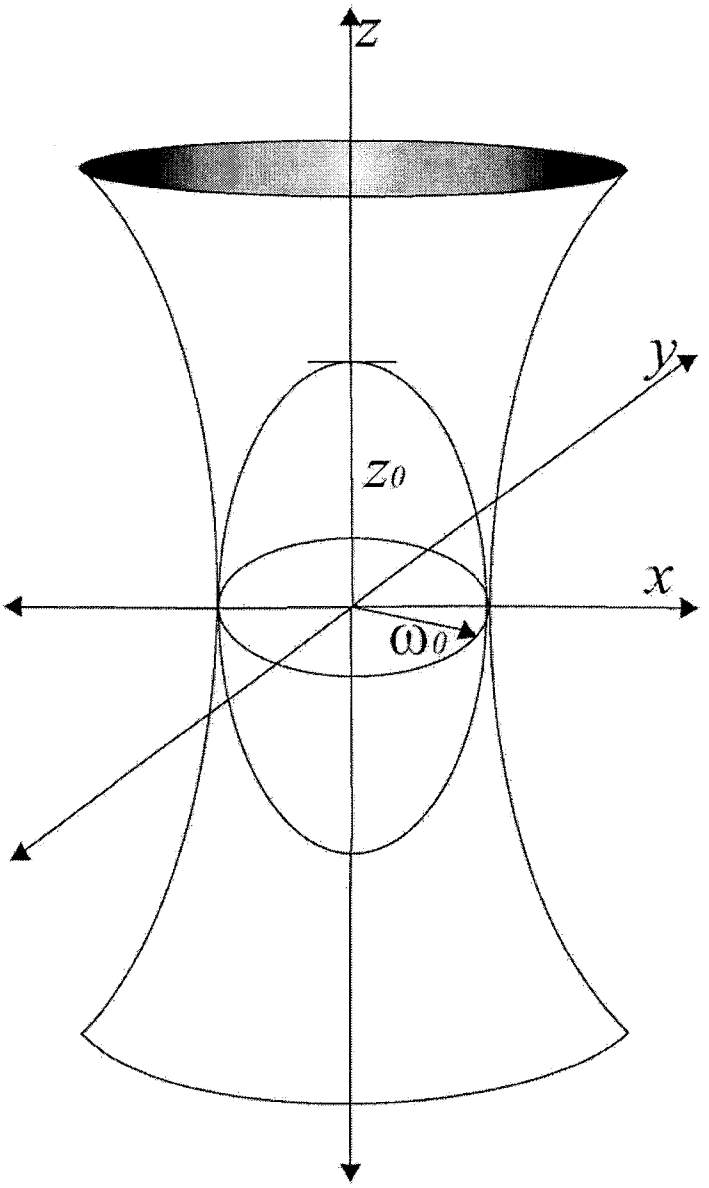

Figure 2.1: A schematic of the focus of laser beam with axes and dimensions defined. The border of the focal region is defined as where the laser intensity drops to $1/e^2$ the intensity at the center.

fluorescent species involved. Figure 2.1 depicts a schematic of the laser focus. The volume is determined by ω_o and z_o, the dimensions at which the incident laser intensity, I, drops to $1/e^2$ the laser intensity at the center of the focus, I_0, in the xy plane and z axis, respectively. The correlation of these concentration fluctuations can be represented by a concentration correlation function, $\Phi_{jl}(\mathbf{r},\mathbf{r}',\tau)$, which compares the size of the concentration fluctuation of component j at one position and time to the size of the concentration fluctuation of component l at another position and a time τ later. The concentration of the j th component at position $\mathbf{r}$ and time t can be represented by $C_j(\mathbf{r},t)$. The mean thermodynamic concentration of this component is independent of position and time, and can be represented by: $\overline{C}_j = \langle C_j(\mathbf{r},t)\rangle$. The concentration fluctuation at position $\mathbf{r}$ and time t is $\delta C_j(\mathbf{r},t) = C_j(\mathbf{r},t) - \overline{C}_j$. With this information the concentration correlation function can be defined as[6]:

$$\Phi_{jl}(\mathbf{r},\mathbf{r}',\tau) = \langle \delta C_j(\mathbf{r},t)\delta C_l(\mathbf{r},t+\tau)\rangle \qquad (2.2)$$

For τ's which are short compared to the characteristic times of diffusion and reaction $\Phi_{jl}(\mathbf{r},\mathbf{r}',\tau) \approx \Phi_{jl}(\mathbf{r},\mathbf{r}',0)$. $\Phi_{jl}(\mathbf{r},\mathbf{r}',0)$ is independent of change, and therefore can be calculated from equilibrium properties alone. For τ's much longer than the characteristic times of occurring processes, $\Phi_{jl}(\mathbf{r},\mathbf{r}',\tau) \approx \Phi_{jl}(\mathbf{r},\mathbf{r}',\infty) = 0$. The rate at which $\Phi_{jl}(\mathbf{r},\mathbf{r}',\tau)$ decays to zero with increasing τ gives a measure of how quickly diffusion, flow, and chemical reaction change the configuration of the system.

In order to express the concentration correlation function in terms of measured fluorescent intensity fluctuations, one must find an expression for the measured fluorescence intensity, $i(t)$, from a detector in terms of the concentration functions discussed above[6]:

$$i(t) = \kappa \sum_j \varepsilon_j Q_j \int I(\mathbf{r}) C_j(\mathbf{r},t) d^3\mathbf{r} \tag{2.3}$$

The factor κ represents the percentage of fluorescent photons that are converted into photocounts, accounting for losses due to optics and the quantum efficiency of the detector. ε_j is the optical extinction coefficient of the jth component. Q_j is the fluorescent quantum efficiency of the jth component. $I(\mathbf{r})$ is the intensity of incident laser light at position $\mathbf{r}$. The laser intensity at any point is dependent on the position relative to the center of the laser focus, which has an intensity of I_0: $I(\mathbf{r}) = I_0 \exp\left[-2\frac{x^2+y^2}{\omega_0^2} - 2\frac{z^2}{z_0^2}\right]$. Fluctuations in the photocounts can be represented by:

$$\delta i(t) = i(t) - \langle i \rangle \tag{2.4}$$

The temporal autocorrelation of the photocounts (after normalization) can be calculated from the intensity fluctuations as[6]:

$$G(\tau) = \frac{\langle \delta i(t) \delta i(t+\tau) \rangle}{\langle i \rangle^2} \tag{2.5}$$

Recall the concentration correlation function, $\Phi_{jl}(\mathbf{r},\mathbf{r}',\tau) = \langle \delta C_j(\mathbf{r},t) \delta C_l(\mathbf{r},t+\tau) \rangle$. In the simplest case where there is only one fluorescent component in solution, there is only diffusion occurring, and the solution is ideal (solutions in FCS are dilute to the point where this assumption is justified), fluctuations caused by

different molecules are completely uncorrelated. This simplifies the concentration correlation function to the case for one species, j, $\Phi_{jj}(\mathbf{r},\mathbf{r}',\tau)=\langle \delta C_j(\mathbf{r},t)\delta C_j(\mathbf{r},t+\tau)\rangle$, which allows the transformation of equation 2.5 into[6]:

$$G(\tau)=\frac{\sum_j (\varepsilon_j Q_j)^2 \iint I(\mathbf{r})I(\mathbf{r}')\Phi_{jj}(\mathbf{r},\mathbf{r}',\tau)d^3\mathbf{r}d^3\mathbf{r}'}{\left(I_0\pi^{3/2}\omega_0^2 z_0 \sum_j \varepsilon_j Q_j \overline{C}_j\right)^2} \tag{2.6}$$

Here, $\left(I_0\pi^{3/2}\omega_0^2 z_0 \sum_j \varepsilon_j Q_j \overline{C}_j\right)^2$ is equivalent to $\langle i\rangle^2$. Simplification of equation 2.6 gives[6]:

$$G(\tau)=\frac{1}{N}\left(\frac{1}{1+\tau/\tau_d}\right)\left(\frac{1}{1+\kappa_0^2\,\tau/\tau_d}\right)^{1/2} \tag{2.7}$$

where $N=\pi^{3/2}\omega_0^2 z_0 \overline{C}_j$, or the average number of fluorophores in the focus volume, κ_0 is the ratio ω_0/z_0, and $\tau_d=\frac{\omega_0^2}{4D_j}$, which is the average time a molecule j with diffusion constant D_j resides in the focal volume. Figure 2.2 depicts experimentally-determined fluorescent time traces and theoretical autocorrelation functions derived from the calculation of equation 2.7 for two different concentrations of fluorophores. The concentration dependence of equation 2.7 can clearly be seen: fluorescent time trace a is of a sub-nM solution of fluorophores, and the individual bursts can be seen clearly above the background, fluorescent time trace b is of a >10-nM solution of fluorophores in

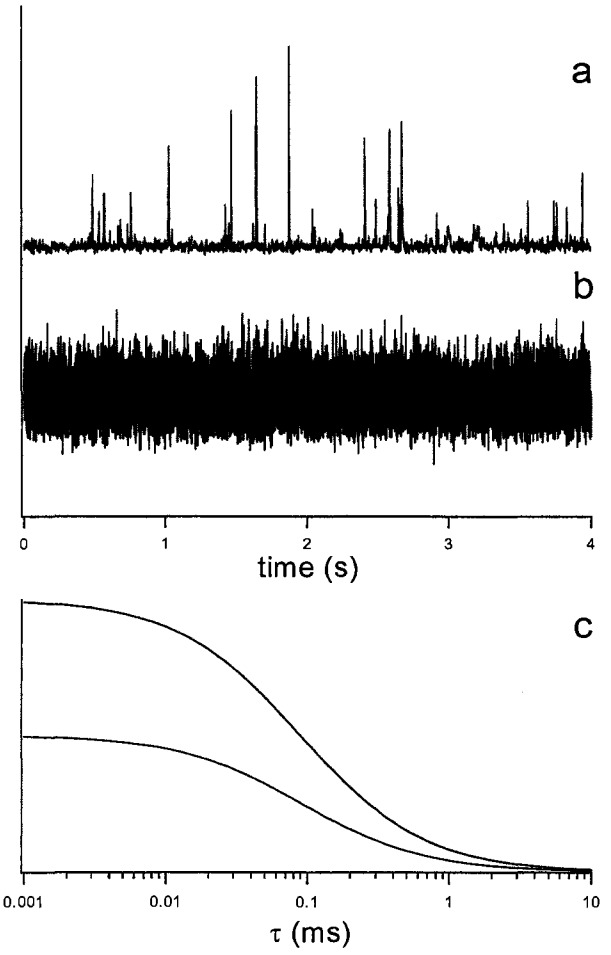

Figure 2.2: Time dependent fluorescent photon count data (*a,b*) and theoretical autocorrelation functions calculated using equation 2.7 (*c*) for two different sample solutions of the fluorescent dye Rhodamine 6G (R6G). The red trace in *a* is photon count data from a sub-nM solution of R6G. Photon bursts from single molecules are clearly resolved. The red trace in *c* was calculated using equation 2.7 and the data from *a*. The blue trace in *b* is photon count data from a >10-nM solution of R6G. The solution is too concentrated to clearly discern single molecule bursts. The blue trace in *c* was calculated using equation 2.7 and the data from *b*. The dependence of the amplitude of the autocorrelation on concentration can be seen in *c*; the solution with higher fluorophore concentration results in autocorrelation functions with lower amplitude

which the fluorescent fluctuations due to concentration fluctuations are much more difficult to observe.

2.1.2.2 Two-Beam Cross-Correlation

In two-beam cross-correlation (2bFCCS) analysis, the correlation analysis is a comparison of fluorescence intensity fluctuations in one volume (V_1) to fluctuations in a spatially separated, equivalently sized volume (V_2) at a time τ later. The volumes are formed by two laser foci, spatially separated by a distance R (see Figure 2.3). In this situation, diffusion alone is not sufficient to transport molecules from one beam to another in enough numbers to generate meaningful correlation data. This problem is overcome by introducing uniform flow (at least on the scale of the foci) either through electrophoretic flow or pressure-driven flow. The theoretical derivation for cross-correlation analysis mirrors that of autocorrelation analysis, except that the comparison of fluorescent intensities is between two, spatially separated volumes[24, 25]:

$$G_C(\tau) = \frac{\left\langle i_1\left(t,\vec{r}\right) i_2\left(t+\tau,\vec{r'}\right)\right\rangle}{\langle i_1\rangle\langle i_2\rangle} \tag{2.8}$$

where $i_1(t,\vec{r})$ and $i_2(t+\tau,\vec{r'})$ are the fluorescent intensities measured at focal volume 1 and 2 at times t and $t + \tau$ respectively as a function of their respective coordinate systems ($\vec{r} = (x,y,z), \vec{r'} = (x',y',z')$). Note that the cross correlation can be reversed:

$$G_R(\tau) = \frac{\left\langle i_2\left(t,\vec{r}\right) i_1\left(t+\tau,\vec{r'}\right)\right\rangle}{\langle i_1\rangle\langle i_2\rangle} \tag{2.9}$$

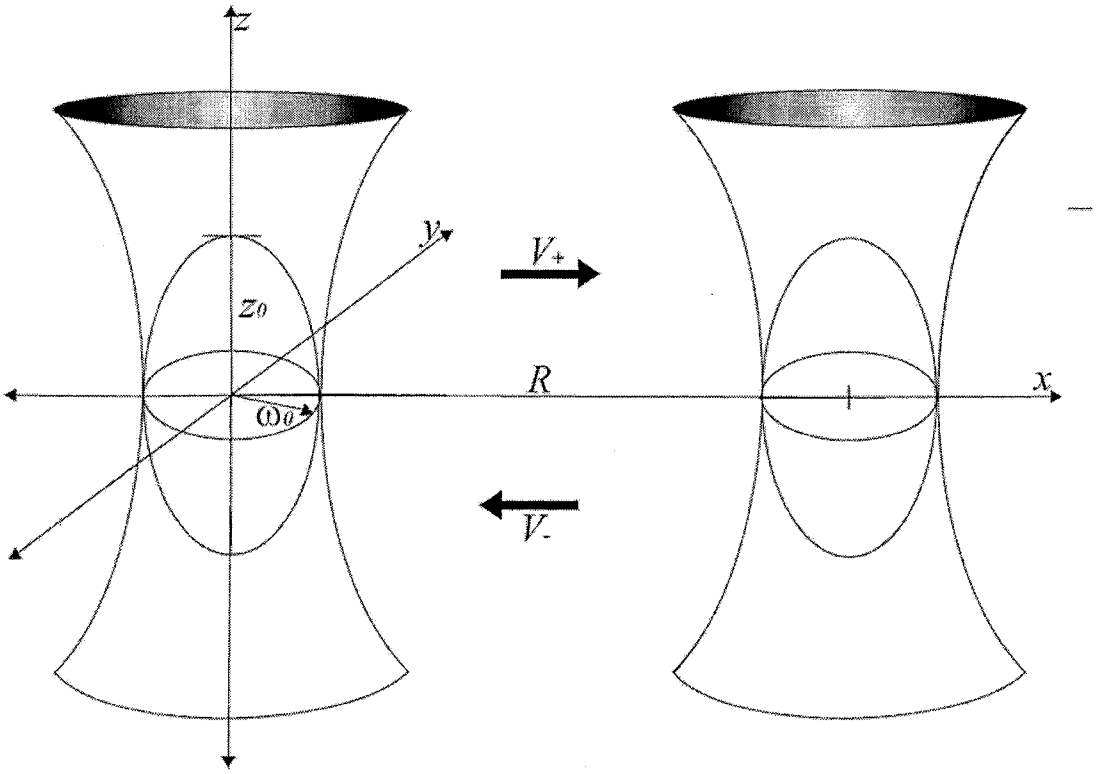

Figure 2.3: Schematic of the two, spatially-separated laser foci used in two-beam fluorescence cross-correlation spectroscopy with axes, dimensions and flow directions defined. R is the distance along the x-axis between the foci. V_+ and V_- represent the migration velocity of the fluorophore in the forward case and the reverse case, respectively.

Where focus 1 is now the volume monitored at time delay, τ. Equation 2.8 is said to be the "forward" correlation, or $G_F(\tau)$. Theoretical derivation conceptually similar to the autocorrelation case yields[24, 25]:

$$G_F(\tau) = \frac{1}{N}\left(\frac{1}{1+\tau/\tau_d}\right)\left(\frac{1}{1+\kappa_0^2\,\tau/\tau_d}\right)^{1/2} \exp\left[-\frac{\left(\vec{V}_\rho\tau - \vec{R}\right)^2}{\omega_0^2\left(1+\tau/\tau_d\right)} - \frac{V_z^2\tau^2}{z_0^2\left(1+\kappa_0^2\,\tau/\tau_d\right)}\right] \qquad (2.9)$$

Note that this resembles the autocorrelation function with an exponential expression added to take into account the flow and distance between focal volumes. $\vec{V}_\rho$ is the xy component of the flow that transports the fluorophore from focus 1 to focus 2, and V_z is the z component of the flow. $\vec{R}$ is the distance between the two foci. If the spatial separation of the two focal volumes is solely on the x-axis, and the flow is also confined to the x-axis, equation 2.9 simplifies to[24]:

$$G_F(\tau) = \frac{1}{N}\left(\frac{1}{1+\tau/\tau_d}\right)\left(\frac{1}{1+\kappa_0^2\,\tau/\tau_d}\right)^{1/2} \exp\left[-\frac{R^2\left(1-\tau/\tau_F\right)^2}{\omega_0^2\left(1+\tau/\tau_d\right)}\right] \qquad (2.10)$$

where R is the spatial separation of the two foci on the x-axis, and τ_F is the characteristic time it takes the fluorophore to traverse the distance between the two foci, given by $\tau_F = R/V_x$, where V_x is the velocity of flow along the x-axis.

For $G_R(\tau)$:

$$G_R(\tau) = \frac{1}{N}\left(\frac{1}{1+\tau/\tau_d}\right)\left(\frac{1}{1+\kappa_0^2\,\tau/\tau_d}\right)^{1/2} \exp\left[-\frac{R^2\left(1+\tau/\tau_F\right)^2}{\omega_0^2\left(1+\tau/\tau_d\right)}\right] \qquad (2.11)$$

The addition here that replaces the subtraction in the forward correlation expression is due to the fact that the fluorophore must migrate with negative

velocity to contribute to the reverse cross-correlation function. It should be noted that the forward and reverse correlation functions are completely independent of one another. Forward cross-correlation analysis is only sensitive to fluorophores migrating from focus 1 to focus 2, while in reverse cross-correlation only fluorophores migrating in the opposite direction are measured. Figure 2.4 depicts a representative, experimentally-obtained cross-correlation function and its theoretical fit obtained from the calculation of equation 2.10. Note that this function is conceptually similar to the electropherogram peaks obtained from conventional CE experiments. At low τ the fluorophore has not had sufficient time to migrate from focus 1 to focus 2, resulting in zero correlation. At high τ the fluorophore has migrated past focus 2 and no longer contributes to the correlation. It is only at τ values near τ_F that the fluorophore is present in focus 1 at time t and focus 2 at time $t + \tau$ to generate cross-correlation signal. The function rises to a maximum at τ_{max}:

$$\tau_{\max} = -\left(\tau_d + \frac{\tau_F^2}{2\tau_d}\left(\frac{\omega_0}{R}\right)^2\right) + \left[\left(\tau_d + \frac{\tau_F^2}{2\tau_d}\left(\frac{\omega_0}{R}\right)^2\right)^2 + \tau_F^2\left(1 + \left(\frac{\omega_0}{R}\right)^2\right) + 2\tau_d\tau_F\right]^{1/2} \quad (2.12)$$

In the case where $R >> \omega_0$, $\tau_{\max} \approx \tau_F$.

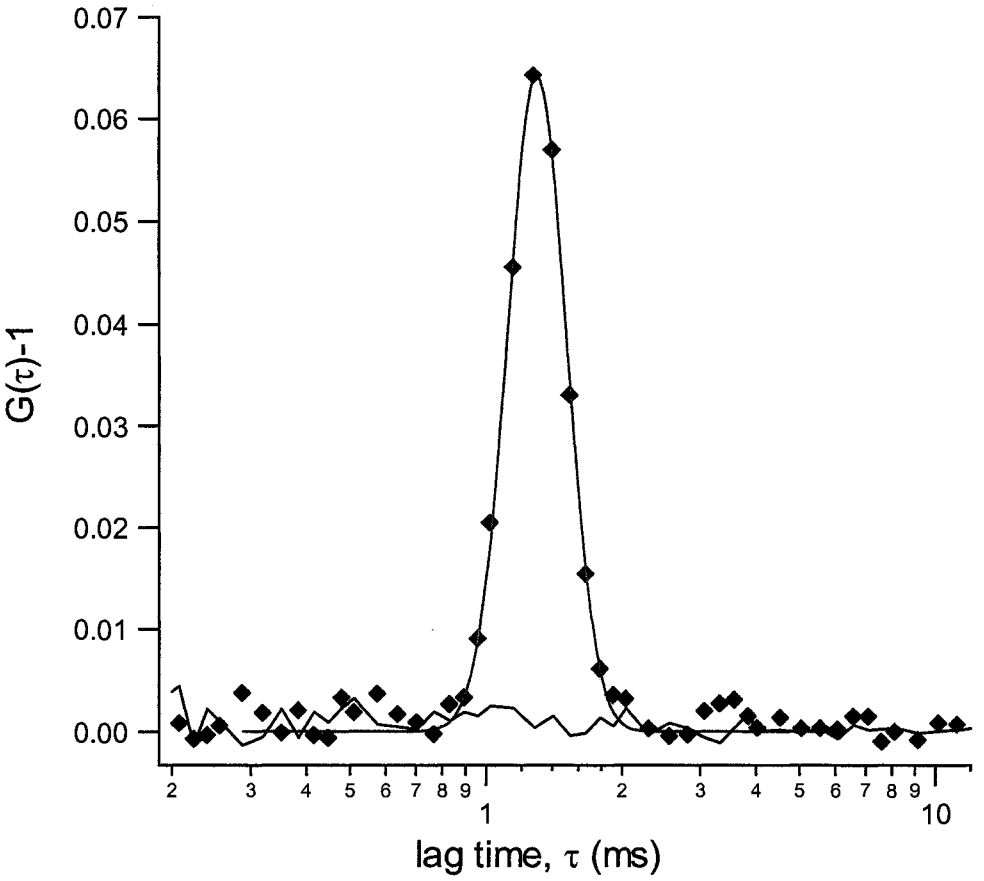

Figure 2.4: 2bFCCS data (black dots, black solid line) and theoretical fit obtained from equation 2.10 (red solid line). The experimentally determined data was obtained from a ~2.5 nM solution of Rhodamine 6G labeled single-stranded DNA (40-mer of polythymine) electrophoretically migrating in the forward direction. The only significant signal appears in the forward channel (black dots). No discernable signal appears in the reverse correlation channel (black solid line) because there were no fluorescent species migrating in the opposite direction of the DNA. The red solid line is a fit to the experimental data using equation 2.10.

2.2 Measurement of Correlation Functions

2.2.1 Calculation

In confocal microscopy-based FCS single photon counting methods are used to measure the autocorrelation function. Experimentally, this is accomplished by accumulating the detected photons into successive time bins of duration Δt. The fluorescence intensity, *i(t)*, at any given time is equivalent to the number of detected photons, n_i, divided by the time interval, Δt, corresponding to $t = i\Delta t$. The autocorrelation function for a given lagtime is calculated from Equation 2.13, after an appropriately large number of time intervals have been accumulated[14]:

$$G(\tau) = (M-k)\sum_{i=1}^{M-k} n_i n_{i+k} \Big/ \left(\sum_{i=1}^{M-k} n_i\right)^2 \qquad (2.13)$$

Here, M is the total number of time bins, and k indicates the time interval corresponding to lagtime $\tau = k\Delta t$. In practice, it is often convenient to allow the lengths of the successive time intervals to vary. Photons are initially collected into time bins of a few nanoseconds duration. Subsequent photons are then accumulated into time bins of increasingly longer durations ranging from tens of nanoseconds to seconds. This "multiple-tau" technique imparts sensitivity to fluctuations over a broad range of time scales (nanoseconds to tens of seconds) without requiring excessively long data accumulations.

In the case of cross-correlation analysis, equation 2.13 takes on the form[26]:

$$G_F(\tau) = \frac{\frac{1}{M-k}\sum_{t=1}^{M-k} n_1(t)n_2(t+\tau)}{\left(\frac{1}{M-k}\right)^2 \sum_{t=1}^{M-k} n_1(t)\sum_{t=1}^{M-k} n_2(t+\tau)} \quad (2.14)$$

Where n_1 is the photocounts obtained from detector 1 monitoring focus 1, and n_2 corresponds to the photocounts obtained from detector 2 monitoring focus 2. In reverse correlation, the n_1 and n_2 terms are switched. Note that if both n's were measured from focus 1, or both were measured from focus 2, equation 2.14 would simplify to equation 2.13.

2.2.2 Instrumentation

2.2.2.1 Capillary Preparation

2bFCCS-CFCE is a specialized capillary electrophoresis technique that uses a unique method of detection, yet it is still a capillary electrophoresis technique, and so choosing an appropriate capillary and preparing it for experimentation was an important part of performing a 2bFCCS-CFCE experiment. The capillary chosen for the experiments was a 50-μm inner diameter, 375-μm outer diameter square-bore fused-silica capillary (Polymicro, Phoenix, AZ), which was coated on the outer surface with polyimide. Commonly, the capillaries used in CE are cylindrical[27]. Square-bore capillary was chosen for the 2bFCCS-CFCE technique because the flat, rectangular surfaces allow for

easier focusing of the lasers into the capillary. Cylindrical capillaries were found to have lensing effects on the lasers, causing distortions in the shape of the laser foci imaged in the capillary. The polyimide coating on the outer surface of the capillary serves as support for the fused silica, making it much harder to break, but also acts as a barrier to imaging the lasers in the capillary. In order to monitor fluorescence occurring inside the capillary, it was necessary to burn a ~1-cm window in the polyimide coating. This was accomplished one of two ways; either a match was used to burn off the coating using a flame, or 75°C H_2SO_4 was used to dissolve the polyimide coating. The capillary was then mounted on a stage, and laser foci could be aligned inside the capillary. The total distance from the outside window wall to the center of the capillary was ~170μm, or roughly the thickness of a microscope cover slip.

As discussed in the introduction, wall effects can have negative effects on capillary electrophoresis, and so coatings are often applied to minimize analyte-wall interactions. It was found that 2bFCCS-CFCE was also negatively impacted by wall effects, and so a procedure adopted from Belder et al.[28] was used to apply a coating of poly(vinyl alcohol) (PVA, $M_W \approx 4\times10^4$ g/mol, Sigma) to the interior wall of the capillary. Belder and co-workers found that PVA coatings were successful in limiting analyte-wall interactions in addition to suppressing the EOF. A clean, ~25-cm long capillary with a window burned in the polyimide coating was filled with an acidified aqueous glutaraldehyde solution, prepared from 200 μL of 50 wt% aqueous glutaraldehyde (Fisher, Houston, TX) in 800 μL of 1 M hydrochloric acid (Mallinckrodt, Hazelwood, MO). A plug of 2.5 wt% PVA

in 0.6 M hydrochloric acid was injected into the glutaraldehyde-filled capillary using 0.5 MPa of N_2 for 10s. The capillary was then emptied and dried with continuous nitrogen flow for ~ 4 hours, after which it was ready for use. The glutaraldehyde served as a cross-linking agent which reacted with PVA molecules in solution to form a sleeve of PVA on the capillary's interior walls. Before use, capillaries were equilibrated with blank buffer solutions.

2.2.2.2 Optical Instrumentation

Several different optical setups were used for the 2bFCCS-CFCE experiments described in this dissertation, but they all were comprised of the same basic elements. Future chapters will illuminate the specific differences between the optical setups used. Figure 2.5 illustrates the basic concept of the optical instrumentation used in a 2bFCCS-CFCE experiment. Pressure flow was used to wash the capillaries, coat the capillaries, and introduce the sample prior to experimentation. This was accomplished by placing a micro-centrifuge tube containing the desired solution into a custom-built pressure chamber attached to a tank of N_2. One capillary end, which was sealed into the pressure chamber, is inserted into the solution present in the chamber. A pneumatic pressure regulator (Fairchild Model 81, Winston-Salem, NC) was used to control the pressure of N_2 in the chamber, which pushed solution through the capillary. In 2bFCCS-CFCE experiments, once the capillary was filled with sample, sample solution was placed at equal heights on either end of the capillary, and a platinum wire, connected to a high voltage power supply (Spellman, model CZE1000R, Plainview, NY), also in the pressure chamber, was inserted into the

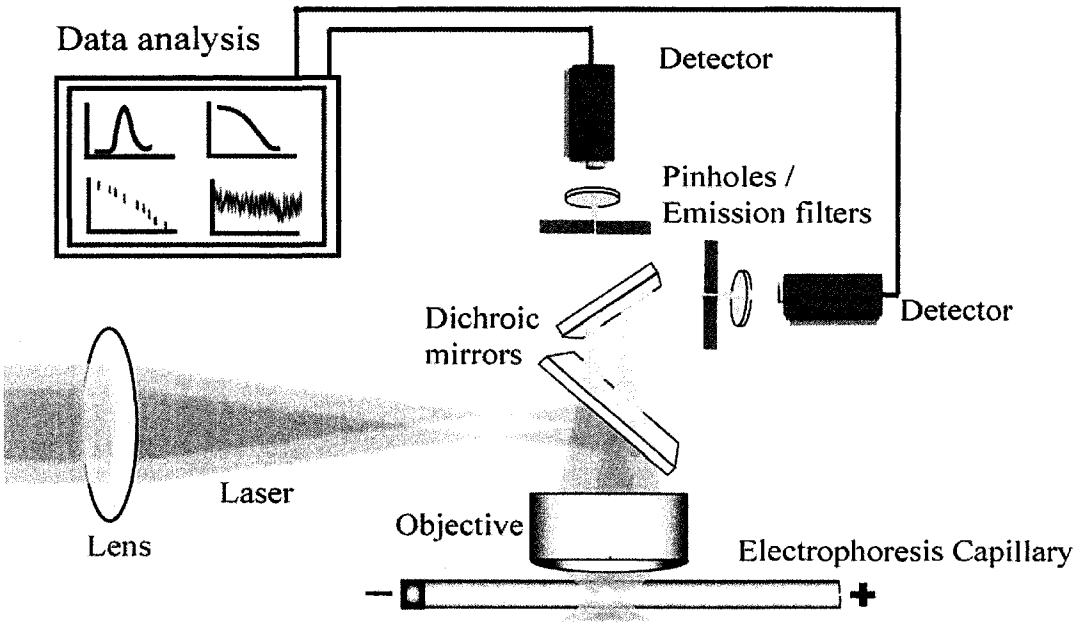

Figure 2.5: Schematic representation of the two-beam fluorescence cross-correlation/continuous flow capillary electrophoresis experiment. The optical setup was designed to position two diffraction limited laser foci in the center of a square capillary, separated by a distance of ~5 μm. The capillary is filled with sample solution using applied gas pressure, which is then turned off and voltage is applied for the electrophoresis experiment. Fluorescence signal from each focus is collected and used for the analysis of auto and cross-correlation.

sample solution present in the chamber. A grounded platinum wire was placed in the solution at the other end of the capillary. Voltage applied across the capillary resulted in electrophoretic migration of the sample components, allowing cross-correlation analysis to be performed.

The 2bFCCS-CFCE apparatus (Figure 2.5) has been described elsewhere[29, 30]. A 514.5-nm laser beam from an air-cooled, continuous wave Ar^+ laser (Midwest Laser Products, Frankfort, IL) was expanded and collimated by a 4x telescope, split, and then recombined into two nearly parallel beams by two 50/50 beamsplitters (Newport, Irvine, CA). The two beams were adjusted to equal power using the appropriate absorptive neutral density filters (Newport). The two laser beams were prefocused using a 150-mm focal-length spherical lens, reflected by a 530-nm long pass dichroic beamsplitter (CVI, Albuquerque, NM), and focused by a 100×, 1.25-numerical aperture oil immersion microscope objective (Edmund Industrial Optics, Barrington, NJ) through a small window created in the 25-cm length of the PVA coated capillary. The size of the foci was controlled by precise positioning of the 150-mm focal-length lens. The lens was positioned such that it was approximately 300 mm from the back of the microscope objective and then adjusted to minimize the size of the foci, limit clipping of the beams on the sides of the objective, and ensure near-ideal Gaussian beam profile. Fluorescence from each focal region was collected by the same objective, split by a 50/50 cubic beamsplitter (Thorlabs, Newton, NJ), spatially filtered by 50 μm pinholes (Thorlabs, Newton, NJ), and filtered by 535-nm long pass interference filters (Omega Optical, Brattleboro, VT). The spatially

and spectrally filtered light was then focused onto two single photon counting avalanche photodiode detectors (PerkinElmer Optoelectronics, model SPCM-AQR-14, Wellesley, MA) using aspheric lenses (Newport, Irvine, CA).

The two laser beams formed nearly identical diffraction-limited focal regions, positioned near the center of the inner capillary space (~25 μm from the inner surfaces), and separated along the axial dimension of the capillary by a distance, R. The e^{-2} focal radius, ω_0, in the radial dimension of the focal volume is typically ~0.3 μm. The ratio of the radial and axial e^{-2} radii ($\kappa_0 = \omega_0 / z_0$, where z_0 is the axial radius) is typically ~0.1. The separation distance, R, between the two foci is determined by cross-correlation analysis and is on the scale of ~5 μm. The position of the laser beam foci relative to the inner surface of the capillary was reproducibly controlled using a submicrometer resolution differential micrometer (Newport) mounted on the *z*-axis of the sample stage. Additionally, a precision rotation stage (Newport) was mounted on the sample stage to allow adjustment of the flow axis relative to the axis defined by the position of the two laser beams. The optimum position of the lasers relative to the capillary walls and relative to each other was determined by cross-correlation analysis. Ideally, laser foci were positioned near the center of the capillary, to reduce the impact of analytes adsorbed to the walls on the cross-correlation analysis. In addition the axis defined by the position of the two laser beams had to be exactly aligned with the flow to optimize the number of species that passed through the focal regions of both lasers. Finally R had to be precisely controlled to optimize the cross-correlation analysis. If R is too small, fluorescence from each region can be

detected by the other region's detector, which can generate what is known as pseudo-autocorrelation, or false correlation signals. If R is too large, not enough analytes are detected in both focal regions to perform successful cross-correlation analysis.

The photocounts from the two detectors were cross-correlated using an ALV-6010/160 digital correlator card (ALV, Langen, Germany) mounted in a Pentium computer. The digital correlator card uses a multiple-tau correlation technique like that discussed in section 2.2.1. The correlator card performs hardware-based correlation analysis as opposed to software-based correlation, or, in other words, the correlation analysis is performed on-chip as opposed to the raw photon data being correlated by software. This means that the digital correlator card used is incapable of recording raw photon-count data. If the raw photon-count data was desired for analysis by means other than correlation, a two-channeled 800-MHz gated photon counter card (PMS-400, Becker & Hickl GmbH, Berlin, Germany) interfaced to a Pentium computer was used.

1. Van Orden, A.; Fogarty, K.; Jung, J., Fluorescence fluctuation spectroscopy: A coming of age story. *Applied Spectroscopy* **2004,** 58, (5), 122A-137A.

2. Berne, B.; Pecora, R., *Dynamic Light Scattering: With Applications to Chemistry, Biology, and Physics*. ed.; Dover Publications, Inc.: New York, 2000; 'Vol.' p 376.

3. Schmitz, K. S., *An introduction to dynamic light scattering of macromolecules*. ed.; San Diego, CA (USA);Academic Press Inc.: United States, 1990; Pages: (472 p).

4. Magde, D.; Webb, W. W.; Elson, E. L., Fluorescence Correlation Spectroscopy.3. Uniform Translation and Laminar-Flow. *Biopolymers* **1978,** 17, (2), 361-376.

5. Magde, D.; Elson, E. L.; Webb, W. W., Fluorescence correlation spectroscopy. II. Experimental realization. *Biopolymers* **1974,** 13, (1), 29-61.

6. Elson, E. L.; Magde, D., Fluorescence correlation spectroscopy. I. Conceptual basis and theory. *Biopolymers* **1974,** 13, (1), 1-27.

7. Magde, D.; Elson, E.; Webb, W. W., Thermodynamic fluctations in a reacting system. Measurement by fluorescence correlation spectroscopy. *Phys Rev Letters* **1972,** 29, (11), 705-8.

8. Shera, E. B.; Seitzinger, N. K.; Davis, L. M.; Keller, R. A.; Soper, S. A., Detection Of Single Fluorescent Molecules. *Chemical Physics Letters* **1990,** 174, (6), 553-557.

9. Rigler, R., Fluorescence Correlations, Single-Molecule Detection And Large Number Screening - Applications In Biotechnology. *Journal Of Biotechnology* **1995,** 41, (2-3), 177-186.

10. Rigler, R.; Mets, U.; Widengren, J.; Kask, P., Fluorescence Correlation Spectroscopy With High Count Rate And Low-Background - Analysis Of Translational Diffusion. *European Biophysics Journal With Biophysics Letters* **1993,** 22, (3), 169-175.

11. Nie, S. M.; Chiu, D. T.; Zare, R. N., Real-Time Detection Of Single-Molecules In Solution By Confocal Fluorescence Microscopy. *Analytical Chemistry* **1995,** 67, (17), 2849-2857.

12. Nie, S. M.; Chiu, D. T.; Zare, R. N., Probing Individual Molecules With Confocal Fluorescence Microscopy. *Science* **1994,** 266, (5187), 1018-1021.

13. Elson, E. S.; Rigler, R., Eds., *Fluorescence Correlation Spectroscopy: Theory and Applications*. 1 ed.; Springer-Verlag: Berlin, 2001; Vol. 65, p 487.

14. Zander, C.; Enderlein, J.; Keller, R. A., Eds., *Single-Molecule Detection in Solution: Methods and Applications*. ed.; Wiley-VCH: Berlin, 2002; p 400.

15. Ambrose, W. P.; Goodwin, P. M.; Jett, J. H.; Van Orden, A.; Werner, J. H.; Keller, R. A., Single molecule fluorescence spectroscopy at ambient temperature. *Chemical Reviews* **1999,** 99, (10), 2929-2956.

16. Keller, R. A.; Ambrose, W. P.; Goodwin, P. M.; Jett, J. H.; Martin, J. C.; Wu, M., Single molecule fluorescence analysis in solution. *Applied Spectroscopy* **1996,** 50, (7), A12-A32.

17. Widengren, J.; Rigler, R., Fluorescence correlation spectroscopy as a tool to investigate chemical reactions in solutions and on cell surfaces. *Cell. Mol. Bio.* **1998,** 44, (5), 857-879.

18. Eigen, M.; Rigler, R., Sorting Single Molecules - Application To Diagnostics And Evolutionary Biotechnology. *Proceedings Of The National Academy Of Sciences Of The United States Of America* **1994,** 91, (13), 5740-5747.

19. Haustein, E.; Schwille, P., Ultrasensitive investigations of biological systems by fluorescence correlation spectroscopy. *Methods* **2003,** 29, (2), 153-166.

20. Bohmer, M.; Enderlein, J., Fluorescence spectroscopy of single molecules under ambient conditions: Methodology and technology. *Chemphyschem* **2003,** 4, (8), 793-808.

21. Bacia, K.; Schwille, P., A dynamic view of cellular processes by in vivo fluorescence auto- and cross-correlation spectroscopy. *Methods* **2003,** 29, (1), 74-85.

22. Thompson, N. L.; Lieto, A. M.; Allen, N. W., Recent advances in fluorescence correlation spectroscopy. *Current Opinion In Structural Biology* **2002,** 12, (5), 634-641.

23. Pawley, J. B., Ed., *Handbook of Biological Confocal Microscopy.* 2 ed.; Plenum Press: New York, 1995; p 632.

24. Brinkmeier, M.; Doerre, K.; Stephan, J.; Eigen, M., Two-beam cross-correlation. A method to characterize transport phenomena in micrometer-sized structures. *Analytical Chemistry* **1999,** 71, (3), 609-616.

25. Brinkmeier, M.; Rigler, R., Flow analysis by means of fluorescence correlation spectroscopy. *Exp. Techn. Phys.* **1995,** 41, (2), 205-210.

26. Jung, J.; Van Orden, A., Folding and Unfolding Kinetics of DNA Hairpins in Flowing Solution by Multiparameter Fluorescence Correlation Spectroscopy. *Journal of Physical Chemistry B* **2005,** 109, (8), 3648-3657.

27. Landers, J. P., Ed., *Handbook of Capillary Electrophoresis.* 2nd ed.; CRC Press: Boca Raton, 1997; p 894.

28. Belder, D.; Deege, A.; Husmann, H.; Koehler, F.; Ludwig, M., Cross-linked poly(vinyl alcohol) as permanent hydrophilic column coating for capillary electrophoresis. *Electrophoresis* **2001,** 22, (17), 3813-3818.

29. LeCaptain, D. J.; Van Orden, A., Two-beam fluorescence cross-correlation spectroscopy in an electrophoretic mobility shift assay. *Analytical Chemistry* **2002,** 74, (5), 1171-1176.

30. Fogarty, K.; Van Orden, A., Two-beam fluorescence cross-correlation spectroscopy for simultaneous analysis of positive and negative ions in continuous-flow capillary electrophoresis. *Analytical Chemistry* **2003,** 75, (23), 6634-6641.

Chapter 3: 2bFCCS-CFCE for Simultaneous Analysis of Positive and Negative Ions.

This chapter describes the application of two-beam fluorescence cross-correlation spectroscopy coupled with continuous-flow capillary electrophoresis (2bFCCS-CFCE) for the monitoring of ions migrating opposite directions in an electrophoresis capillary. A paper based on this work was published in the december issue of *Analytical Chemistry* in 2003[1]. This work demonstrated the ability of the 2bFCCS-CFCE technique to overcome a limitation of separations-based CE by monitoring ions moving in different directions.

3.1 Introduction:

In conventional CE, analyte species must all migrate in the same direction in order to be detected downstream from the injection point. This can be

problematic when an analyte sample one hopes to study by CE contains both positive and negative ions. Such samples are studied by conventional CE utilizing electroosmotic flow (EOF). If the magnitude of EOF is larger than the migration velocity of negative ions towards the anode, the net direction of negative ion migration will be in the same direction as positive ions, and both positive and negative ions will migrate through the detection zone. If, however, the negative ions have greater migration velocities than the EOF velocity, this technique is unable to detect them. In addition, the requirement of relatively large EOF velocities to analyze samples containing both positive and negative ions increases the impact of sample dispersion caused by phenomena related to electroosmotic flow[2-6]. Kuban and Karlberg[7] overcame the dilemma of ions migrating in opposite directions by injecting the sample at both ends of the capillary, while placing the detector in the middle. This technique eliminated the requirement of high EOF by positioning the detector in such a way that ions migrating in opposite directions both migrated towards the detection region. Unfortunately, the technique requires much more complicated experiments, in that two injection steps are required. The additional complexity of sample introduction also dramatically increases the possibility of non-reproducibility and high peak dispersion.

This work demonstrates the ability of 2bFCCS-CFCE to overcome the limitations of conventional, separations-based CE and easily monitor ions flowing in opposite directions without specialized requirements that increase experimental complexity or error. As discussed in previous chapters, 2bFCCS-

CFCE cross-correlates the fluorescence signals detected from two spatially offset laser excitation zones, referred to as focal regions 1 and 2 (Refer to Figure 2.3, chapter 2). If the signal from region 2 is cross-correlated relative region 1, one obtains the "forward" cross-correlation function. Only molecules flowing from region 1 to region 2 (*i.e.* the "forward" direction) contribute to the forward cross-correlation function. The "reverse" cross-correlation function is obtained by cross-correlating the signal from region 1 relative to region 2 and is only sensitive to molecules flowing in the "reverse" direction. Hence, the forward and reverse cross-correlation functions contain exclusive information about molecules flowing in the forward and reverse directions, respectively. The experiment is configured such that anions flow in the forward direction, and cations flow in the reverse direction. By measuring the forward and reverse cross-correlation functions simultaneously, monitoring both anions and cations in the same experiment is possible. Resolving the analytes into two different cross-correlation functions in this way effectively doubles the peak capacity of CFCE. In addition, due to the continuous-flow nature of the experiment, only the sample-containing buffer is required for the experiment, eliminating the sample injection step of conventional CE entirely. These principles are demonstrated by analyzing a model three-component mixture containing the cation Rhodamine 6G and the anions tetramethyl-6-carboxyrhodamine (TAMRA) and TAMRA labeled poly$(dT)_{39}$ single stranded DNA in aqueous buffer solution.

3.2 Experimental Section:

3.2.1 Sample Preparation:

Nanomolar solutions of Rhodamine 6G (R6G, Eastman Kodak, Rochester, NY), TAMRA (Molecular Probes, Eugene, OR), and 39-oligo poly(dT) single stranded DNA, labeled at the 5' end with TAMRA (TAMRA-ssDNA, Qiagen, Alameda, CA), were prepared in tris-Glycine buffer at pH 8.3 (0.025-M Tris-HCl, 0.192-M Glycine, Sigma, St. Louis, MO). The buffer solution also contained 0.055-wt% poly(vinylpyrrolidone) (PVP, $M_W \approx 10^6$ g/mol, Sigma), which served as a dynamic coating to further suppress EOF and prevent adsorption to the capillary walls.[8] PVP does not alter the viscosity of the solution at this concentration and was assumed to have no effect on the motion of the analytes.

3.2.2 Capillary Coating:

As stated in the previous chapter, a procedure adopted from Belder et al.[9] was used to apply a coating of poly(vinyl alcohol) (PVA, $M_W \approx 4\times10^4$ g/mol, Sigma) to the interior wall of a 50-μm inner diameter, 100-μm outer diameter cylindrical glass capillary (Polymicro, Phoenix, AZ), coated on the outer surface with polyimide. A clean, 25-cm long capillary was filled with an acidified aqueous glutaraldehyde solution, prepared from 200 μL of 50 wt% aqueous

glutaraldehyde (Fisher, Houston, TX) in 800 µL of 1 M hydrochloric acid (Mallinckrodt, Hazelwood, MO). A plug of 2.5 wt% PVA in 0.6 M hydrochloric acid was injected into the glutaraldehyde-filled capillary using 0.5 MPa of N_2 for 10s. The capillary was then emptied and dried with continuous nitrogen flow for ~ 4 hours, after which it was ready for use.

3.2.3 Instrumentation:

The 2bFCCS-CFCE apparatus used was similar to that described in the previous chapter, with some slight differences (see Figure 3.1). Briefly, a 514.5-nm laser beam from an air-cooled, continuous wave Ar^+ laser (Midwest Laser Products, Frankfort, IL) was split and then recombined into two nearly parallel beams by two 50/50 beamsplitters (Newport, Irvine, CA). The two beams were adjusted in power to 4.1 mW using the appropriate absorptive neutral density filters (Newport), reflected by a 530-nm long pass dichroic beamsplitter (CVI, Albuquerque, NM), and focused by a 100×, 1.25-numerical aperture oil immersion microscope objective (Edmund Industrial Optics, Barrington, NJ) through a small window created in a 25-cm length of the PVA coated capillary. The window was created by dissolving a small section of the outer polyimide coating in concentrated sulfuric acid heated to a temperature of 75°C. The two laser beams formed nearly identical diffraction limited focal regions, separated along the axial dimension of the capillary by a distance of ~5-µm and positioned ~ 6 µm below the inner glass surface of the capillary. A –22-kV potential was

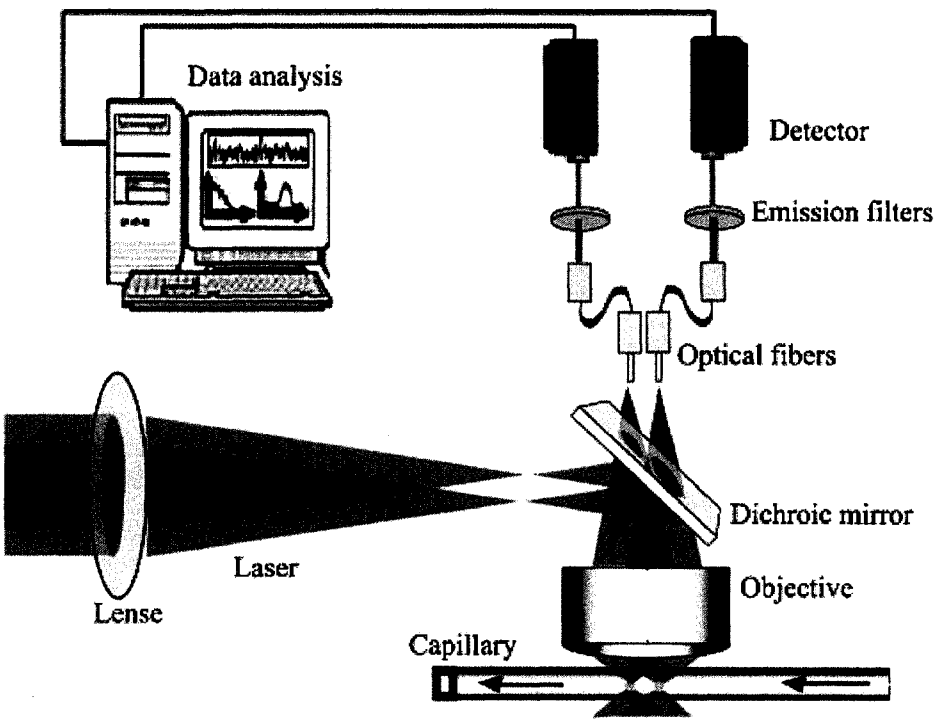

Figure 3.1: Schematic representation of the 2bFCCS-CFCE experiment. This differs from the setup described in chapter 2 (see Figure 2.5) in that optical fibers are used to direct fluorescence from the two focal volumes to their respective detectors.

applied to the capillary by means of platinum electrodes connected to a high voltage power supply (Spellman, model CZE1000R, Plainview, NY). Fluorescence from each focal region, was collected by the same objective, filtered by a 535-nm long pass interference filter (Omega Optical, Brattleboro, VT), and imaged onto the apertures of two 100 μm core diameter multimode optical fibers (Thorlabs, Newton, NJ), which transmitted the fluorescence to two single photon counting avalanche photodiode detectors (PerkinElmer Optoelectronics, model SPCM-AQR-14, Wellesley, MA). The photocounts from the two detectors were cross-correlated using an ALV-6010/160 digital correlator card (ALV, Langen, Germany) mounted in a Pentium computer.

The primary safety hazards of this experiment are electric shock due exposure to the high voltage electrodes and eye injury from exposure to laser light. The entire experiment was placed inside an enclosure to block stray laser light. Access to the enclosure was interlocked to the high-voltage power supply to prevent exposure to the high voltage electrodes during the operation of the experiment.

3.3 Theory:

The theory for 2bFCCS-CFCE was discussed in the previous chapter. Briefly, the forward and reverse cross-correlation functions are obtained through

monitoring the fluorescence intensity at each focus. The forward cross-correlation function can be represented by[10]:

$$G_F(\tau) = \frac{\left\langle i_1\left(t, \vec{r}\right) i_2\left(t+\tau, \vec{r'}\right)\right\rangle}{\langle i_1\rangle\langle i_2\rangle} \tag{3.1}$$

where $i_1(t, \vec{r})$ and $i_2(t+\tau, \vec{r'})$ are the fluorescent intensities measured at focal volume 1 and 2 at times t and $t+\tau$ respectively as a function of their respective coordinate systems ($\vec{r} = (x, y, z), \vec{r'} = (x', y', z')$). $\langle i_1\rangle$ and $\langle i_2\rangle$ are the average fluorescent intensities from focus 1 and focus 2, respectively. The reverse cross-correlation function is similar to the forward cross-correlation:

$$G_R(\tau) = \frac{\left\langle i_2\left(t, \vec{r}\right) i_1\left(t+\tau, \vec{r'}\right)\right\rangle}{\langle i_1\rangle\langle i_2\rangle} \tag{3.2}$$

where focus 1 is now the volume monitored at time delay, τ. Theoretical derivation like that discussed in the previous chapter transforms equations 3.1 and 3.2 into[1, 10]:

$$G_F(\tau) = \frac{1}{N}\left(\frac{1}{1+\tau/\tau_d}\right)\left(\frac{1}{1+\kappa_0^2\,\tau/\tau_d}\right)^{1/2} \exp\left[-\frac{R^2(1-\tau/\tau_F)^2}{\omega_0^2(1+\tau/\tau_d)}\right] \tag{3.3}$$

$$G_R(\tau) = \frac{1}{N}\left(\frac{1}{1+\tau/\tau_d}\right)\left(\frac{1}{1+\kappa_0^2\,\tau/\tau_d}\right)^{1/2} \exp\left[-\frac{R^2(1+\tau/\tau_F)^2}{\omega_0^2(1+\tau/\tau_d)}\right] \tag{3.4}$$

where ω_0 is the radius of laser focus on the xy-axis, κ_0 is the ratio ω_0/z_0, where z_0 is the radius of the beam on the z-axis, N is the average number of molecules occupying the laser beam foci (*i.e.* the occupancy), defined as $N = \overline{C}\,\omega_0^2 z_0 \pi^{3/2}$, τ_F is the characteristic time it takes the fluorophore to traverse the distance

between the two foci, given by $\tau_F = R/V_x$, where V_x is the velocity of flow along the x-axis, and τ_d is the characteristic molecular diffusion time through one of the focal volumes. The latter term is related to the diffusion constant by $\tau_d = \omega_o^2 / 4D$.

The experiments described in this chapter used a two-dimensional approximation, which neglects fluctuations caused by diffusion along the *z*-axis. This approximation is justified when z_0 is significantly larger than ω_0. However, even in confocal microscopy-based FCS, fluctuations caused by *z*-axis diffusion constitute a small perturbation to the correlation function and can often be neglected[11]. A three-dimensional model was used to analyze some cross-correlation data and it was found that the results did not differ significantly from those of the two-dimensional model presented here. With the assumption of a two-dimensional model, equations 3.3 and 3.4 can be rewritten as:

$$G_F(\tau) = \frac{1}{N}\left(\frac{1}{1+\tau/\tau_d}\right)\exp\left[\frac{-(R-V_x\tau)^2}{\omega_0^2(1+\tau/\tau_d)}\right] \tag{3.5}$$

$$G_R(\tau) = \frac{1}{N}\left(\frac{1}{1+\tau/\tau_d}\right)\exp\left[\frac{-(R+V_x\tau)^2}{\omega_0^2(1+\tau/\tau_d)}\right] \tag{3.6}$$

Equations 3.5 and 3.6, as discussed earlier, are used as the basis for analysis of the cross-correlation data of the anion and cation components, respectively.

Samples containing mixtures of fluorophores were analyzed by treating the cross-correlation functions as linear combinations of the single-component cross-correlation functions, according to equation [12].

$$G_{F,R}(\tau) = \frac{1}{\langle F\rangle^2}\sum_i N_i^2 Q_i^2 G_{F,R,i}(\tau). \tag{3.7}$$

Here, $\langle F \rangle$ is the time-averaged photodetection rate from each focal volume due to the total fluorescence from all species plus the background radiation, N_i is the occupancy of species i, Q_i is the specific brightness of species i (defined as the average number of detected photons per molecule per second), and $G_{F,R,i}(\tau)$ are the pure-component cross-correlation functions for species i, given by Equations 3.5 and 3.6. Mixtures containing both positive and negative ions flowing in opposite directions can be analyzed due to the presence of cross-correlation peaks in both correlation channels, as will be demonstrated below.

3.4 Results and Discussion:

3.4.1 Control Experiments:

Control autocorrelation and cross-correlation experiments were carried out to determine the parameters R, ω_o, and $\tau_{d,R6G}$, the diffusion time of R6G. These parameters remained constant through all subsequent experiments (Table 3.1). This was accomplished by analyzing a pure solution of 3-nM R6G in Tris-Glycine buffer. A static solution of the R6G was first measured using autocorrelation analysis (Figure 3.2) to determine the value $\tau_{d,R6G}$. The value of ω_o was then obtained from $\tau_{d,R6G}$ using the literature value of $D_{R6G} = 3.0 \times 10^{-6} cm^2/s$ [13]. The experimental autocorrelation functions of the 3-nM R6G solution were fit according to the equation:

Table 3.1: Control Experiment Data[a]

Parameter	R6G control experiments[b]		
ω_o (μm)	0.3277(41)		
R (μm)	4.54(17)		
τ_{dR6G} (ms)	0.0895(23)		
T_{eq}	0.4266(49)		
τ_T (10^{-3} ms)	1.989(91)		
	Cross-Correlation Analysis of Single Component Standards[c]		
	R6G	TAMRA	TAMRA-ssDNA
V_x (mm/s)	-2.524(40)	1.283(19)	4.2017(32)
τ_F (ms)	1.7779(65)	3.54(14)	1.081(41)
τ_d (ms)	0.0895(23)	0.0749(66)	0.3832(89)
A	0.004032(52)	0.001091(38)	0.02735(22)

[a]Numbers in parenthesis are the uncertainties in the last digits reported to one standard deviation. [b]$\tau_{d,R6G}$, T_{eq}, and τ_T were obtained from the fitting of autocorrelation data, ω_o was obtained from $\tau_{d,R6G}$ through the relation, $\tau_{d,R6G} = \omega_o^2 / 4D_{R6G}$, using the value of $D_{R6G} = 3.0 \times 10^{-6}\,\mathrm{cm}^2/\mathrm{s}$, and R was determined from fitting R6G cross-correlation data. [c]R and ω_o were held constant at 4.54(17) μm and 0.3277(41) μm, respectively in the analysis of the TAMRA and TAMRA-ssDNA standard solutions.

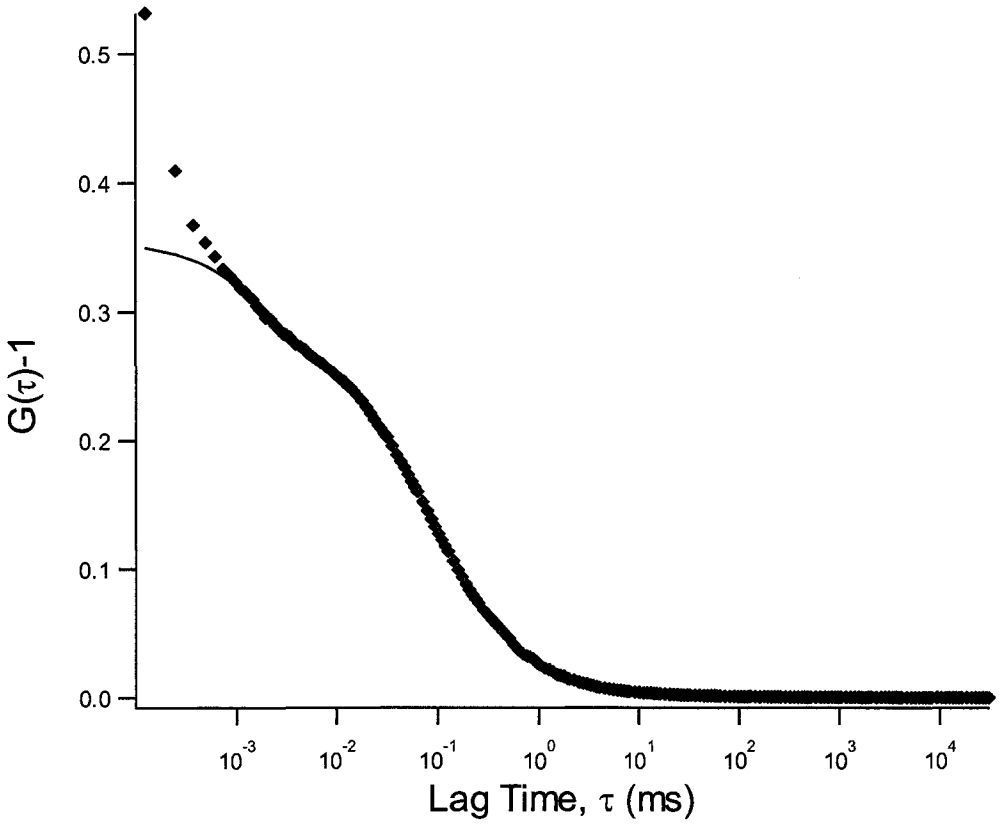

Figure 3.2: Control autocorrelation data (black diamonds) for R6G with the theoretical fit (red solid line) according to equation 3.8. The theoretical fit deviates from the experimental data at low lag times due to afterpulsing of the detector, a form of electronic feedback that impacts correlation data at lag times less than 10^{-3} ms. The fits eliminated the impact of afterpulsing by only fitting data at lag times greater than 10^{-3} ms.

$$G_{R6G}(\tau)-1 = A\left(\frac{1}{1+\tau/\tau_{d,R6G}}\right)\left(1+T_{eq}e^{-\tau/\tau_T}\right) \tag{3.8}$$

where A is the amplitude of the autocorrelation function, related to the concentration of R6G and the molecular brightness of the R6G fluorophore, T_{eq} is defined as $T_{eq} = T/(1-T)$, where T is the quantum yield, and τ_T is a time constant for population and depopulation of the triplet state. The parameters in the last term of equation 3.8 account for the fact that a fraction of molecules exist in a nonfluorescent triplet state, which lowers the effective fluorophore concentration. The theoretical derivation accounting for triplet state impact on autocorrelation analysis was based on work by Rigler and coworkers[14].

Figure 3.3d shows the cross-correlation functions for the pure R6G solution as it flowed through the capillary under the influence of the applied electric field. This reverse correlation function was analyzed by fitting to Equation 3.9.

$$G_R(\tau) = B_R + A_{PA}\left(\frac{1}{1+\tau/\tau_{PA}}\right) + A_{R6G}\exp\left[\frac{-\left|V_{x,R6G}\right|^2\left(\tau_{F,R6G}-\tau\right)^2}{\omega_o^2\left(1+\tau/\tau_{d,R6G}\right)}\right] \tag{3.9}$$

This function is assumed to be a linear combination of three components. The first, B_R, is the baseline, given by $\lim_{\tau\to\infty} G_R(\tau)$. The second component represents the pseudo-autocorrelation function, which appears as a decay from lagtime zero. This arises because of cross-talk between the two detection volumes. A small fraction of the fluorescence from focal region 1 is detected on detector 2, and vice versa, giving rise to autocorrelation of R6G molecules flowing through the individual focal volumes[15]. The parameters A_{PA} and τ_{PA} are used only for fitting this region of the cross-correlation function. No physical meaning is

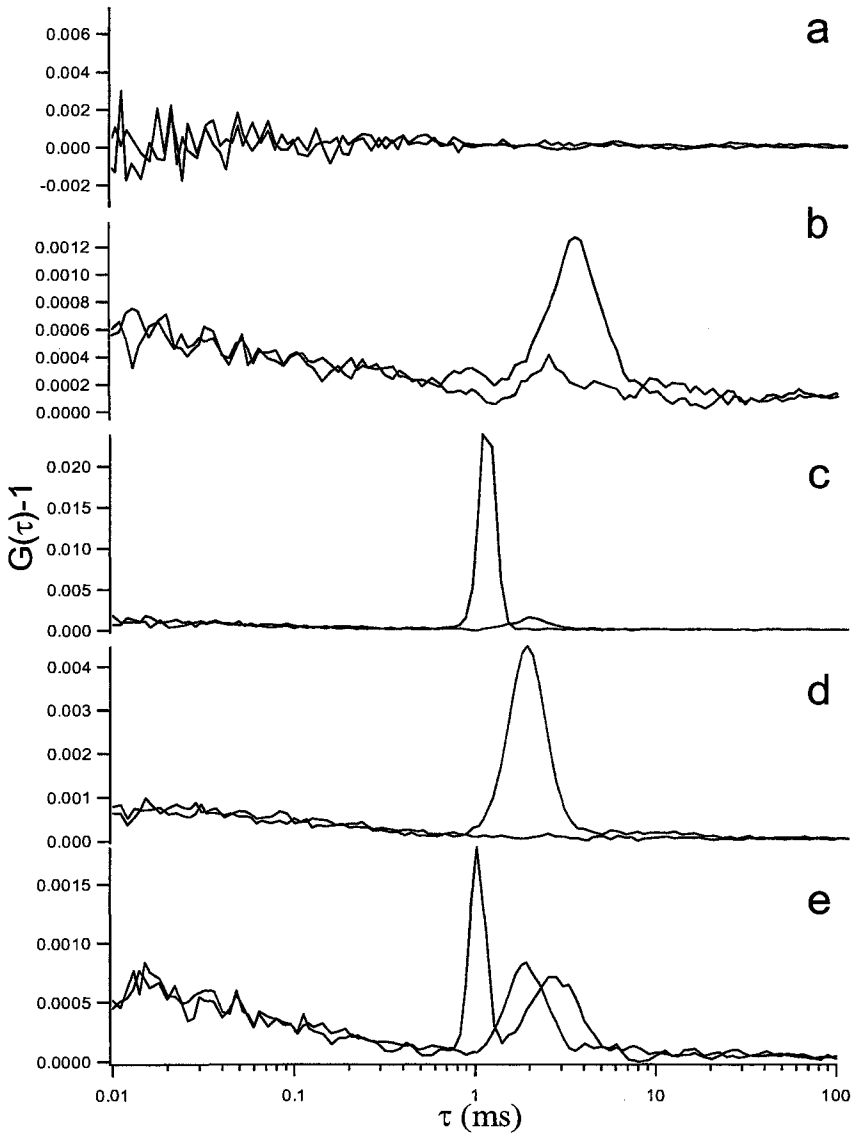

Figure 3.3: Forward (black) and reverse (red) cross-correlation functions for (a) blank Tris-Glycine buffer; pure solutions of (b) 3-nM TAMRA, (c) 0.5-nM TAMRA-ssDNA, (d) 2-nM R6G in Tris-Glycine buffer; and (e) a mixture containing 2-nM R6G, 3-nM TAMRA, and 0.5-nM TAMRA-ssDNA in Tris-Glycine buffer. The data aquisition times were 5-min per sample.

ascribed to these parameters. The third component is the reverse cross-correlation function due to R6G molecules flowing from focal region 2 to focal region 1. The parameter A_{R6G} is the intensity of the cross-correlation peak at τ= $\tau_{F,R6G}$. The physical meaning of this parameter is related to the concentration and photophysical properties of R6G, as will be discussed below. The values of A_{R6G}, $V_{x,R6G}$, and $\tau_{F,R6G}$ were determined from the least-squares fitting procedure by fixing ω_o and $\tau_{d,R6G}$ to the values obtained by autocorrelation analysis. The distance, R, between focal regions 1 and 2 could then be determined from the expression, $R = V_{x,R6G}(\tau_{F,R6G})$.

3.4.2 Analysis of a Three-Component Mixture.

Figure 3.3e shows the forward and reverse cross-correlation functions for a three component mixture containing 2-nM R6G, 3-nM TAMRA, and 0.5-nM TAMRA-ssDNA flowing through the capillary under the influence of the applied electric field. Forward and reverse cross-correlation functions from a blank buffer solution and from pure solutions of each analyte are also shown for comparison (Figures 3.3a-3.3d). Since TAMRA and TAMRA-ssDNA are both negative ions, the corresponding peaks occur in the forward correlation channel. The cross-correlation peak for R6G occurs in the reverse correlation channel. Note that there appears to be a slight contamination in the TAMRA-ssDNA standard, giving rise to a small peak in the reverse correlation channel. Cross-correlation analysis of the pure solutions yielded the data presented in Table 3.1. The peak

positions measured for the pure solutions enable identification of the corresponding peaks in the three component mixture. The peaks in the forward channel are attributed to TAMRA-ssDNA and TAMRA, occurring at earlier and later lagtimes, respectively, while the peak in the reverse channel is assigned to R6G. The TAMRA-ssDNA peak occurs at the earliest time owing to its higher charge state and, hence, its greater electrophoretic mobility. The apparent mobility of TAMRA is less than that of R6G, possibly due to residual electroosmotic flow, which may oppose the flow of the negative ions.

The reverse correlation function for the three component mixture was analyzed by fitting the data to Equation 3.9, and the forward correlation function was analyzed using Equation 3.10, with R and ω_0 held fixed to the values reported in Table 3.1:

$$G_F(\tau) = B_F + A_{PA}\left(\frac{1}{1+\tau/\tau_{PA}}\right) + A_1 \exp\left[\frac{-(R - V_{x,1}\tau)^2}{\omega_o^2(1+\tau/\tau_{d,1})}\right] + A_2 \exp\left[\frac{-(R - V_{x,2}\tau)^2}{\omega_o^2(1+\tau/\tau_{d,2})}\right] \quad (3.10)$$

subscripts 1 and 2 denote the parameters corresponding to TAMRA-ssDNA and TAMRA, respectively. The results of these analyses are displayed graphically in Figure 3.4. The fitted parameters and their associated standard deviations are presented in Table 3.2.

The intensities of the cross-correlation peaks depend on the concentrations and photophysical properties of the fluorophores, and the molecular transit times for diffusion and flow, according to the following relationship, which was derived from Equations 3.5-3.7 for $G_{F,R}(\tau = \tau_{F,i})$:

$$A_i = \frac{N_i(1 - T_{eq,i})Q_i^2}{\langle I \rangle^2 (1 + \tau_{F,i}/\tau_{d,i})} \quad (3.11)$$

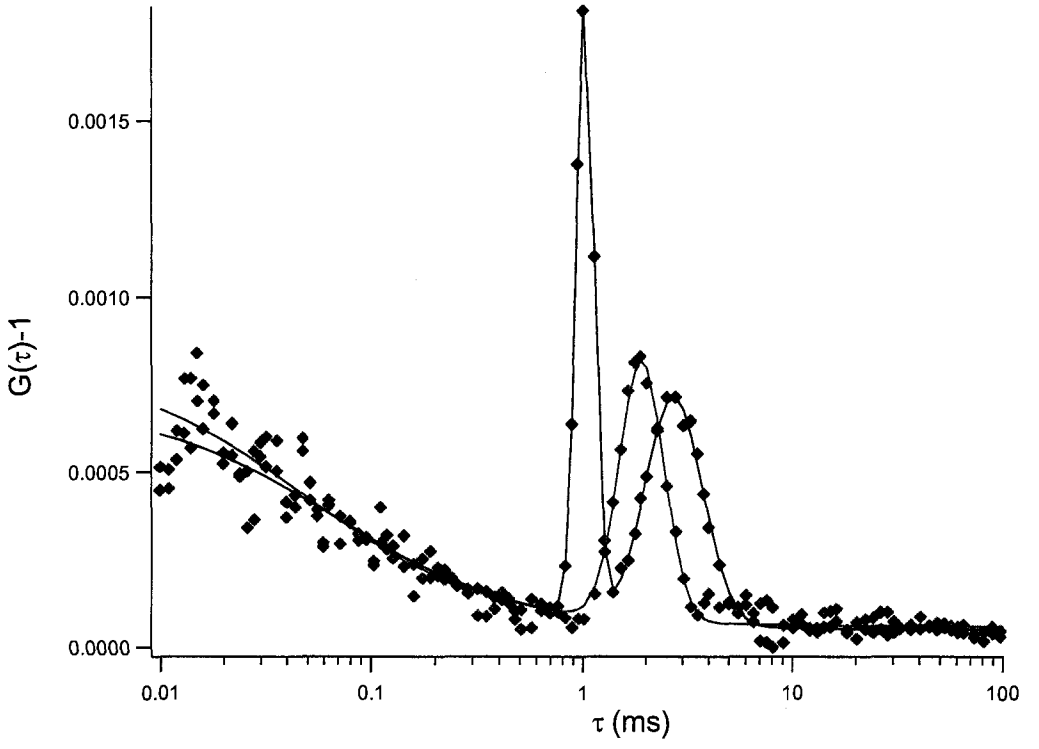

Figure 3.4: Experimental and fitted forward (black) and reverse (red) cross-correlation functions obtained for the TAMRA, TAMRA-ssDNA, and R6G mixture from Figure 3.3e. The diamonds represent the experimental data and the solid curves are fits to equations 3.9 (red) and 3.10 (black).

Table 3.2: Determination of Relative Concentrations[a]

Parameter	Cross-Correlation Analysis of a Three-Component Mixture[b]		
	R6G	TAMRA	TAMRA-ssDNA
V_x (mm/s)	-2.22(15)	1.649(25)	4.362(14)
τ_F (ms)	1.933(34)	2.75(11)	1.041(40)
τ_d (ms)	0.079(11)	0.0676(69)	0.379(34)
D (μm^2/ms)	0.339(47)	0.397(42)	0.0708(65)
A	0.000756(42)	0.000663(28)	0.001768(53)
	Photophysical Parameters[c]		
	R6G	TAMRA	TAMRA-ssDNA
T_{eq}	0.4266(49)	0.3590(28)	0.4146(18)
ϕ_f	0.8095(30)	0.3882(18)	0.5350(52)
τ_f (ns)	3.935(39)	2.310(23)	2.974(30)
	Relative Concentrations[d]		
	R6G	TAMRA	TAMRA-ssDNA
$N_{i,corr}$ (%)	31.4(4.1)	55.8(4.3)	12.7(1.6)
$N_{i,exp}$ (%)	38.2(3.7)	52.7(3.7)	9.1(1.1)

[a]Numbers in parenthesis are the uncertainties in the last digits reported to one standard deviation. [b]R and ω_o were held constant at 4.54(17)μm and 0.3277(41)μm respectively for all the fits in the analysis of the mixture. D was calculated using the expression, $D = \omega_0^2/4\tau_d$ [c]τ_f was measured by time-correlated single photon counting performed on pure solutions of each species in the tris-glycine buffer. T_{eq} was obtained from autocorrelation analysis of the pure solutions. [d]$N_{i,corr}$ is the relative concentration as determined from cross-correlation analysis. $N_{i,exp}$ is the expected relative concentration as determined from dilution of known stock solutions.

here, $T_{eq,i}$ is the triplet yield of species i. This parameter accounts for the fact that a fraction of molecules exist in a nonfluorescent triplet state, which lowers the effective fluorophore concentration. The specific brightness, Q_i, is the product of the fluorescence excitation rate, $k_{exc,i}$, the fluorescence quantum yield, $\phi_{f,i}$, and the fluorescence collection/detection efficiency, κ_i, for species i. Since the laser intensity used in these experiments was above the threshold for optical saturation of the fluorophores, we assume $k_{exc,i} = 1/\tau_{f,i}$ for each species, where $\tau_{f,i}$ is the fluorescence lifetime of species i. Hence, $Q_i = \kappa_i \phi_{f,i} / \tau_{f,i}$

In principle, it is possible to determine the absolute concentration of each species by calculating N_i from equation 3.11 and using the relationship between N and $\overline{C}$ above. However, there are a number of factors affecting A_i that are difficult to measure or calculate theoretically, which makes determining the absolute concentrations impractical. These factors may include slight differences in the laser intensity distributions in the two focal volumes, off-axis components in the flow velocities or R value, a slight distribution in the flow velocity across the z dimension of the focal regions, distortion of the focal regions from an ideal Guassian shape due to focusing through the curved capillary walls, photobleaching (presumed to be a small effect because of the fast transit times of the molecules through the focal regions), and Joule heating. Nevertheless, most of these factors are likely to cancel when calculating the ratios N_i/N_j, given by

$$\frac{N_i}{N_j} = \frac{A_i}{A_j} \cdot \left(\frac{1 + \tau_{F,i}/\tau_{d,i}}{1 + \tau_{F,j}/\tau_{d,j}} \right) \cdot \left(\frac{\tau_{f,i}}{\tau_{f,j}} \cdot \frac{\kappa_j \phi_{f,j}}{\kappa_i \phi_{f,i}} \right)^2 \cdot \left(\frac{1 - T_{eq,j}}{1 - T_{eq,i}} \right) \qquad (3.12)$$

The relative concentrations, $N_{rel,i}=N_i/(N_i+N_j+N_k)$, can then be obtained from these ratios using:

$$N_{rel,i} = \left(1 + \frac{N_j}{N_i} + \frac{N_k}{N_i}\right)^{-1}. \tag{3.13}$$

The relative concentrations of each species in the three component mixture are presented in Table 3.2, along with the parameters used to calculate these values.

The values of A, τ_F, and τ_d were obtained from the cross-correlation analyses. The diffusion constants, D_i, of the different components of the mixture are also presented in table 3.2. They were found according to the expression, $D_i = \omega_0^2/4\tau_{d,i}$, where $\tau_{d,i}$ indicates the characteristic diffusion time of fluorescent species i. All values agreed well with literature values[16-21]. The τ_f's were measured by time-correlated single photon counting performed by Dr. Peter Goodwin of Los Alamos National Laboratory on pure solutions of each species in the tris-glycine buffer (Data not shown).

The fluorescence quantum efficiencies were measured for each species using static spectrofluorimetry with reference to standard solutions of R6G and TAMRA in methanol. This was accomplished by comparing the measured fluorescent intensities of TAMRA and R6G in methanol to the tris-glycine buffers used in the cross-correlation experiments:

$$\frac{\phi_{R6G,MeOH}}{\phi_i} = \frac{I_{R6G,MeOH}}{I_i} \tag{3.14}$$

where $\phi_{R6G,MeOH}$ is the fluorescence quantum efficiency of R6G in methanol, a value obtained from the literature[22]. $I_{R6G,MeOH}$ is the intensity of the R6G

fluorescence measured on the spectrofluorimeter, and ϕ_i and I_i are the fluorescence quantum efficiencies and measured fluorescence intensities of the dyes in different buffer conditions, respectively.

Finally, the T_{eq} values were obtained from autocorrelation analysis of the pure static solutions according to the procedure outlined by Rigler and co-workers, as discussed above[14]. Note that the relative concentrations of the three analytes are determined with ~10-% precision, and that they agree with the expected values within experimental error. The errors in the expected concentrations were estimated from the precision of the pipettes used to prepare the solutions and the errors in the standard solution concentrations.

3.4.3 Data Acquisition Time:

The data presented in Figure 3.3 were obtained after 5-min data acquisition times. Clearly it would be desirable to minimize this time. From our data, we can estimate the minimum time required to obtain statistically significant cross-correlation functions, in which the signal-to-noise ratios (S/N) of the cross-correlation peaks are equal to 3. The noise was estimated to be the standard deviation of the blank solution cross-correlation functions (Figure 3.3a) between lagtimes of 1- and 10-ms. This yielded a noise value of 9.85×10^{-5}. The S/N values for each cross-correlation peak were then obtained by dividing this number into the peak amplitudes. For the pure TAMRA, R6G, and TAMRA-ssDNA solutions (Figure 3.3b-3.3d), the S/N values were found to be 13, 40, and

240, respectively. A larger S/N for TAMRA-ssDNA was obtained because of the higher electrophoretic mobility and lower diffusion rate of TAMRA-ssDNA compared to the other analytes. Given that S/N is proportional to the square root of the acquisition time, the minimum times required to analyze each of the pure solutions are 16-, 1.3-, and 0.05-s, for TAMRA, R6G, and TAMRA-ssDNA, respectively. This indicates that 2bFCCS is capable of extremely fast data acquisition times (tens of milliseconds to seconds) under favorable conditions.

For the three-component mixture (Figure 3.3e), the S/N values were 7, 8, and 18 for the TAMRA, R6G, and TAMRA-ssDNA peaks, respectively. The minimum time needed to analyze all components in this solution, based on S/N=3 for the TAMRA peak, is thus 60-s. The lower S/N values for the three-component mixture, and, hence, the longer minimum data acquisition time, was due to the higher total fluorophore concentration compared to that of the pure solutions. This increased the average detected photocount rate, $\langle I \rangle$, and lowered S/N, due to the inverse relationship of S/N and $\langle I \rangle^2$ (Equation 3.11). By optimizing the analyte concentrations, it should be possible to achieve total analysis times on the order of tens of seconds or less in most cases.

3.4.4 Analyte Resolution:

The efficiency for multicomponent analysis of different species flowing in the same direction, but at different speeds, can be expressed by calculating the analyte resolution of the TAMRA and TAMRA-ssDNA peaks in the forward cross-

correlation function. Both peaks were fit to Gaussian functions, and the resolution, ρ, was determined from

$$\rho = \frac{2(\tau_{F,2} - \tau_{F,1})}{W_2 + W_1}, \tag{3.15}$$

where W_1 and W_2 are the baseline widths of the TAMRA-ssDNA and TAMRA peaks, respectively. These values were determined from the standard deviations, σ_i, of the Gaussian function using $W_i = 4\sigma_i$. From this we obtain $\rho = 0.96$. This is comparable to the resolution of two-component mixtures obtained using high-speed separations-based CE on the millisecond time scale[23, 24]. It should also be noted that the ability to resolve different components into separate cross-correlation channels effectively doubles the efficiency for multicomponent analysis in our experiment. This confirms that 2bFCCS-CFCE can be performed with comparable efficiency to high-speed separations-based CE, and thus should be considered a viable approach to electrophoretic analysis of molecular processes occurring on a millisecond to sub-millisecond time scale.

3.5 Conclusion:

In summary, it has been demonstrated that 2bFCCS-CFCE can be used to discriminate molecules as they flow continuously through an electrophoresis capillary, based on the magnitudes and directions of their electrophoretic flow velocity. The sensitivity to molecular processes occurring on a millisecond time

scale and the chemical selectivity of 2bFCCS-CFCE compared favorably to millisecond separations-based CE techniques[23, 24]. The 2bFCCS-CFCE technique has proved itself to be an elegant and efficient alternative to separations-based CE. Its ability to monitor ions migrating in opposite directions overcomes a limitation of conventional CE and allows for greater versatility in analysis of complex samples.

3.6 Acknowledgements:

I would like to thank Dr. Peter Goodwin from the Los Alamos National Laboratory for carrying out the time-correlated single photon counting measurements on our samples. This research was supported by the National Institutes of Health (Grant Number R21RR17025).

1. Fogarty, K.; Van Orden, A., Two-beam fluorescence cross-correlation spectroscopy for simultaneous analysis of positive and negative ions in continuous-flow capillary electrophoresis. *Analytical Chemistry* **2003,** 75, (23), 6634-6641.

2. Huang, X.; Coleman, W. F.; Zare, R. N., Analysis of factors causing peak broadening in capillary zone electrophoresis. *Journal of Chromatography* **1989,** 480, 95-110.

3. Xuan, X. C.; Xu, B.; Sinton, D.; Li, D. Q., Electroosmotic flow with Joule heating effects. *Lab On A Chip* **2004,** 4, (3), 230-236.

4. Roberts, G. O.; Rhodes, P. H.; Synder, R. S., Dispersion effects in capillary zone electrophoresis. *Journal of Chromatography* **1989,** 480, 35-67.

5. Mayer, B. X., How to increase precision in capillary electrophoresis. *Journal of Chromatography, A* **2001,** 907, (1-2), 21-37.

6. Landers, J. P., Ed., *Handbook of Capillary Electrophoresis.* 2nd ed.; CRC Press: Boca Raton, 1997; p 894.

7. Kuban, P.; Karlberg, B., Simultaneous Determination of Small Cations and Anions by Capillary Electrophoresis. *Analytical Chemistry* **1998,** 70, (2), 360-365.

8. Gao, Q.; Yeung, E. S., A matrix for DNA separation: genotyping and sequencing using poly(vinylpyrrolidone) solution in uncoated capillaries. *Analytical Chemistry* **1998,** 70, (7), 1382-1388.

9. Belder, D.; Deege, A.; Husmann, H.; Koehler, F.; Ludwig, M., Cross-linked poly(vinyl alcohol) as permanent hydrophilic column coating for capillary electrophoresis. *Electrophoresis* **2001,** 22, (17), 3813-3818.

10. Brinkmeier, M.; Rigler, R., Flow analysis by means of fluorescence correlation spectroscopy. *Exp. Techn. Phys.* **1995,** 41, (2), 205-210.

11. Rigler, R.; Widengren, J.; Mets, Ü., Interaction and Kinetics of Single Molecules as Observed by Fluorescence Correlation Spectroscopy. In *Fluorescence Spectroscopy*, ed.; Wolfbeis, O. S., Ed. Springer: Berlin, 1992.

12. Elson, E. L.; Magde, D., Fluorescence correlation spectroscopy. I. Conceptual basis and theory. *Biopolymers* **1974,** 13, (1), 1-27.

13. Hansen, R. L.; Zhu, X. R.; Harris, J. M., Fluorescence Correlation Spectroscopy with Patterned Photoexcitation for Measuring Solution Diffusion Coefficients of Robust Fluorophores. *Analytical Chemistry* **1998,** 70, (7), 1281-1287.

14. Widengren, J.; Mets, U.; Rigler, R., Fluorescence correlation spectroscopy of triplet states in solution: a theoretical and experimental study. *J. Phys. Chem.* **1996,** 99, (36), 13368-79.

15. Brinkmeier, M.; Doerre, K.; Stephan, J.; Eigen, M., Two-beam cross-correlation. A method to characterize transport phenomena in micrometer-sized structures. *Analytical Chemistry* **1999,** 71, (3), 609-616.

16. Doose, S.; Barsch, H.; Sauer, M., Polymer properties of polythymine as revealed by translational diffusion. *Biophysical Journal* **2007,** 93, (4), 1224-1234.

17. Stellwagen, E.; Lu, Y.; Stellwagen, N. C., Unified Description of Electrophoresis and Diffusion for DNA and Other Polyions. *Biochemistry* **2003,** 42, (40), 11745-11750.

18. Nkodo, A. E.; Garnier, J. M.; Tinland, B.; Ren, H.; Desruisseaux, C.; McCormick, L. C.; Drouin, G.; Slater, G. W., Diffusion coefficient of DNA molecules during free solution electrophoresis. *Electrophoresis* **2001,** 22, (12), 2424-2432.

19. Stellwagen, E.; Stellwagen, N. C., Determining the electrophoretic mobility and translational diffusion coefficients of DNA molecules in free solution. *Electrophoresis* **2002,** 23, (16), 2794-2803.

20. Rigler, R.; Mets, U.; Widengren, J.; Kask, P., Fluorescence Correlation Spectroscopy With High Count Rate And Low-Background - Analysis Of Translational Diffusion. *European Biophysics Journal With Biophysics Letters* **1993,** 22, (3), 169-175.

21. Egele, C.; Schaub, E.; Piemont, E.; de Rocquigny, H.; Mely, Y., Investigation by fluorescence correlation spectroscopy of the chaperoning interactions of HIV-1 nucleocapsid protein with the viral DNA initiation sequences. *Comptes Rendus Biologies* **2005,** 328, (12), 1041-1051.

22. Magde, D.; Wong, R.; Seybold, P. G., Fluorescence quantum yields and their relation to lifetimes of rhodamine 6G and fluorescein in nine solvents: Improved absolute standards for quantum yields. *Photochemistry And Photobiology* **2002,** 75, (4), 327-334.

23. Jacobson, S. C.; Culbertson, C. T.; Daler, J. E.; Ramsey, J. M., Microchip Structures for Submillisecond Electrophoresis. *Analytical Chemistry* **1998,** 70, (16), 3476-3480.

24. Gordon, M. J.; Okerberg, E.; Gostkowski, M. L.; Shear, J. B., Electrophoretic characterization of transient photochemical reaction products. *J. Am. Chem. Soc.* **2001,** 123, (43), 10780-10781.

Chapter 4: 2bFCCS-CFMCCE: Cross-Correlation Analysis Coupled with Continuous-Flow Microchip Capillary Electrophoresis

This chapter describes the development of two-beam fluorescence cross-correlation spectroscopy coupled with continuous-flow microchip capillary electrophoresis (2bFCCS-CFMCCE). This technique couples the advantage of a sensitive technique for continuous-flow CE with the added fluid handling and miniaturization design advantages offered by microfluidic platforms. The techique allows for simpler fluid handling and increased miniaturization compared with conventional microchip capillary electrophoresis (MCCE) techniques. The work that contributes to this chapter was performed over the period from July 2003 to January 2005.

4.1 Introduction:

The concept of MCCE was introduced in chapter 1. Briefly, microfabrication techniques developed in the semiconductor industry have been used to develop capillary electrophoresis microdevices in which CE experiments are conducted using microchannels fabricated in a microdevice rather than the fused silica capillaries used in conventional CE[1-20]. Commonly used substrates for MCCE include glass, polydimethylsiloxane (PDMS), and poly(methyl methacrylate) (PMMA). MCCE has two distinct advantages over conventional CE; 1) MCCE microchannels are formed in a block of insulating material, which allows for the use of much higher applied electric fields than those used for conventional capillary electrophoresis, and 2) the ability to precisely control the fabrication geometry of microchannels allows for more complex fluid handling than is possible with conventional CE[3-11]. The combination of these two advantages allows for the separation channels used in MCCE to be fabricated on much smaller scales, which, in turn, leads to faster analysis times[1]. The high aspect ratio of the microchannels used also allows for more efficient heat dissipation, and thus, higher voltages[16].

MCCE, like conventional CE, is a separations technique. In other words, in order for the analysis to be performed, macroscopic separation of the analytes must be realized. The requirement of macroscopic separation necessitates the use of multiple buffers (typically a run buffer and sample buffer) and fluid

handling capabilities that allow for a sample injection step prior to separation. The most common, and perhaps simplest, way to achieve these requirements in microchip format is through the style of microfluidic device known as the "T-chip" (refer to figure 1.5, chapter 1)[11, 16]. Sample injection is accomplished on T-chip devices through the careful manipulation of applied potentials at a microchannel intersection. Sample solution is caused to flow across an intersection by applying the appropriate potential between sample and sample waste wells. The applied voltage is then switched to the other channel of the intersection, the separations channel, which has been prefilled with a blank run buffer. This causes a plug of the sample buffer to be injected into the separations channel for macroscopic separation.

The primary advantage that MCCE has over conventional CE is in design flexibility[3]. Conventional CE is ultimately a more efficient, higher resolution technique than MCCE, but MCCE can be integrated into multi-step fluid handling devices for online analysis, and MCCE experiments can be performed on shorter timescales. Unfortunately, the very thing that makes MCCE such a powerful analytical technique, macroscopic separation, limits its versatility. The sample injection step requires multi-microchannel formats with complex buffer systems which can limit the ability of MCCE to be incorporated into multifunctional devices. The requirement for macroscopic separation of analytes, along with the multichannel format, also limits the miniaturization of MCCE devices[21]. An ideal MCCE device would be able to perform electrophoretic analysis without the separation and injection requirements that traditionally limit its flexibility.

A technique that is seems to be perfectly situated to overcome the design limitations of MCCE is two-beam fluorescence cross-correlation spectroscopy coupled with continuous-flow microchip capillary electrophoresis (2bFCCS-CFMCCE)[22-27]. As stated in previous chapters, 2bFCCS –CFCE techniques are able to perform sample analysis without the requirement of macroscopic separation. This eliminates the need for a sample injection step, and thus allows analysis to be performed using a single buffer, the sample-containing buffer. In addition, the minimum distance required for the analysis, the distance in-between the two focal regions, is on the scale of <10 microns, which is much shorter than that required for efficient MCCE separations. The ability to eliminate the complex multichannel geometry of MCCE and perform analysis over extremely short distances makes 2bFCCS-CFMCCE a much more design-versatile technique than conventional MCCE.

The goal of the work presented in this chapter was to successfully perform 2bFCCS-CFMCCE analysis on microchips that demonstrate the design advantages that the technique allows in relation to conventional MCCE. PDMS and glass microchips used for 2bFCCS-CFMCCE experiments were fabricated by myself and Vinod Anumareddy[28], respectively. These microchips exhibited design advantages over conventional MCCE microdevices in that they consisted of a single microfluidic channel, rather than the multichannel design typically required for sample injection and macroscopic separation in MCCE. In addition, the technique could be performed in channels much shorter in length than microchannels used in traditional MCCE devices. Analysis was performed using

channels with lengths as short as 1 mm. Though the technique showed much promise, my study of 2bFCCS-CFMCCE was ultimately limited by the fact that construction and use of microdevices for MCCE-based analysis is more expensive and time-consuming than performing identical analyses on conventional capillaries.

4.2 Fabrication of PDMS microchips:

The procedure used to fabricate the PDMS microchips used in the 2bFCCS-CFMCCE experiments was adopted from a procedure developed by Henry and coworkers[29-32]. Jon Vickers aided me in PDMS microchip fabrication, especially in the fabrication of PDMS mold masters and masks. A schematic outlining the fabrication of PDMS microchips can be seen in figure 4.1.

4.2.1 Fabrication of Masks:

The masks used in fabrication of the molds were constructed of high-resolution transparancies. Negative drawings of the channel patterns were composed to scale in Adobe Illustrator 9.0. High-resolution transparancies were then printed using a high-resolution printer located in the Colorado State University Academic Computing and Networking Services Weber building lab.

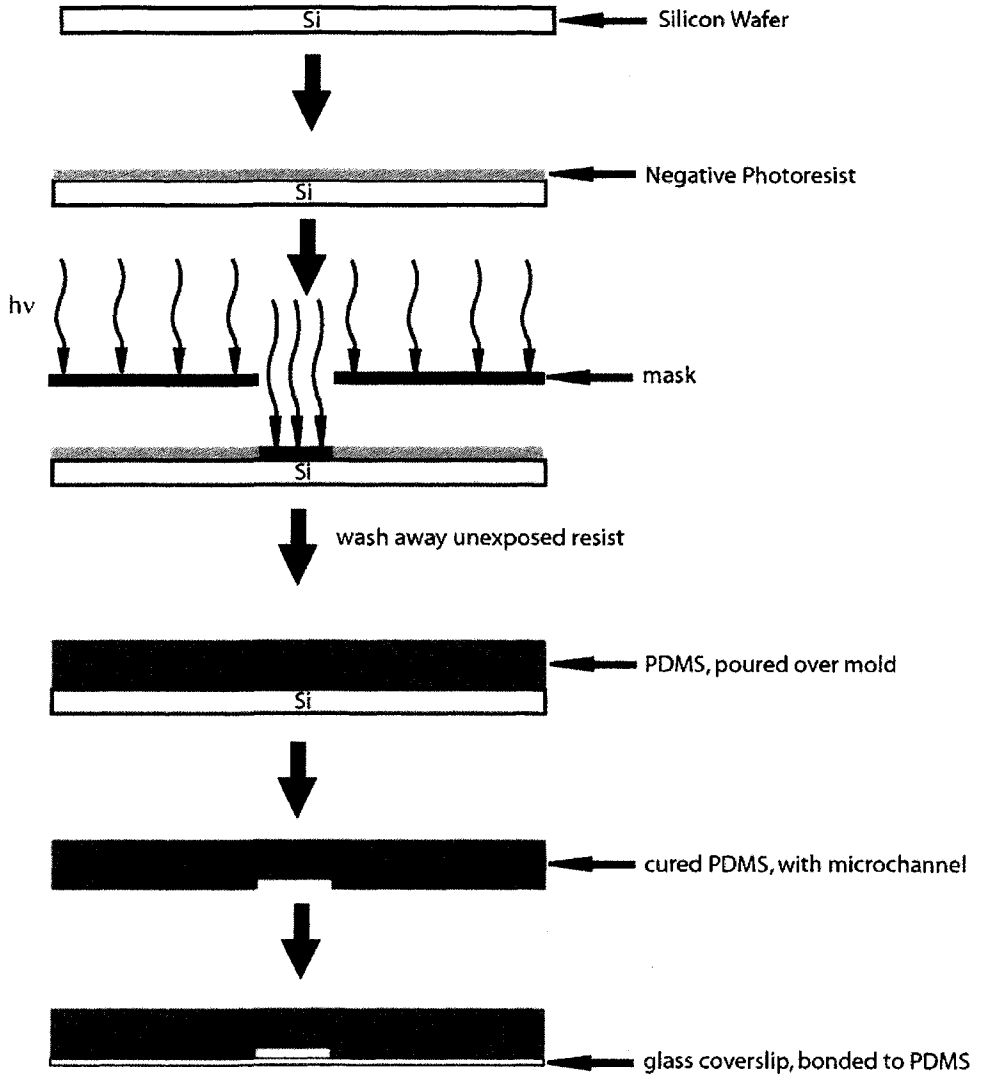

Figure 4.1: Schematic of PDMS microchip fabrication. A silicon wafer is cleaned and then coated with a negative photoresist. The wafer is then exposed to light filtered by a high-resolution mask. The unexposed photoresist is washed away, and PDMS is poured over the resulting mold. The PDMS is then cured by baking, and subsequently bonded to a glass microscope coverslip, at which point the microchip is ready for use.

Masks were used for patterning channel widths from approximately 25 μm to 75 μm, with 50 μm being the channel width used to collect the data presented here.

4.2.2 Fabrication of PDMS Mold Masters:

A 3-inch silicon wafer (Silicon Valley Microelectronics, Inc.) is first cleaned and oxidized with piranha solution (2:1 H_2SO_4:H_2O_2) for approximately 5 min followed by a thorough rinse with ultrapure 18 MΩ water. The wafer is then placed in an oven at 65°C to dry for approximately 15 min. The dry wafer is then coated with SU-8 2035 negative photoresist (MicroChem Co.) using a spin coater with ~1 mL of photoresist/inch of wafer coated. A spread cycle of 500 rpm for 10-s, followed by 2500 rpm for 30 s was used. The photoresist-coated wafer is then soft baked by placing it on a 65°C hot plate for 3 min followed by a 95°C hot plate for 5 min. The soft-baked photoresist-coated wafer is then exposed through a mask to a near-UV light source for 7 s. The exposed wafer is then baked again at 65°C for 2 min, followed by 95°C for 6 min. The unexposed photoresist is removed by immersing the wafer in propylene glycol methyl ether acetate for approximately 30 min followed by baking/drying on a hot plate at 65°C for another 30 min. This process forms a positive-relief pattern approximately 20 μm in height on the surface of the wafer. Once dry, the wafer is washed with acetone, methanol, and ultrapure water and dried under an N_2 stream. The exposed silicon surface of the mold is then made hydrophobic by reaction with

hexadimethyldisilazane at 65°C for approximately 6 hours. This prevents the PDMS from adhering irreversibly to the mold during PDMS microchip fabrication.

4.2.3 PDMS Microchip Fabrication:

A degassed mixture of Sylgard 184 elastomer and curing agent (10:1) (Dow Corning, Midland, MI) was poured over the mold master to a depth of ~0.5-cm and allowed to cure for ~2-3 hours at 65°C. Once the PDMS has cured, it can simply be peeled away from the mold master, with channel(s) shaped by the positive relief pattern on the mold master. Reservoirs are punched at the ends of the channels using a 6 mm hole-punch. The surface of the PDMS is cleaned using methanol and then dried in an oven at 65°C. The PDMS is then placed in an air plasma cleaner (Harrick Plasma Cleaner/Sterilizer PDS-32G) and is oxidized at high power for 30 s. The PDMS is then brought into conformal contact with a piranha-cleaned glass microscope cover slip (~170 μm thick) to form an irreversible seal which is strong enough such that the PDMS and glass cannot be pulled apart without destroying the microchip. A picture of a PDMS microchip fabricated in the above manner can be seen in figure 4.2.

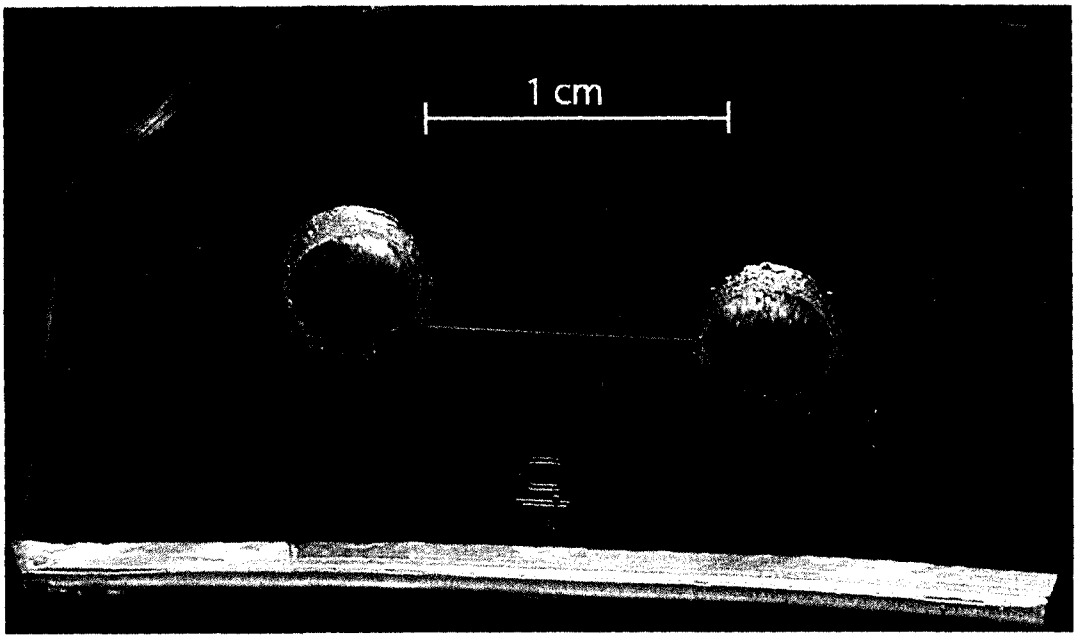

Figure 4.2: A single channel electrophoresis PDMS microchip with an electrophoresis channel 1-cm in length, 40-μm in width, and 20-μm deep. This microchip was fabricated at Colorado State University. The chip is operated in continuous flow mode by applying an electrical potential across the two sample wells. Platinum electrodes are immersed into the wells and connected to a high voltage power supply.

4.3 Fabrication of Glass Microchips:

All glass microchips were fabricated by Vinod Anumareddy[28] according to a procedure adopted from the literature[33-35]. A schematic outlining the fabrication of glass microchips can be seen in figures 4.3 and 4.4.

4.3.1 Fabrication of Masks:

Masks were fabricated by Vinod Anumareddy using the same procedure outlined in section 4.2.1.

4.3.2 Etching Microchannels in Glass Substrates:

All of the procedure information presented here was developed and implemented by Vinod Anumareddy[28].

4.3.2.1 Selection of Glass Substrate Used:

The glass selected for the study was Pyrex 7740 (Chemglass Inc, Vineland, NJ). This glass was selected for two reasons; it exhibits favorable etching properties, and it is the same type of glass as the microscope cover slips (Fisher Scientific, Pittsburgh, PA) to which it was thermally bonded. If the thermally bound glasses are of two different types, the bonds are relatively unstable and susceptible to fracture.

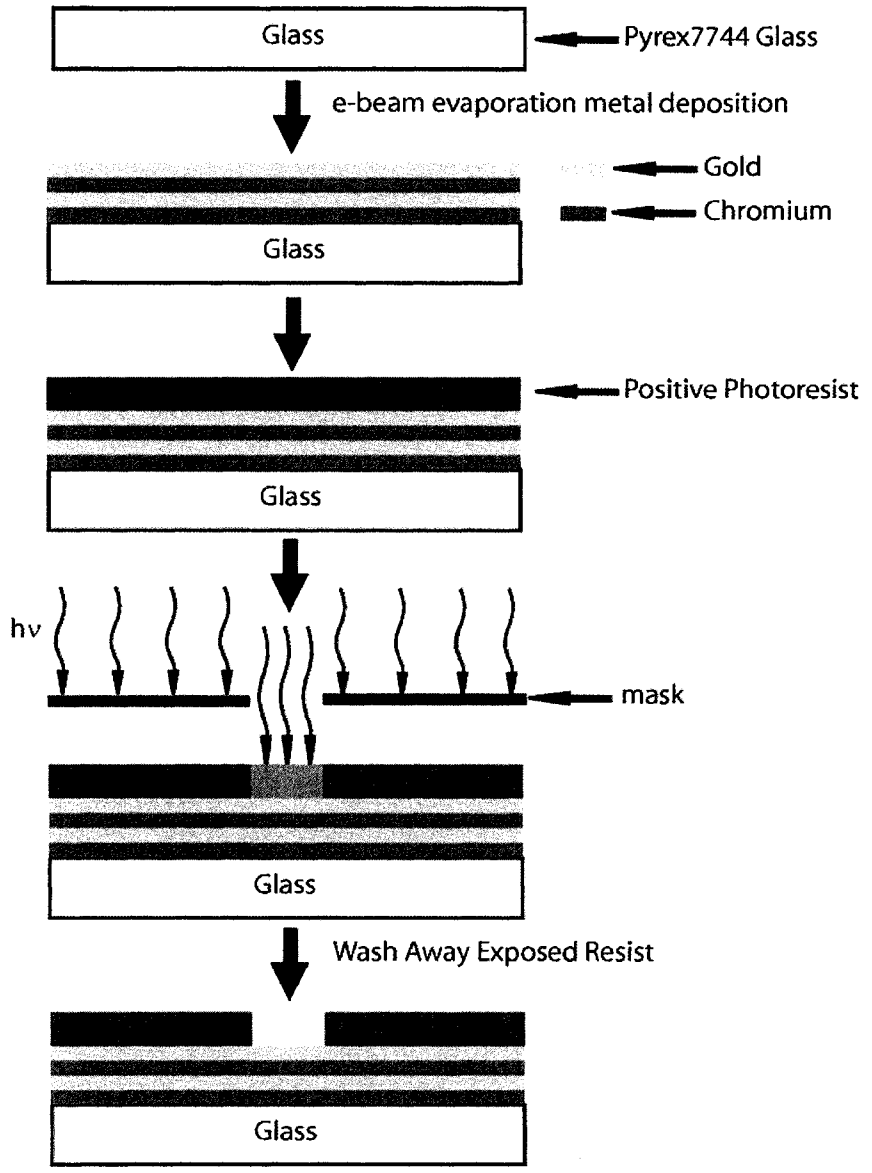

Figure 4.3: Schematic of the initial process of glass microchip fabrication. Piranha-cleaned glass is coated with alternating gold and chromium metal layers deposited through e-beam evaporation. A positive photoresist is then spin-cast on top of the metal layers. The photoresist/metal coated glass is then exposed to UV light through a mask. The exposed resist is then removed, exposing the metal layers underneath in the pattern defined by the mask.

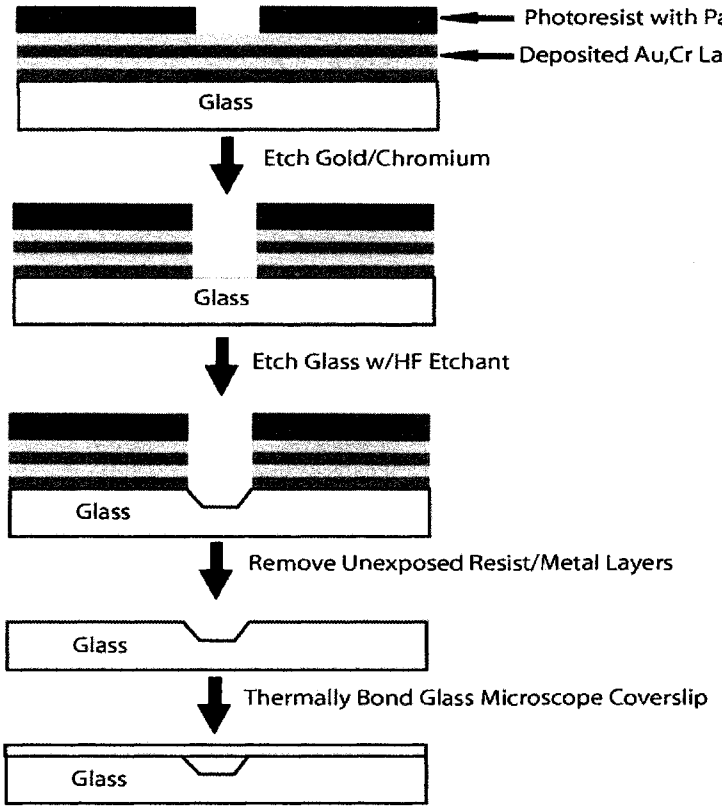

Figure 4.4: Schematic of the second half of the process of glass microchip fabrication. The top image depicts the photoresist/metal coated glass with exposed regions of the resist having been washed away, exposing the metal underneath regions where the resist was exposed to UV light. The exposed metal is then etched away, exposing the glass surface in the desired patterned locations. The glass is then etched with an HF solution. The remaining unexposed photoresist and metal layers are then removed to yield the etched glass substrate. The glass substrate is then thermally bonded to a glass microscope cover slip to yield microchannels in the desired configuration.

4.3.2.2 Deposition of Metal Layers:

Due to the extremely reactive nature of the HF solution used to etch channels in the glass substrate, it was necessary to deposit protective metal layers in addition to the photoresist used in order to prevent the etchant solution undercutting the photoresist layer, which would cause non-specific etching of the glass substrate. Gold and Chromium (Electronic Space Products International) were deposited in alternating layers for a total of 4 layers (2 each of Au and Cr) using electron-beam evaporation. The metal-coated glass substrate was then baked at 110°C for 1 hour to remove stresses from the metal layers.

4.3.2.3 Photolithography:

After the protective metal layers have been applied to the glass substrate, the photoresist used to create patterns can be applied. The photoresist used was Shipley 1818 (Shipley Corporation, Marlborough, MA), a positive photoresist. The photoresist was applied by spin casting at 4000 rpm for 30 s. The photoresist coated substrate was then baked at 90°C for 2 min. The photoresist coated substrate is then exposed through a mask to a near-UV light source for 11 s. Development of the photoresist coated substrate in 4:1 AZ 400K developer(Clariant Corporation, Somerville, NJ):ultrapure water results in dissolution of the photoresist regions exposed to the UV light, exposing the metal underneath. The developed substrate is then baked at 110°C for 5 min prior to metal etching. The exposed gold metal layers were etched using a solution of 4:1:40 $KI:I_2:H_2O$. The exposed chromium layers were etched using chrome etchant (Alfa Aesar, Ward Hill, MA). The etchant steps resulted in exposed glass

confined to the areas in which the microchannels are to be formed, with photoresist and metal layers still coating the regions of the glass substrate which were to be kept as-is.

4.3.2.4 Wet Chemical Etching and Removal of Remaining Photoresist and Metal:

Microchannels and other features were etched into the exposed glass using a solution of 48% HF. The HF etched the glass at a rate of ~10 μm/min. After HF etching, the glass substrate was washed with ultrapure water, then with acetone, which removed the remaining photoresist. After the photoresist is removed the remaining gold and chromium layers were removed using the etchants described in the previous section. The patterned glass substrate was then cleaned in piranha solution to remove remaining contamination prior to thermal bonding.

4.3.3 Reservoir Formation and Thermal Bonding:

Reservoirs were formed at the ends of the microchannels by drilling with a diamond-tipped drill bit. After drilling, the patterned glass substrate and a microscope coverslip (~170 μm thick) were piranha cleaned for 12 hours to ensure removal of all contaminants. The patterned glass substrate and glass coverslip were then arranged in the preferred configuration, placed between two quartz blocks, weighted with a 1 kg steel block, and bonded for 4 hours at 656°C. Figure 4.5 shows a picture of a 44 channel-array glass microchip fabricated by

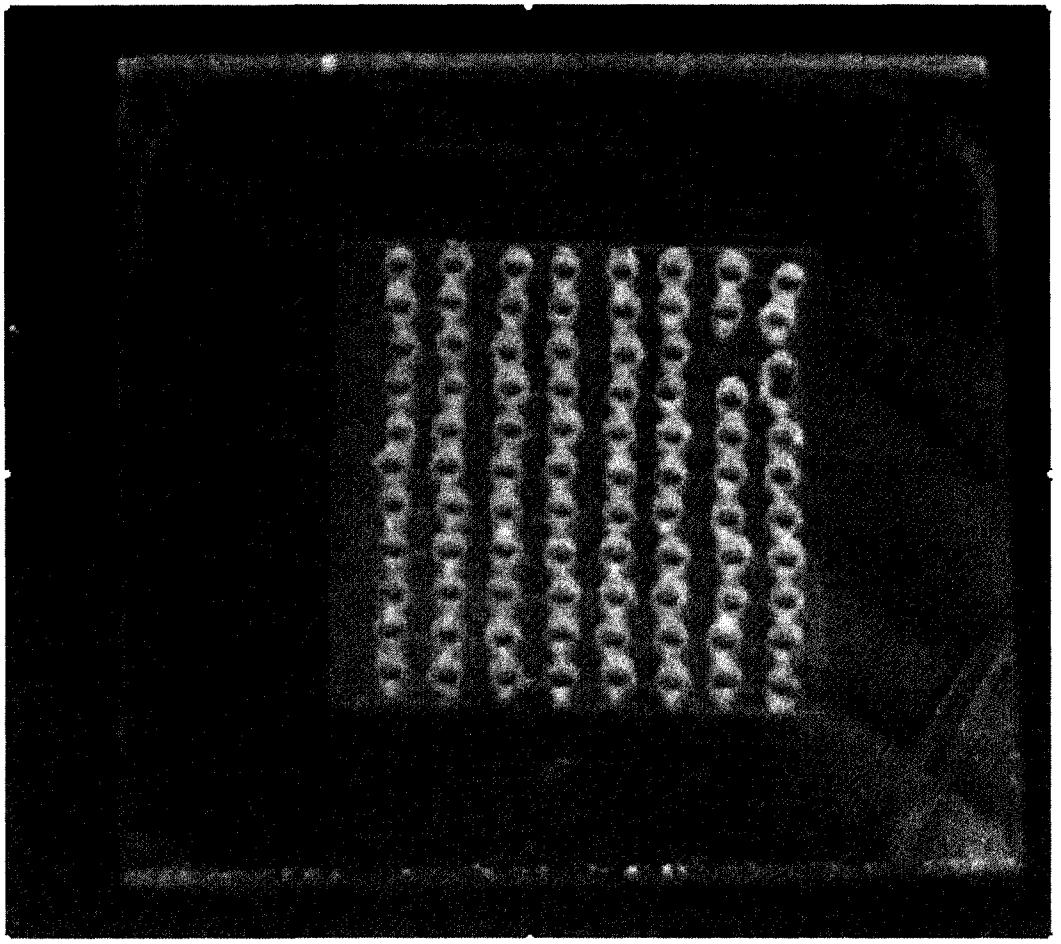

Figure 4.5: A glass microchip containing an array of 40 electrophoresis channels on a 1×1-in^2 glass slide. A glass coverslip is thermally bonded to the channel array. The drilled holes are fluid and electrode access ports. Each pair of access holes is connected by a different electrophoresis channel. The channel dimensions are 50-μm width, 15-μm depth, and 1-mm length.

Vinod Anumareddy using the above procedure. The channels are 1 mm in length by 50 μm in width by 15 μm in depth.

4.4 Experiments Conducted on PDMS Microchips:

4.4.1 Sample Preparation:

Nanomolar solutions of Rhodamine 6G (R6G, Eastman Kodak, Rochester, NY), TAMRA (Molecular Probes, Eugene, OR), and 39-oligo poly(dT) single stranded DNA, labeled at the 5' end with TAMRA (TAMRA-ssDNA, Qiagen, Alameda, CA), were prepared in tris-Glycine buffer at pH 8.3 (0.025-M Tris-HCl, 0.192-M Glycine, Sigma, St. Louis, MO). In the experiments, one of two different coatings was used to suppress wall interactions and control EOF. A dynamic coating added to the sample buffer solutions was 0.055-wt% poly(vinylpyrrolidone) (PVP, $M_W \approx 10^6$ g/mol, Sigma), which suppresses EOF and prevents adsorption to the capillary walls.[36] PVP does not alter the viscosity of the solution at this concentration and was assumed to have no effect on the motion of the analytes. The other coating, which was applied through pretreatment of the microchip, was a 5% solution of hexadimethrine bromide (polybrene)(Sigma, St. Louis, MO). Polybrene is a positively charged surfactant that adsorbs to the walls of the channel, and in so doing, reverses the EOF by

reversing the charge state of the surface. Polybrene also suppresses wall interactions of the analytes[37].

4.4.2 Instrumentation:

The 2bFCCS-CFMCCE apparatus used was similar to that described in chapter 2. Briefly, a 514.5-nm laser beam from an air-cooled, continuous wave Ar^+ laser (Midwest Laser Products, Frankfort, IL) was split and then recombined into two nearly parallel beams by two 50/50 beamsplitters (Newport, Irvine, CA). The two beams were adjusted in power to 4.1 mW using the appropriate absorptive neutral density filters (Newport). The two laser beams were then directed into the back of a Nikon TE2000 U inverted optical microscope (Nikon, Inc., Melville, NY), reflected by a 514 dichroic beamsplitter, and focused by a 100X, 1.3NA Nikan Plan Fluor objective (Nikon, Inc., Melville, NY) into the PDMS (or glass) microchips mounted on a scanning stage with ~100 nm resolution (Applied Scientific Instrumentation MS-2000 XYZ-stage, Applied Scientific Instrumentation, Eugene, OR). The two laser beams formed nearly identical diffraction limited focal regions, separated along the axial dimension of the capillary by a distance of ~3-μm and positioned ~ 6 μm below the inner glass surface of the capillary. A ~200-500 V/cm electric field was applied to the microchip by means of platinum electrodes connected to a high voltage power supply (custom built by Colorado State University Chemistry Department's electronics technician). Fluorescence from each focal region, was collected by

the same objective, split by a 50/50 cubic beamsplitter (Thorlabs, Newton, NJ), spatially filtered by 50 μm pinholes (Thorlabs, Newton, NJ), and filtered by 535-nm long pass interference filters (Omega Optical, Brattleboro, VT). The spatially and spectrally filtered light was then focused onto two single photon counting avalanche photodiode detectors (PerkinElmer Optoelectronics, model SPCM-AQR-14, Wellesley, MA) using aspheric lenses (Newport, Irvine, CA). The photocounts from the two detectors were cross-correlated using an ALV-6010/160 digital correlator card (ALV, Langen, Germany) mounted in a Pentium computer.

4.4.3 Results and Discussion:

4.4.3.1 PDMS T-Chip

Initial 2bFCCS-CFMCCE experiments were performed on a PDMS "T-chip" microchip like that in figure 4.6 in order to demonstrate the feasibility of performing 2bFCCS analysis on PDMS microchips. The masks and mold masters had been previously fabricated by Jon Vickers of the Henry lab in the Colorado State University Chemistry Department. I constructed the PDMS microchip in figure 4.6 using the mold master.

Figure 4.7 shows the forward and reverse cross-correlation functions and their respective theoretical fits for a three component mixture containing 1.5-nM R6G, 4-nM TAMRA, and 1-nM TAMRA-ssDNA flowing through the microchip under the influence of an applied electric field of 429 V/cm. This data was

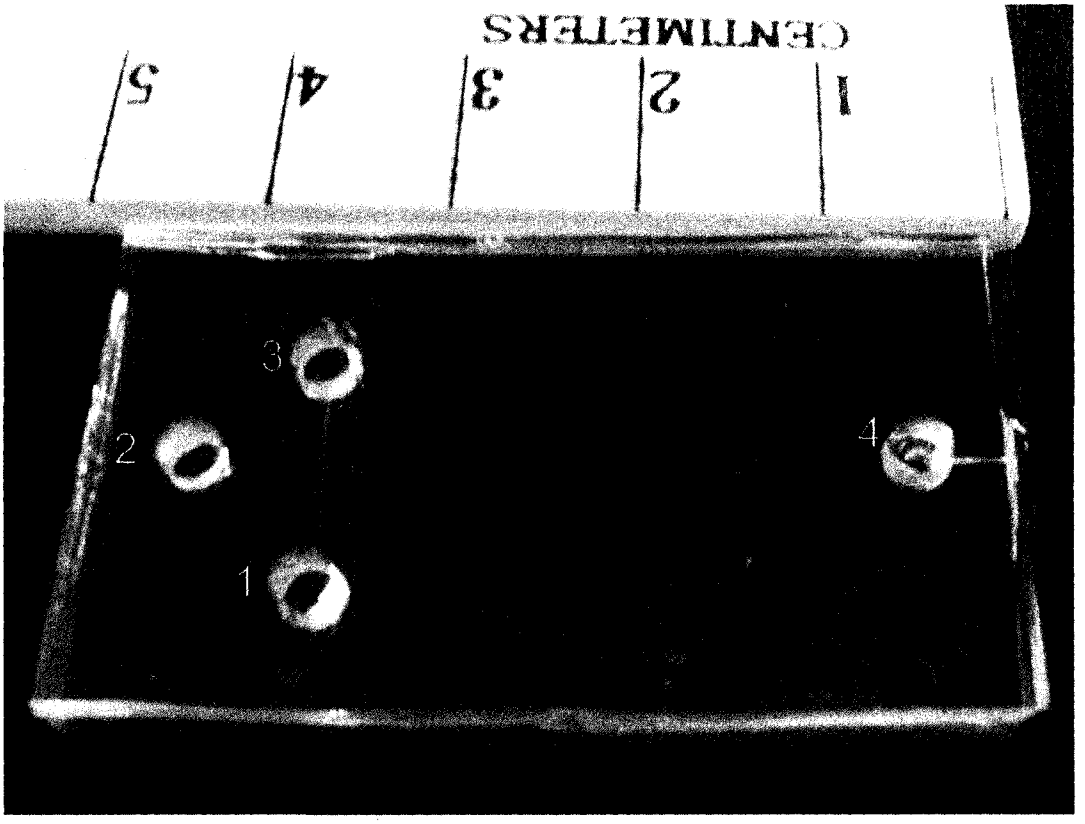

Figure 4.6: A crossed-T electrophoresis microchip with a centimeter ruler for scale. This chip was fabricated at Colorado State University. The main electrophoresis channel is 3.5 cm in length, 50 μm in width, and 20 μm deep. Fluid flow is induced by means of platinum electrodes immersed in the sample wells and connected to a switching high-voltage power supply. The chip can be operated in both separations mode and continuous flow mode. When operated in continuous flow mode, the analyte solution fills all sample wells and both channels. Sample wells 1, 2, and 3 are held at the same potential, and well 4 is connected to ground. This causes the fluid to sample to flow continuously through the main electrophoresis channel.

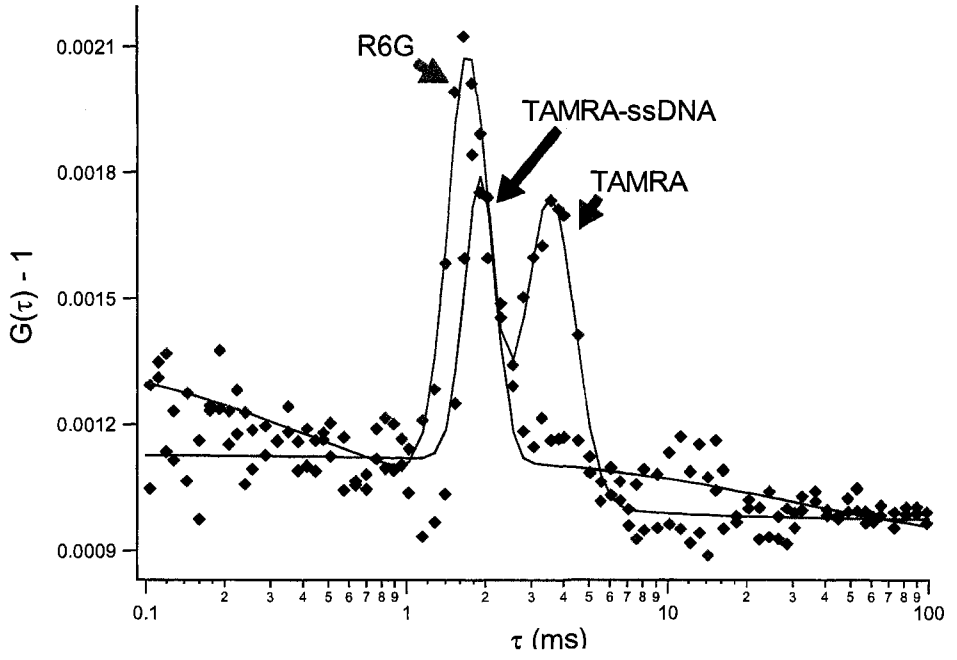

Figure 4.7: Experimental data (diamonds) obtained from a mixture of TAMRA, R6G, and TAMRA-ssDNA that has been fit (solid lines) using the appropriate theoretical models. A solution of 4 nm TAMRA, 1.5 nm R6G, and 1 nm TAMRA-ssDNA in a pH 8.3 Tris-Glycine buffer with 0.055-wt% PVP was analyzed by applying an electric field of 429 V/cm across the channel between wells 2 and 4 on the microchip in figure 4.6. The individual cross-correlation peaks were identified using control experiments conducted at the same conditions.

Table 4.1: PDMS T-Chip Data[a]

Parameter			
	R6G control experiments[b]		
ω_o (μm)	0.2706(12)		
R (μm)	3.158(95)		
τ_{dR6G} (ms)	0.0610(52)		
	Cross-Correlation Analysis of 3-Component Mixture[c]		
	R6G	TAMRA	TAMRA-ssDNA
V_x (mm/s)	-1.823(14)	-0.883(11)	1.641(23)
τ_F (ms)	1.733(54)	3.58(12)	1.924(64)
τ_d (ms)	0.212(22)	0.306(42)	0.44(11)
D (μm^2/ms)	0.0863(90)	0.0598(82)	0.041(10)
A	0.001036(33)	0.000725(30)	0.000675(52)
	Relative Concentrations[d]		
	R6G	TAMRA	TAMRA-ssDNA
$N_{i,corr}$ (%)	19.1(25)	65.9(50)	15.0(18)
$N_{i,exp}$ (%)	23.5(22)	57.7(40)	18.7(23)

[a]Numbers in parenthesis are the uncertainties in the last digits reported to one standard deviation. [b]$\tau_{d,R6G}$ was obtained from the fitting of autocorrelation data, ω_o was obtained from $\tau_{d,R6G}$ through the relation, $\tau_{d,R6G} = \omega_o^2 / 4D_{R6G}$, using the value of $D_{R6G} = 3.0 \times 10^{-6} \text{cm}^2/\text{s}$, and R was determined from fitting R6G cross-correlation data. [c]R and ω_o were held constant at 3.158(95) μm and 0.2706(12) μm, respectively in the analysis of the cross-correlation data presented in figure 4.7. [d]$N_{i,corr}$ is the relative concentration as determined from cross-correlation analysis. $N_{i,exp}$ is the expected relative concentration as determined from dilution of known stock solutions.

obtained using PVP as the coating used to suppress wall interactions and EOF. The parameters obtained from the theoretical fits can be seen in Table 4.1. The theory used to determine the theoretical fits has already been discussed in chapters 2 and 3. Control experiments to determine the parameters ω_0 and R using a R6G standard solution were conducted using the same procedure as presented in chapter 3. Note that on the PDMS microchip EOF must be nonzero, because the TAMRA, a negative ion in the buffer conditions used, now appears in the same cross-correlation channel as the R6G, a positive ion. The TAMRA and R6G cross-correlation peaks in the reverse channel (red peaks in figure 4.7) were fit according to the equation:

$$G_R(\tau) = B_R + A_{PA}\left(\frac{1}{1+\tau/\tau_{PA}}\right) + A_1 \exp\left[\frac{-(R+V_{x,1}\tau)^2}{\omega_o^2(1+\tau/\tau_{d,1})}\right] + A_2 \exp\left[\frac{-(R+V_{x,2}\tau)^2}{\omega_o^2(1+\tau/\tau_{d,2})}\right] \quad (4.1)$$

subscripts 1 and 2 denote the parameters corresponding to R6G and TAMRA, respectively. The parameters ω_0 and R were held constant to the values presented in table 4.1 when fitting the data using equation 4.1.

The TAMRA-ssDNA appears in the forward channel of the cross-correlation experiment (black peaks in figure 4.7), indicating its migration velocity is enough to overcome the EOF. The TAMRA-ssDNA cross-correlation peak was fit according to the equation:

$$G_F(\tau) = B_F + A_{PA}\left(\frac{1}{1+\tau/\tau_{PA}}\right) + A_{DNA} \exp\left[\frac{-(R-V_{x,DNA}\tau)^2}{\omega_o^2(1+\tau/\tau_{d,DNA})}\right] \quad (4.2)$$

The parameters ω_0 and R were held constant to the values presented in table 4.1 when fitting the data using equation 4.1.

The relative concentrations of the respective species (table 4.1) were found using the methodology described in chapter 3 and the equation:

$$N_{i,corr}(\%) = \frac{A_i \tau_{f,i} / (\kappa_i \phi_{f,i})}{\sum_j A_j \tau_{f,j} / (\kappa_j \phi_{f,j})} \tag{4.3}$$

The fluorescent lifetime $(\tau_{f,i})$, fluorescence detection/collection efficiency (κ_i), and fluorescence quantum yield $(\phi_{f,i})$ of each species, *i*, were assumed to be identical to the values presented in table 3.2 in chapter 3, due to the similarity of the optical components and experimental conditions used. Note that the relative concentrations of the three analytes are determined with ~10-% precision, and that they agree with the expected values within experimental error. The errors in the expected concentrations were estimated from the precision of the pipettes used to prepare the solutions and the errors in the standard solution concentrations.

Inspection of figure 4.7 and of the values presented in table 4.1 brings to light two somewhat disconcerting features. In figure 4.7, the pseudo-autocorrelations (refer to section 3.4.1, chapter 3 for a discussion of pseudo-autocorrelation) and baselines of the forward and reverse cross-correlation data appear to be particularly noisy when compared to those presented in figure 3.3 (chapter 3). In addition, the diffusion constants of all three species, in similar buffer conditions, are approximately 3 times smaller than those presented in table 3.2, chapter 3. Both of these experimental anomalies point to a possible source of experimental error with the analysis performed in the PDMS T-chip. The anomalies are consistent with what might be expected if there are strong

wall interactions between the analyte species and the PDMS microchannel walls. It should be noted that the data in chapter 3 was obtained in a glass capillary coated with a permanent PVA polymer coating. The chemistry, surface roughness, and porosity of PDMS is significantly different from that of PVA-coated glass. If the analyte species' wall interactions are significant, one would expect two things to happen that would cause the experimental anomalies discussed above; analyte species would have slower effective diffusion times, and the background noise in the experiment would be elevated, making correlation analysis more difficult. Numerous experiments in PDMS microchannels of multiple microchips seemed to confirm this hypothesis. Background fluorescence was found to be a significant problem. PDMS microchips used for only 1 or 2 experiments exhibited high rates of background fluorescence even after extended washing with detergents and blank buffer solutions. In addition, the migration velocites of the different analyte species varied significantly from run to run. This was most likely due to variable and unpredectible EOF. Because it was necessary for optical reasons to use glass coverslips to focus the laser light through, the microchannel was formed from heterogenuous materials (PDMS and glass), which can contribute to nonuniform, sporadic EOF. It was nearly impossible to obtain reproducible cross-correlation data. For this reason, different buffer and coating conditions were used in later experiments to try to address the difference in using PDMS as the microchannel material in place of glass.

4.4.3.2 PDMS Single-Channel Chip:

Further 2bFCCS-CFMCCE experiments on PDMS microchips were performed on a chip like that seen in figure 4.2. This demonstrated the capability of 2bFCCS-CFMCCE to perform analysis on PDMS microchips that have a design format incompatible with conventional MCCE analysis. The single-channel design and relatively short (1-cm) microchannel are two features that show the design advantage offered by 2bFCCS-CFMCCE. Jon Vickers fabricated the mask used to fabricate the single-channel chip, while I fabricated the mold master and PDMS microchip.

Figure 4.8 shows the forward and reverse cross-correlation functions and their respective theoretical fits for a two component mixture containing 1-nM R6G and 1.5-nM TAMRA flowing through the microchip under the influence of an applied electric field of 285 V/cm. This data was obtained using polybrene as the coating used to suppress wall interactions. Note that use of the polybrene reverses the electroosmotic flow. The parameters obtained from the theoretical fits can be seen in Table 4.2. The theory used to determine the theoretical fits has already been discussed in chapters 2 and 3. Control experiments to determine the parameters ω_0 and R using a R6G standard solution were conducted using the same procedure as presented in chapter 3. The TAMRA and R6G cross-correlation peaks in the reverse channel (red peaks in figure 4.8) were fit according to equation 4.1. The subscripts 1 and 2 in equation 4.1 denote the parameters corresponding to TAMRA and R6G, respectively (the opposite denotation used for equation 4.1 with the T-chip data). The parameters ω_0 and R

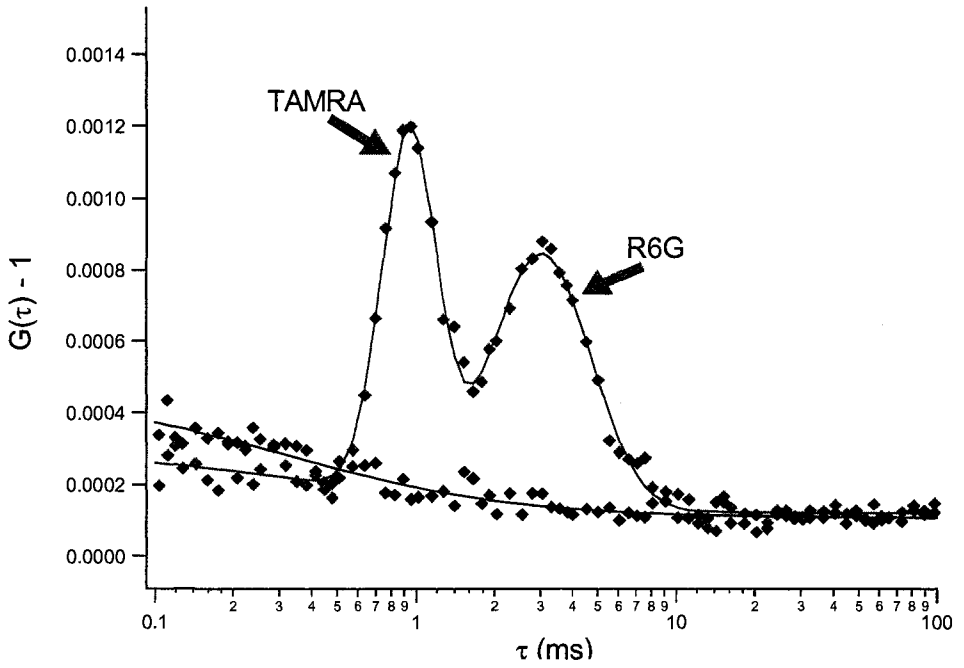

Figure 4.8: Experimental data (diamonds) obtained from a mixture of TAMRA and R6G that has been fit (solid lines) using the appropriate theoretical models. The electrophoresis channel of the microchip in figure 4.2 was pretreated with the cationic polymer Polybrene (PB) to reduce interaction of analytes with PDMS. Note that treatment with PB results in a reversal in the direction of electroosmotic flow. A solution of 1.6 nm TAMRA and 1 nm R6G in a pH 8.3 Tris-Glycine buffer was then analyzed by applying an electric field of 285 V/cm across the microchip. The individual cross-correlation peaks were identified using control experiments conducted at the same conditions.

Table 4.2: PDMS Single Channel Chip Data[a]

Parameter		
	R6G control experiments[b]	
ω_o (μm)	0.329(55)	
R (μm)	3.30(11)	
τ_{dR6G} (ms)	0.090(30)	
	Cross-Correlation Analysis of 2-Component Mixture[c]	
	R6G	TAMRA
V_x (mm/s)	-1.079(32)	-3.583(48)
τ_F (ms)	3.06(14)	0.921(33)
τ_d (ms)	0.072(12)	0.0819(94)
D (μm^2/ms)	0.377(89)	0.331(67)
A	0.000590(32)	0.001087(39)
	Relative Concentrations[d]	
	R6G	TAMRA
$N_{i,corr}$ (%)	35.1(46)	64.9(50)
$N_{i,exp}$ (%)	39.2(37)	60.8(42)

[a]Numbers in parenthesis are the uncertainties in the last digits reported to one standard deviation. [b]$\tau_{d,R6G}$ was obtained from the fitting of autocorrelation data, ω_o was obtained from $\tau_{d,R6G}$ through the relation, $\tau_{d,R6G} = \omega_o^2 / 4D_{R6G}$, using the value of $D_{R6G} = 3.0 \times 10^{-6} \text{cm}^2/\text{s}$, and R was determined from fitting R6G cross-correlation data. [c]R and ω_o were held constant at 3.30(11) μm and 0.329(55) μm, respectively in the analysis of the cross-correlation data presented in figure 4.8. [d]$N_{i,corr}$ is the relative concentration as determined from cross-correlation analysis. $N_{i,exp}$ is the expected relative concentration as determined from dilution of known stock solutions.

were held constant to the values presented in table 4.2 when fitting the data using equation 4.1.

The forward channel of the cross-correlation experiment (black data in figure 4.8) is essentially blank cross-correlation data. Pseudo-autocorrelation contributed to the signal in the forward channel and was fit according to the equation:

$$G_F(\tau) = B_F + A_{PA}\left(\frac{1}{1+\tau/\tau_{PA}}\right) \tag{4.4}$$

The data obtained from fitting the forward cross-correlation channel data to equation 4.4 has no physical meaning, and so none of the information obtained from the fit is presented here

The relative concentrations of the respective species were found using the same procedure discussed earlier, with the use of equation 4.3. The data is presented in table 4.2. Note that the relative concentrations of the three analytes are determined with ~10-% precision, and that they agree with the expected values within experimental error. The errors in the expected concentrations were estimated from the precision of the pipettes used to prepare the solutions and the errors in the standard solution concentrations.

Comparison of figures 4.7 and 4.8 as well as the information in tables 4.1 and 4.2 reveal some interesting insights into the performance of the polybrene coating in relation to the PVP dynamic coating used for the T-chip data. Inspection of the diffusion constants found for TAMRA and R6G reveals values similar to those found in chapter 3 (Table 3.2), which, as discussed in chapter 3, agreed well with literature values. In addition, the baselines appear to be much

better defined in figure 4.8 versus figure 4.7. This indicates that the polybrene was better than the PVP at suppressing analyte wall interactions in PDMS. Unfortunately, despite these promising results, it was found that it was still difficult to achieve reproducible results in PDMS microchips, even with the polybrene coating. Chips could only be used for a few experiments before background fluorescence and sporadic EOF became a problem. This problem necessitated the frequent fabrication of new chips, which was both time-consuming and expensive. For this reason, my focus switched to glass microchips. The success and reproducibility of experiments conducted on fused-silica capillaries indicated that perhaps glass was a better suited wall material for 2bFCCS-CFMCCE than PDMS. In the next section, data obtained on glass microchips will be described.

4.5 Experiments Conducted on Glass Microchip:

While 2bFCCS-CFMCCE showed promise on PDMS microchips, the difficulty in obtaining reproducible results led to the decision to investigate 2bFCCS-CFMCCE on glass microchips. Reproducible 2bFCCS-CFCE experiments were obtained in fused silica capillaries coated with PVA, and it was thought that if glass microchips could be fabricated and subsequently coated with PVA, the similarity between fused-silica capillaries' and glass microchips' wall chemistry could possibly indicate that glass microchips would be a platform more

suited for 2bFCCS-CFMCCE than PDMS microchips. Unfortunately, the fabrication of glass microchips is somewhat more involved than the fabrication of PDMS microchips. For this reason, Vinod Anumareddy, an electrical and computer engineering masters student at Colorado State University, made it his goal to perfect the glass microchip fabrication process for our group, and supply me with glass microchips for the purpose of performing 2bFCCS-CFMCCE analysis.

4.5.1 Coating Procedure:

The PVA coating procedure described in detail in chapter 2 could not be used to coat the glass microchips used in the 2bFCCS-CFMCCE experiments. The reason for this is that we did not have the appropriate equipment for injecting the PVA solutions into the microchannels at the required pressures. For this reason, a modified PVA coating procedure was developed which did not require high pressure. A solution of 0.25% PVA, 5% glutaraldehyde, and 1M HCl was made and immediately drawn into the microchip channel through the use of a syringe. The chip was then completely submersed in the reacting polymer solution and allowed to incubate for ~15 min. During this time, the polymerization reaction could be monitored by observation of the appearance of white PVA precipitate in the reaction solution. After the incubation period was complete, the chip was removed from the solution and washed with blank tris-glycine buffer and was ready for use. Two assumptions were made in the development of this

coating procedure for microchips; the polymerization reaction proceeded slowly enough such that the bulk of the polymerization occurred after introduction into the microchannel, and that the polymer produced in the polymerization reaction would preferentially deposit on the walls of the microchannel in a relatively uniform manner. Microchips coated in this manner proved to yield more reproducible results and to suffer from less fluorescence background problems than uncoated glass chips, so it was apparent that the coating procedure was at least somewhat successful.

4.5.2 Sample Preparation and Instrumentation:

40-oligo poly(dT) single-stranded DNA (polythymine) labeled at the 5' end with Rhodamine 6G (R6G-ssDNA, Operon Biotechnologies, Huntsville, AL) was prepared in tris-EDTA buffer at pH 8.0 (10mM Tris-HCl, 1mM EDTA, Sigma, St. Louis, MO). The buffer solution also contained 0.125-wt% poly(vinylpyrrolidone) (PVP, $M_W \approx 10^6$ g/mol, Sigma), which served as a dynamic coating to suppress EOF and prevent adsorption to the capillary walls.[36] The instrumentation used in the glass microchip experiments is the same as that used in the PDMS microchip experiments.

4.5.3 Results and Discussion:

2bFCCS-CFMCCE experiments were performed on glass microchips like that seen in figure 4.5, and on ones with the same design format as figure 4.2 (1-cm length channel, 40-μm wide X 20-μm deep) but made of glass instead of PDMS. All glass microchips were fabricated by Vinod Anumareddy.

4.5.3.1 Glass Microchip with 44 channels:

The glass microchip pictured in figure 4.5 was an intriguing starting point for the study of 2bFCCS-CFMCCE on glass microchips. The channel dimensions and compact array of microchannels fully illustrated, conceptually, the advantage that 2bFCCS-CFMCCE offers over conventional MCCE. It is impossible to arrange 44 separate MCCE separation channels in 1X1 in^2; the requirement of macroscopic separation in conventional MCCE simply cannot be met on such scales and with the channel format shown. Unfortunately, the fluid handling requirements of the microchip in figure 4.5 proved to hinder the ability to take data. The close proximity and small size of the access wells of the glass microchip in figure 4.5 made it extremely difficult to introduce sample, perform channel buffer washes, and keep the fluid levels in the wells at both ends of the microchannel even. In addition, evaporation of sample buffer from the wells quickly introduced bubbles into the channels, and altered the conductivity of solutions. Every attempt to obtain meaningful 2bFCCS-CFMCCE data fell short. While some experimental cross-correlation data was seen, the flourescent signal was extremely unstable due to the factors listed above, and no data worthy of

theoretical fitting was obtained. In addition, the construction of the 44 microchannel chip was labor-intensive. The separate hand drilling of 88 wells to serve as fluid ports proved to be a real pain, and difficult to perform precisely. A more elegant microchip fabrication strategy and fluid handling strategy would have allowed more extensive testing of this particular microchip format. Unfortunately, given the state of development of the 2bFCCS-CFMCCE technique, it was deemed more prudent to investigate a simpler glass microchip system.

4.5.3.2 Single-Channel Glass Microchip

Figure 4.9 shows 2bFCCS-CFMCCE data collected on a glass microchip with the same dimensions as the PDMS microchip pictured in figure 4.2. As one can see, as the voltage is increased, the ssDNA migrates faster, and thus the peaks are positioned at shorter lag times on the x-axis. Unfortunately, while this data appears to be good, and the voltage trend makes intuitive sense, the theoretical fitting of this data was inconclusive. In other words, determination of parameters such as τ_d, V_x, etc. from the fitting procedure yielded nonsensical values. Unfortunately problems such as this plagued the data obtained on glass microchips. Perhaps the coating procedure, though it seemed to yield better data than uncoated chips, was insufficient, and the experiments were still plagued by sporadic EOF and wall effects. Other possible sources of error involved with glass microchips are related to the fabrication process. Glass microchannels that are formed through HF etching can have high surface

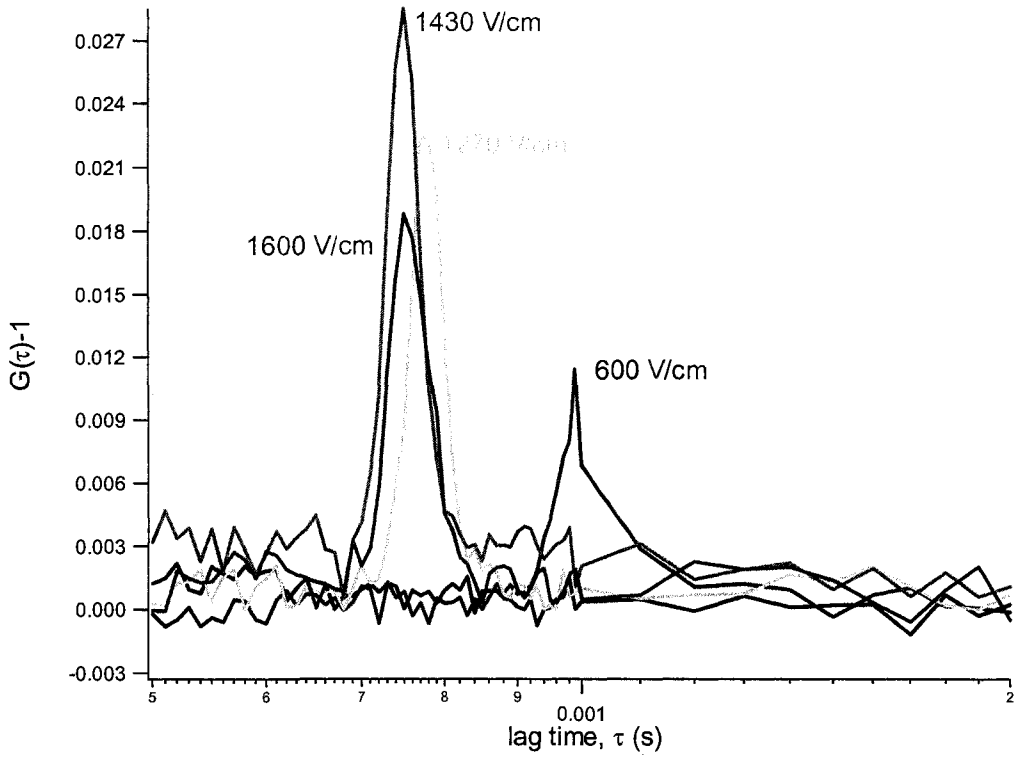

Figure 4.9: Cross-correlation data obtained from the observation of nanomolar solutions of 40-oligo poly(dT) single-stranded DNA (polythymine) labeled at the 5' end with Rhodamine 6G (R6G-ssDNA). The dependence of the migration velocity on applied voltage can be seen. Shorter lag times indicate faster R6G-ssDNA migration between the two laser-foci.

roughness when compared to the inner walls of fused silica capillaries. This could potentially lead to unpredictable effects in the EOF on-chip.

Another possibility which would help explain the difficulty in fitting the data presented in figure 4.9 is related to the glass bonding process. The 2bFCCS theoretical model, and thus data fitting, is extremely dependent on the geometry of the laser focus used to excite the fluorophores studied by 2bFCCS analysis. In the fused silica capillaries and PDMS microchips, the laser is focused through smooth capillary walls, or through microscope coverslips of high optical quality. While the glass surface the laser was focused through in glass microchips was a microscope coverslip, this was a microscope coverslip that had been bonded to a glass microchip at high temperature. Numerous glass microchips had to be disposed of after the thermal bonding process because the coverslips interacted unfavorably with the quartz blocks which pressed the coverslip and microchip together. The coarse surface texture of the quartz blocks was often imprinted onto the coverslip at high temperature. In addition, distortions visible to the naked eye were visible on some coverslips after bonding. If the laser was focused through coverslips with optical defects, then the laser focus would no longer be the gaussian, oval-like shape used in the theoretical model for data fitting. Thus, the model would no longer be valid, and any data fit using the wrong model would provide meaningless information.

Ultimately, though glass microchips had promising microchannel chemistry, the difficulties involved in fabricating microchips with favorable optical properties limited their application. The process of glass microchip fabrication

was time-consuming and expensive and the failure rate was high. Though tantalizing data like that seen in figure 4.9 was obtained, it proved to be unamenable to theoretical fits.

4.6 Conclusion:

The technique of 2bFCCS-CFMCCE showed a lot of promise for expanding the design options of MCCE techniques. Cross-correlation analysis was successfully performed on PDMS microchips, some with design features unique to the 2bFCCS-CFMCCE technique. Cross-correlation data was also obtained on glass microchips, though comprehensive analysis of the data proved to be problematic.

Although bringing the 2bFCCS-CFMCCE technique to maturity was beyond the scope of the work performed here, possibilities remain for further development of the technique. Fabrication processes for both PDMS and glass microchips could be performed to greater control the wall chemistry and surface roughness. For instance, the hardness and porosity of the PDMS can be controlled by using varying ratios of elastomer and curing agent[38]. In addition, there are a multitude of possible coatings and plasma oxidation techniques that can be used to tailor PDMS surface chemistry. Glass microchips have the same multitude of options for coating chemistry[39]. Both types of chips could be equipped with more elegant fluid handling technology, which would enable such

things as applying the PVA coating under the same conditions as used in fused silica capillaries[40].

There were numerous possible routes for optimization of the fabrication techniques used for the microchips, especially glass. A variety of possible HF-based etchants can be used to fabricate the microchannels. Careful selection and optimization of HF etching conditions can lead to smoother microchannel walls, and thus more stable EOF[28]. In addition, perhaps the most difficult step of the glass microchip fabrication is the thermal bonding process. Careful optimization of the thermal bonding step could yield glass microchips with higher optical quality. The thermal bonding process is extremely dependent on the bonding surfaces of the two glass pieces[28]. Any dirt or contamination can completely alter the bonding process. Though all glass surfaces to be bonded were thoroughly cleaned, the bonding process was not performed in a clean room, opening the possibility of greater surface contamination. In addition, once the glass surfaces are bonded, it is possible to perform grinding on glass surfaces to improve their optical quality[28].

The scope of the 2bFCCS-CFMCCE experimentation performed here barely scratches the surface of possible microchip design and optimization. As a proof of concept, the work was successful in showing the promise of the technique for expanding the design options and experimental possibilities of MCCE. Ultimately the expense and time involved in optimization of the technique proved to be beyond the scope intended for the work, and so 2bFCCS

on microchips was discontinued in favor of the study of interesting systems on the more stable and predictable platform of fused silica capillaries.

1. Landers, J. P., Ed., *Handbook of Capillary Electrophoresis*. 2nd ed.; CRC Press: Boca Raton, 1997; p 894.

2. Landers, J. P., Molecular Diagnostics on Electrophoretic Microchips. *Analytical Chemistry* **2003,** 75, (12), 2919-2927.

3. Vilkner, T.; Janasek, D.; Manz, A., Micro Total Analysis Systems. Recent Developments. *Analytical Chemistry* **2004,** 76, (12), 3373-3386.

4. Dolnik, V.; Liu, S.; Jovanovich, S., Capillary electrophoresis on microchip. *Electrophoresis* **2000,** 21, (1), 41-54.

5. Effenhauser, C. S.; Bruin, G. J. M.; Paulus, A., Integrated chip-based capillary electrophoresis. *Electrophoresis* **1997,** 18, (12-13), 2203-2213.

6. Manz, A.; Harrison, D. J.; Verpoorte, E. M. J.; Fettinger, J. C.; Paulus, A.; Ludi, H.; Widmer, H. M., Planar Chips Technology For Miniaturization And Integration Of Separation Techniques Into Monitoring Systems - Capillary Electrophoresis On A Chip. *Journal Of Chromatography* **1992,** 593, (1-2), 253-258.

7. Manz, A.; Effenhauser, C. S.; Burggraf, N.; Harrison, D. J.; Seiler, K.; Fluri, K., Electroosmotic pumping and electrophoretic separations for miniaturized chemical analysis systems. *J. Micromech. Microeng.* **1994,** 4, (4), 257-65.

8. Seiler, K.; Harrison, D. J.; Manz, A., Planar glass chips for capillary electrophoresis: repetitive sample injection, quantitation, and separation efficiency. *Analytical Chemistry* **1993,** 65, (10), 1481-8.

9. Harrison, D. J.; Fluri, K.; Seiler, K.; Fan, Z. H.; Effenhauser, C. S.; Manz, A., Micromachining A Miniaturized Capillary Electrophoresis-Based Chemical-Analysis System On A Chip. *Science* **1993,** 261, (5123), 895-897.

10. Effenhauser, C. S.; Manz, A.; Widmer, H. M., Glass chips for high-speed capillary electrophoresis separations with submicrometer plate heights. *Analytical Chemistry* **1993,** 65, (19), 2637-42.

11. Harrison, D. J.; Manz, A.; Fan, Z.; Luedi, H.; Widmer, H. M., Capillary electrophoresis and sample injection systems integrated on a planar glass chip. *Analytical Chemistry* **1992,** 64, (17), 1926-32.

12. Khandurina, J.; McKnight, T. E.; Jacobson, S. C.; Waters, L. C.; Foote, R. S.; Ramsey, J. M., Integrated system for rapid PCR-based DNA analysis in microfluidic devices. *Analytical Chemistry* **2000,** 72, (13), 2995-3000.

13. Waters, L. C.; Jacobson, S. C.; Kroutchinina, N.; Khandurina, J.; Foote, R. S.; Ramsey, J. M., Microchip Device for Cell Lysis, Multiplex PCR Amplification, and Electrophoretic Sizing. *Analytical Chemistry* **1998,** 70, (1), 158-162.

14. Jacobson, S. C.; Culbertson, C. T.; Daler, J. E.; Ramsey, J. M., Microchip Structures for Submillisecond Electrophoresis. *Analytical Chemistry* **1998,** 70, (16), 3476-3480.

15. Jacobson, S. C.; Ramsey, J. M., Microchip Electrophoresis With Sample Stacking. *Electrophoresis* **1995,** 16, (4), 481-486.

16. Jacobson, S. C.; Moore, A. W.; Ramsey, J. M., Fused Quartz Substrates For Microchip Electrophoresis. *Analytical Chemistry* **1995,** 67, (13), 2059-2063.

17. Jacobson, S. C.; Hergenroder, R.; Koutny, L. B.; Warmack, R. J.; Ramsey, J. M., Effects Of Injection Schemes And Column Geometry On The Performance Of Microchip Electrophoresis Devices. *Analytical Chemistry* **1994,** 66, (7), 1107-1113.

18. Jacobson, S. C.; Hergenroder, R.; Koutny, L. B.; Ramsey, J. M., High-Speed Separations On A Microchip. *Analytical Chemistry* **1994,** 66, (7), 1114-1118.

19. Shi, Y.; Simpson, P. C.; Scherer, J. R.; Wexler, D.; Skibola, C.; Smith, M. T.; Mathies, R. A., Radial Capillary Array Electrophoresis Microplate and Scanner for High-Performance Nucleic Acid Analysis. *Analytical Chemistry* **1999,** 71, (23), 5354-5361.

20. Simpson, P. C.; Roach, D.; Woolley, A. T.; Thorsen, T.; Johnston, R.; Sensabaugh, G. F.; Mathies, R. A., High-throughput genetic analysis using microfabricated 96-sample capillary array electrophoresis microplates. *P Natl. Acad. Sci. USA* **1998,** 95, (5), 2256-2261.

21. LeCaptain, D. J.; Van Orden, A., Two-beam fluorescence cross-correlation spectroscopy in an electrophoretic mobility shift assay. *Analytical Chemistry* **2002,** 74, (5), 1171-1176.

22. Bayer, J.; Raedler, J. O., DNA microelectrophoresis using double focus fluorescence correlation spectroscopy. *Electrophoresis* **2006,** 27, (20), 3952-3963.

23. Schiro, P. G.; Kuyper, C. L.; Chiu, D. T., Continuous-flow single-molecule CE with high detection efficiency. *Electrophoresis* **2007,** 28, (14), 2430-2438.

24. Brinkmeier, M., Cross-correlated flow analysis in microstructures. In *Fluorescence Correlation Spectroscopy: Theory and Applications*, ed.; Elson, E. S., Ed. Springer: Berlin, 2001; Vol. 65, pp 379-395.

25. Brinkmeier, M.; Doerre, K.; Stephan, J.; Eigen, M., Two-beam cross-correlation. A method to characterize transport phenomena in micrometer-sized structures. *Analytical Chemistry* **1999,** 71, (3), 609-616.

26. Brinkmeier, M.; Dorre, K.; Riebeseel, K.; Rigler, R., Confocal spectroscopy in microstructures. *Biophys. Chem.* **1997,** 66, (2-3), 229-239.

27. Brinkmeier, M.; Rigler, R., Flow analysis by means of fluorescence correlation spectroscopy. *Exp. Techn. Phys.* **1995,** 41, (2), 205-210.

28. Anumareddy, V. Fabrication of Glass Microfluidic Chips and Fabrication of Sub-Micron Features Using E-Beam Lithography. Colorado State University, Fort Collins, 2005.

29. Garcia, C. D.; Henry, C. S., Enhanced determination of glucose by microchip electrophoresis with pulsed amperometric detection. *Analytica Chimica Acta* **2004,** 508, (1), 1-9.

30. Garcia, C. D.; Henry, C. S., Direct detection of renal function markers using microchip CE with pulsed electrochemical detection. *Analyst* **2004,** 129, (7), 579-584.

31. Garcia, C. D.; Henry, C. S., Direct determination of carbohydrates, amino acids, and antibiotics by microchip electrophoresis with pulsed amperometric detection. *Analytical Chemistry* **2003,** 75, (18), 4778-4783.

32. Caulum, M. Detection of Disease Markers Using a Novel Multi-Analyte Immunoassay. Colorado State University, Fort Collins, 2007.

33. Fan, Z. H.; Harrison, D. J., Micromachining Of Capillary Electrophoresis Injectors And Separators On Glass Chips And Evaluation Of Flow At Capillary Intersections. *Analytical Chemistry* **1994,** 66, (1), 177-184.

34. Seiler, K.; Fan, Z. H. H.; Fluri, K.; Harrison, D. J., Electroosmotic Pumping And Valveless Control Of Fluid-Flow Within A Manifold Of Capillaries On A Glass Chip. *Analytical Chemistry* **1994,** 66, (20), 3485-3491.

35. Senturia, S. D., *Microsystem Design.* 2nd ed.; Kluwer Academic Publishers: Boston, 2001; p 689.

36. Gao, Q.; Yeung, E. S., A matrix for DNA separation: genotyping and sequencing using poly(vinylpyrrolidone) solution in uncoated capillaries. *Analytical Chemistry* **1998,** 70, (7), 1382-1388.

37. Liu, Y.; Fanguy, J. C.; Bledsoe, J. M.; Henry, C. S., Dynamic coating using polyelectrolyte multilayers for chemical control of electroosmotic flow in capillary electrophoresis microchips. *Analytical Chemistry* **2000,** 72, (24), 5939-5944.

38. McDonald, J. C.; Duffy, D. C.; Anderson, J. R.; Chiu, D. T.; Wu, H. K.; Schueller, O. J. A.; Whitesides, G. M., Fabrication of microfluidic systems in poly(dimethylsiloxane). *Electrophoresis* **2000,** 21, (1), 27-40.

39. Belder, D.; Ludwig, M., Surface modification in microchip electrophoresis. *Electrophoresis* **2003,** 24, (21), 3595-3606.

40. Belder, D.; Deege, A.; Kohler, F.; Ludwig, M., Poly(vinyl alcohol)-coated microfluidic devices for high-performance microchip electrophoresis. *Electrophoresis* **2002,** 23, (20), 3567-3573.

Chapter 5: 2bFCCS-CFCE for Interrogating the Ionic Atmosphere of Single-Stranded DNA

This chapter describes the development of two-beam fluorescence cross-correlation spectroscopy coupled with continuous-flow capillary electrophoresis (2bFCCS-CFCE) for the investigation of DNA-magnesium interactions. Magnesium-DNA interactions are investigtaed through the measurement of the effective charge of the DNA in a capillary electrophoresis experiment. The effective charge measurement is nearly impossible using conventional capillary electrophoresis. The technique of 2bFCCS-CFCE, however, is shown to be capable of making this measurement. To my knowledge, this is the first experimental determination of the effective charge of DNA in a capillary electrophoresis experiment. The work that contributes to this chapter was performed over the period from Febuary 2005 to present.

5.1 Introduction:

The ionic atmosphere of biological macromolecules in free solution plays an important role in their function and structure[1-9]. An example is the impact of divalent cations, such as Mg^{2+}, on the behavior of DNA. Magnesium counterions have been found to strongly interact with nucleotide bases such as guanine, and with the free oxygens of the phosphate backbone[10-14]. These interactions affect DNA's behavior in replication, tertiary structure formation, and in its interaction with RNA and enzymes. Theoretical studies have found that magnesium's role in the structure of DNA is so important that it cannot be explained by electrostatics alone, as it is also an important contributor to the hydrogen bonding of DNA nucleotides[11, 14]. A possible way to study magnesium binding to DNA is through the measurement of effective charge. A DNA's chemical charge is well known, as it is simply a matter of counting the phosphate groups in the DNA backbone. Effective charge, however, is a much more difficult quantity to determine, as it is the chemical charge of the DNA minus the collective charge of associated counterions. Comparison of chemical and effective charge can provide quantitative information about magnesium-DNA interactions and new insight into the important role magnesium plays in our biochemistry.

An apparently ideal method for measuring effective charge is capillary zone electrophoresis (CZE). In CZE, the effective charge of a species is determined through an examination of the species' electrophoretic mobility, μ:

$$\mu = \frac{q_{eff}}{f} \tag{5.1}$$

where q_{eff} is the effective charge and f is the frictional factor, which is related to the diffusion constant, D, of the species by:

$$f = \frac{k_B T}{D} \tag{5.2}$$

where k_B is the Boltzmann constant and T is the temperature. Combining equations 5.1 and 5.2 leads to:

$$\mu = \frac{D q_{eff}}{k_B T} \tag{5.3}$$

Thus, if one wants to determine the effective charge of a species, one would determine the electrophoretic mobility and diffusion constant of the species experimentally and calculate its effective charge using equation 5.3.

In CZE, the electrophoretic mobility of a species can be found from the migration velocity, v, of a species in a particular electric field, E:

$$\mu = \frac{v}{E} \tag{5.4}$$

The migration velocity of a species in CZE can be found from the length of the capillary in which the separation occurs and the timescale of the experiment, $v = L/t$. At this point, it is important to remember the contribution by electroosmotic flow (EOF) to the apparent electrophoretic mobility of a species in CZE. The inner surface of the fused silica capillaries commonly used in CZE is negatively charged. This creates a positively charged ionic double layer near the capillary walls which migrates toward the cathode when an electric field is

applied. The migration towards the cathode results in bulk solvent flow, or electroosmotic flow, due to drag. The migration velocity of a species thus has two contributions: the interaction of the species with the electric field as depicted in equation 5.3, and the electroosmotic flow contribution. Equation 5.4 must therefore be rewritten as:

$$(\mu_e + \mu_{EOF}) = \frac{v}{E} \tag{5.5}$$

where μ_e is the electrophoretic mobility of the species (eq. 5.3), and μ_{EOF} is the contribution to the mobility from electroosmotic flow[15]. If the electroosmotic flow of the CZE experiment can be determined, μ_e can be obtained.

The other important experimental variable calculation necessary for the determination of effective charge is the diffusion constant of the species, D. In CZE, diffusion impacts the experiment by broadening the zone containing the migrating analyte. This zone broadening means that information relating to D is contained in the peak width, or variance, of an electropherogram. If diffusion were the only contribution to peak variance in CZE, then obtaining the diffusion constants of analytes would be a relatively simple task. Unfortunately there are many more contributions to the variance, and accurately determining diffusion constants by using CZE is an uncertain venture. The total peak variance, σ_{tot}^2, of a CZE electropherogram peak can be represented as a linear summation of variances due to various zone broadening effects:

$$\sigma_{tot}^2 = \sigma_{diff}^2 + \sigma_{inj}^2 + \sigma_{wall}^2 + \sigma_{JH}^2 + \sigma_{\det}^2 + \sigma_{em}^2 + \sigma_{flo}^2 \tag{5.6}$$

where σ^2_{diff} is variance contribution of diffusion, σ^2_{inj} is the variance due to sample injection, σ^2_{wall} is the variance due to wall effects, σ^2_{JH} is the variance due to joule heating effects, $\sigma^2_{\det}$ is the variance due to the size of the detection region, σ^2_{em} is the variance due to electromigration dispersion, and σ^2_{flo} is the variance due to nonuniform velocity flow profile[15-19]. In order to precisely determine σ^2_{diff}, it would be necessary to either eliminate or precisely determine all of the other contributions to the variance. However, many of the above forms of variance are either nonreproducable or are intractable to calculation[17, 20, 21].

Determination of σ^2_{diff}, therefore, requires specialized applications of CZE that attempt to create situations in which the myriad forms of variance can be accounted for. By far the most popular of these specialized techniques is stopped migration CZE[22-30]. In stopped migration CZE, a sample is electrophoresed halfway through the capillary at which point the electric field is turned off, and then, after a certain dwell time, the field is reapplied and the sample proceeds and is detected as normal. When the electric field is off, the sample zone spreads due to the diffusion of the molecule, and so the resulting electropherogram has greater peak variance. If these stopped migration peaks are compared to peaks made from continuous runs, the other forms of variance should cancel out, and the difference in the variance of the peaks is solely due to diffusion, making a calculation of the diffusion constant possible.

A potential drawback to stopped migration CZE is that it makes the assumption that the non-diffusion variances do not vary significantly from run to

run. It has been shown that variances due to inconsistent flow rates and sample injection steps often change significantly from run to run[21]. In addition, the dwell time in stopped migration CZE experiments is often unreasonably long, particularly for larger molecules. Dwell times on the order of 10 hours or more have been reported for larger molecules[22, 23, 28]. Although stopped migration CZE has been successful at measuring both electrophoretic mobility and diffusion constants of biological macromolecules, an ideal technique would measure these two variables simultaneously, quickly, and independent from the many sources of variance present in conventional CZE.

An alternative to conventional, separations based CZE for determining the effective charge is the analysis of individual analyte molecules as they migrate continuously through an electrophoresis channel. We refer to techniques based on this concept as continuous-flow capillary electrophoresis (CFCE). CFCE-based techniques are advantageous because they eliminate the need for chemical separation. By continuously monitoring individual molecules, CFCE techniques are able to quickly generate data that is independent of many of the sources of error, such as sample injection, present in traditional CZE. In addition, the measurements of CFCE are based on phenomena happening on microsecond to millisecond timescales. This is an ideal time regime for molecular diffusion analysis, and has also been shown to be effective for looking at molecular interactions not amenable to study by conventional CZE. Detection methods for CFCE include dynamic light scattering (DLS)[31-33], sequential single-

molecule fluorescence detection[34], single-molecule fluorescence imaging[35-37], and various incarnations of fluorescence correlation spectroscopy (FCS)[38-46].

While all of the above CFCE techniques effectively monitor both diffusion and electrophoretic mobility of analyte molecules, they all have unique advantages and disadvantages. DLS-based CFCE has the advantage of label-free detection, but lacks the sensitivity and selectivity of fluorescence-based CFCE. In addition, DLS can only observe larger macromolecules, while fluorescence CFCE can also monitor smaller species. The single-molecule fluorescence imaging technique developed by Yeung and co-workers[35-37] suffers from the same type of problem in that it requires multiple chromaphores per molecule to obtain sufficient signal, though it does have the advantage of high concentration sensitivity and high-throughput capability. Sequential single-molecule fluorescence detection was used in the first demonstration of CFCE, the single molecule electrophoresis (SME) experiment of Castro and Shera[34]. It monitored individual molecules flowing sequentially between two offset laser focal regions. It also had the advantage of high concentration sensitivity, but suffered from complex instrumentation and the need for multiple chromaphores per molecule.

FCS has proved to be the most popular detection method for CFCE. It offers a greater temporal resolution than any of the previously mentioned CFCE techniques, being able to monitor processes occurring on microsecond to millisecond timescales. In addition FCS-based CFCE utilizes a relatively simple confocal microscope setup, though its concentration sensitivity is not as high as

SME or single-molecule imaging (nanomolar vs femtomolar). FCS-CFCE was first demonstrated by Keller and Van Orden[38] in an experiment which demonstrated its ability to analyze multicomponent mixtures. LeCaptain and Van Orden[40] then used FCS-CFCE to monitor binding interactions between biomolecules, effectively taking advantage of the temporal resolution to obtain information not attainable with conventional CZE. Both of the above examples of FCS-CFCE demonstrated the potential of using FCS as a detection technique in CFCE, but suffered from some disadvantages. The single focus FCS-CFCE technique used has difficulty resolving information from multicomponent mixtures due to the fact that only one data signal curve is generated. In addition, single focus FCS-CFCE is unable to discern the direction of analyte migration, which makes it difficult to differentiate the electrophoretic mobility from the combined mobility and EOF contributions to the migration velocity.

In response to the disadvantages of single focus FCS-CFCE, Van Orden and LeCaptain introduced the technique of two beam fluorescence cross correlation spectroscopy CFCE (2bFCCS-CFCE)[41]. The 2bFCCS-CFCE technique is conceptually similar to the SME of Shera and Castro[34] in that molecular transit times between two spatially offset detection volumes are measured to determine the molecular flow velocities. However, 2bFCCS uses smaller detection volumes (femtoliters vs picoliters) that can be positioned much closer together (micrometers vs hundreds of micrometers), thereby enabling smaller transit times of ~100 μs to ~10 ms to be measured. 2bFCCS was developed by Brinkmeier and Rigler[47] for flow analysis, but was first coupled with

CFCE by Van Orden and LeCaptain[41] as stated above. The advantage of 2bFCCS-CFCE, relative to single focus FCS-CFCE, is that it resolves the different components of a mixture into separate electropherogram peaks corresponding to the molecular transit times of each species. In addition, Fogarty and Van Orden[42] demonstrated that it could determine the direction of analyte migration as well, which allows the simultaneous monitoring of both positive and negative ions migrating in opposite directions. Rädler and Bayer[44] have previously demonstrated the use of 2bFCCS-CFCE to simultaneously measure the electrophoretic mobility and diffusion constant of double-stranded DNA. This information could be used to calculate the effective charge of the DNA, but such a calculation was not reported. In addition, the experiments of Rädler and Bayer were performed in the absence of the small counterions which play an important role in the structure and function of DNA.

This chapter demonstrates the use of 2bFCCS-CFCE to elucidate the role magnesium counterions play in the electrophoretic behavior of single-stranded DNA (ssDNA). To our knowledge, this is the first demonstration of the measurement of effective charge of ssDNA in relation to Mg^{2+} concentration. We demonstrate the use of 2bFCCS-CFCE to monitor diffusion, migration velocity, and migration direction of a 40 base polythymine labeled with a rhodamine 6G derivative at multiple concentrations of Mg^{2+} and at multiple field strengths. By accounting for electroosmotic flow and temperature, we are able to determine the effective charge of the ssDNA in varied conditions. This "snapshot" into the

magnesium-DNA interaction reveals the potential 2bFCCS-CFCE has in the fundamental study of biological macromolecules and their ionic atmospheres.

5.2 Experimental Section:

5.2.1 Sample Preparation:

40-oligo poly(dT) single-stranded DNA (polythymine) labeled at the 5' end with Rhodamine 6G (R6G-ssDNA, Operon Biotechnologies, Huntsville, AL) was prepared in tris-glycine buffer at pH 8.3 (3mM Tris-HCl, 3mM Glycine, Sigma, St. Louis, MO). Magnesium chloride (Fisher Scientific, Houston, TX) was then added in concentrations that ranged from 0-3mM. The buffer solution also contained 0.125-wt% poly(vinylpyrrolidone) (PVP, $M_W \approx 10^6$ g/mol, Sigma), which served as a dynamic coating to suppress EOF and prevent adsorption to the capillary walls.[48] Once made, samples were boiled to denature any possible deoxyribonuclease contamination.

5.2.2 Capillary Coating:

A procedure adopted from Belder et al.[49] was used to apply a coating of poly(vinyl alcohol) (PVA, $M_W \approx 4\times10^4$ g/mol, Sigma) to the interior wall of a 50-μm inner diameter, 375-μm outer diameter rectangular glass capillary (Polymicro, Phoenix, AZ), coated on the outer surface with polyimide. A clean, 25-cm long

capillary was filled with an acidified aqueous glutaraldehyde solution, prepared from 200 µL of 50 wt% aqueous glutaraldehyde (Fisher, Houston, TX) in 800 µL of 1 M hydrochloric acid (Mallinckrodt, Hazelwood, MO). A plug of 2.5 wt% PVA in 0.6 M hydrochloric acid was injected into the glutaraldehyde-filled capillary using 0.5 MPa of N_2 for 10s. The capillary was then emptied and dried with continuous nitrogen flow for ~ 4 hours, after which it was ready for use.

5.2.3 Instrumentation:

Our 2bFCCS-CFCE apparatus (Figure 5.1) has been described previously.[41, 42] Briefly, a 514.5-nm laser beam from an air-cooled, continuous wave Ar^+ laser (Midwest Laser Products, Frankfort, IL) was split and then recombined into two nearly parallel beams by two 50/50 beamsplitters (Newport, Irvine, CA). The two beams were adjusted in power to 43 µW using the appropriate absorptive neutral density filters (Newport), reflected by a 530-nm long pass dichroic beamsplitter (CVI, Albuquerque, NM), and focused by a 100×, 1.25-numerical aperture oil immersion microscope objective (Edmund Industrial Optics, Barrington, NJ) through a small window created in a 25-cm length of the PVA coated capillary. The window was created by dissolving a small section of the outer polyimide coating in concentrated sulfuric acid heated to a temperature of 75°C. Various potentials were applied to the capillary by means of platinum electrodes connected to a high voltage power supply (Spellman, model CZE1000R, Plainview, NY). Fluorescence from each focal region was collected

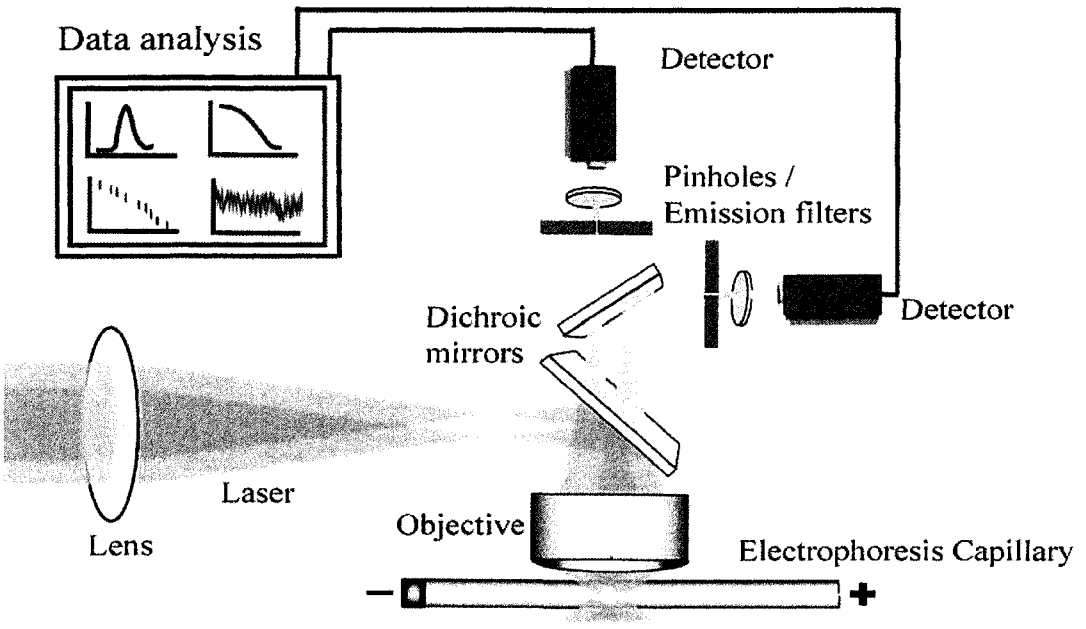

Figure 5.1: Schematic representation of the two-beam fluorescence cross-correlation/continuous flow capillary electrophoresis experiment. The optical setup was designed to position two diffraction limited laser foci in the center of a square capillary, separated by a distance of ~5 μm. The capillary is filled with sample solution using applied gas pressure, which is then turned off and voltage is applied for the electrophoresis experiment. Fluorescence signal from each focus is collected and used for the analysis of auto and cross-correlation. This figure is identical to figure 2.5 in chapter 2, but has been included here for convenience.

by the same objective, split by a 50/50 cubic beamsplitter (Thorlabs, Newton, NJ), spatially filtered by 50 μm pinholes (Thorlabs, Newton, NJ), and filtered by 535-nm long pass interference filters (Omega Optical, Brattleboro, VT), which transmitted the fluorescence to two single photon counting avalanche photodiode detectors (PerkinElmer Optoelectronics, model SPCM-AQR-14, Wellesley, MA). The photocounts from the two detectors were cross-correlated using an ALV-6010/160 digital correlator card (ALV, Langen, Germany) mounted in a Pentium computer. Temperature was monitored using a Digi-Sense Benchtop Thermistor Temperature Controller (model EW-89000-10, Cole Parmer).

The two laser beams formed nearly identical diffraction-limited focal regions, positioned near the center of the inner capillary space (~25 μm from the inner surfaces), separated along the axial dimension of the capillary by a distance, R. From autocorrelation analysis of a standard 5-carboxy-tetramethylrhodamine (TAMRA) solution, the e^{-2} focal radius in the radial dimension, ω_0, of the focal volume was determined to vary from 0.2198 ± 0.0033 μm to 0.2567 ± 0.0037 μm. The ratio of the radial and axial e^{-2} radii ($\kappa_0 = \omega_0 / z_0$, where z_0 is the axial radius) was also determined, and found to be 0.104 ± 0.002 μm. The separation distance, R, between the two foci was determined by cross-correlation analysis to vary from 2.379 ± 0.045 μm to 2.581 ± 0.050 μm. The position of the laser beam foci relative to the inner surface of the capillary was reproducibly controlled using a submicrometer resolution differential micrometer (Newport) mounted on the *z*-axis of the sample stage. Additionally, a precision rotation stage (Newport) was mounted on the sample stage to allow adjustment

of the flow axis relative to the axis defined by the position of the two laser beams. The optimum position of the two laser beam foci relative to the *z*-position of the capillary and the flow axis could be confirmed by cross-correlation analysis.

5.2.4 Electroosmotic Flow Measurements:

The EOF was determined prior to 2bFCCS-CFCE experiments using a procedure adopted from Zare et al.[50] A buffer was made containing lower concentrations of tris-glycine and magnesium chloride. The capillary was then filled with this lower ionic strength buffer, while the higher ionic strength sample buffer was placed at the anode end of the capillary. A 15-kV potential was applied across the capillary, and the voltage drop across a 100 kΩ resistor placed in between ground and the capillary was monitored using a Labview program written in-house. As the higher ionic strength sample buffer flows into the capillary due to electroosmotic flow, more current flows through the resistor, resulting in a continual increase in the voltage. When the higher ionic strength buffer has completely filled the capillary, the current ceases to change, and the measured voltage reaches a steady value. By recording the length of time the voltage was changing, from the first application of the potential to the arrival at a steady state, the velocity of the electroosmotic flow can be determined. While both the dynamic and permanent coatings should have suppressed EOF, it was found by this procedure to be nonzero, and therefore had to be determined for calculation of electrophoretic mobility.

The primary safety hazards of this experiment are electric shock due exposure to the high voltage electrodes and eye injury from exposure to laser light. The entire experiment was placed inside an enclosure to block stray laser light. Access to the enclosure was interlocked to the high-voltage power supply to prevent exposure to the high voltage electrodes during the operation of the experiment.

5.3 Theory:

The theory used to analyze the cross-correlation functions obtained from the magnesium/polythymine experimental study has been developed elsewhere[39, 42, 51, 52]. Briefly, the equation used to fit experimentally determined cross-correlation functions is:

$$G_C(\tau)-1=a\left(\frac{1}{1+\tau/\tau_d}\right)\left(\frac{1}{1+\kappa_0^2\,\tau/\tau_d}\right)^{1/2}\exp\left[\frac{-r^2(1-\tau/\tau_F)^2}{1+\tau/\tau_d}\right] \qquad (5.7)$$

where τ is the lag time, τ_d is the average transit time of molecules through one of the focal volumes due to translational diffusion only, r is the ratio R/ω_0, τ_F is the average transit time for the molecules to flow between the two focal volumes, given by R/V_x, where V_x is the linear flow velocity of the molecules, a is the amplitude, given by $(\gamma/N)(1-T)$, where γ is a geometric factor that corrects for

the deviation in the shape of the excitation volume from an ideal Gaussian function, N is the average number of molecules occupying a focal region, and T is the quantum yield. The parameter κ_0 was held fixed to the value determined from control experiments in all data analysis procedures. Adjustment of this parameter was found to make a negligible contribution to the values of the other fitted parameters in both the auto- and cross-correlation analyses. Cross-correlation data from an experiment can manifest in two independent channels; one corresponding to "forward" flow, and the other corresponding to "reverse" flow. Due to the fact that fluorescently labeled polythymine was the only species contributing to cross-correlation functions in these experiments, relevant cross-correlation data was only observed in one channel, the "forward" channel.

The τ_d parameter can be used to determine the diffusion coefficient, D, of the polythymine using $D = \omega_0^2/(4\tau_d)$. In order to determine the effective charge of the polythymine at various magnesium concentrations, it is also necessary to determine μ_{DNA}, the electrophoretic mobility of the polythymine. This can be obtained by calculation of equations 5.3 and 5.5 from the knowledge of the electric field applied to the capillary, the velocity of the electroosmotic flow determined from control experiments, and the linear flow velocity of the polythymine, V_x. The parameter V_x can be determined from the relation $V_x = (r\omega_0)/\tau_F$, using the ω_0 found from control experiments and the r and τ_F determined from fitting of the cross-correlation data.

5.4 Determination of EOF:

In order to measure the electrophoretic migration of the polythymine molecules independently from EOF contributions, it was necessary to measure the magnitude of the EOF occurring in the capillary from day to day. Figure 5.2 shows representative data used to determine the magnitude of the EOF before cross-correlation analysis was performed. At time zero, a 15 kV voltage was applied across a capillary filled with lower ionic strength buffer, with a reservoir of higher ionic strength buffer at the anode end of the capillary. As the higher ionic strength buffer migrates into the capillary the current flowing through the capillary increases (after a brief equilibration time), and the voltage change, in arbitrary units, measured across a resistor increases as seen in figure 5.2 (keeping in mind the negative scale of the voltage drop). For the experiment represented in figure 5.2 the low ionic strength buffer contained 2 mM Tris-HCl, 2 mM glycine, pH 8.3 with 1 mM magnesium chloride, while the high ionic strength buffer contained 3 mM Tris-HCl, 3 mM glycine, pH 8.3 with 1.5 mM magnesium chloride. The measured voltage for this experiment reaches a steady state at 4118 ± 12 s, corresponding to the moment when the higher ionic strength buffer has completely displaced the lower ionic strength buffer in the capillary. This endpoint time was then used, along with the length of the capillary to calculate V_{EOF}, which in the case of figure 5.2 was determined to be 5.66 ± 0.12 X 10^{-3} cm/s. The determination of the EOF endpoint, though performed as analytically

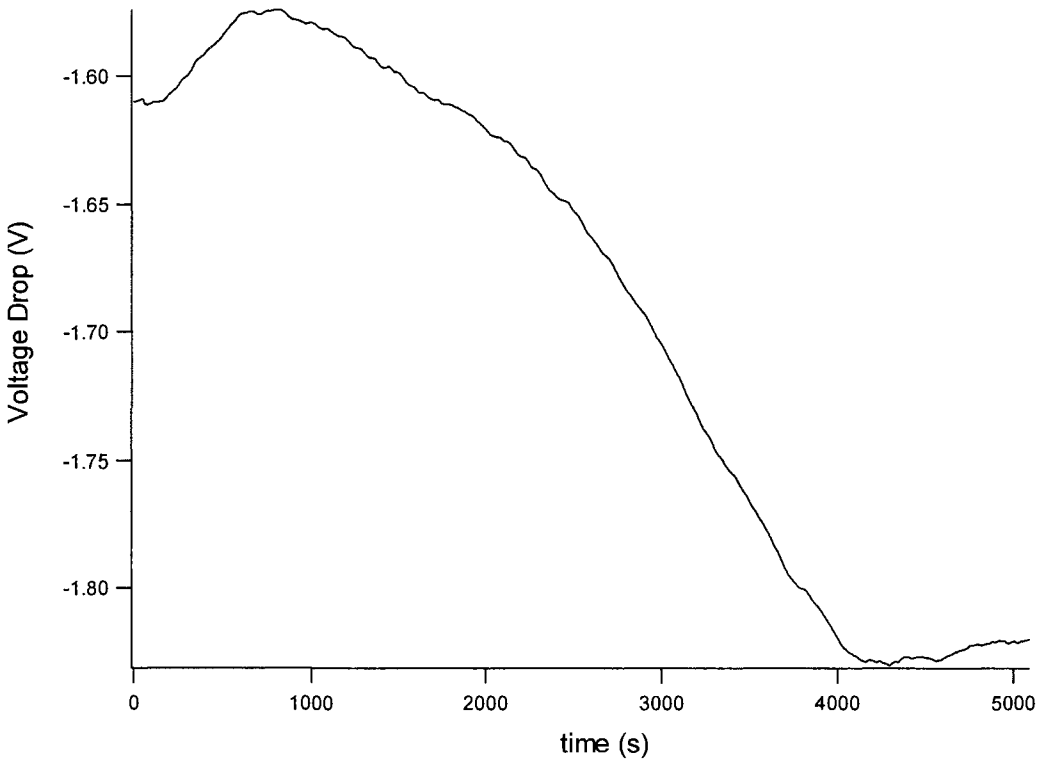

Figure 5.2: Representative electroosmotic flow (EOF) data obtained by the measurement of the voltage drop across a resistor placed in between the capillary and ground, which corresponded to the anode end of the experiment. As a higher ionic strength buffer migrates from the anode to the cathode, it displaces lower ionic strength buffer in the capillary, which results in an increase of current flowing through the capillary (and resistor). In this figure, the higher ionic strength buffer completely displaced the lower ionic strength buffer at ~4100s, which is indicated by the voltage reaching a steady state.

as possible, was ultimately an intuitive endeavor. To obtain statistical error information, control experiments of multiple runs under the same conditions were performed, and the standard deviation of those experiments was assumed to be a constant percentage of other EOF measurements. It should be noted that the magnitude of the EOF was much lower than the migration velocity of the polythymine, and so the impact of EOF on measurements of electrophoretic mobility of polythymine was on the scale of the experimental error.

5.5 Initial Experiments:

During the initial phase of the research into magnesium-DNA interactions, the solutions containing the DNA and magnesium were not boiled as stated in the sample preparation section earlier. Great care was taken in the preparation of buffer solutions (i.e. all buffer containing glassware was piranha cleaned, and all solutions were filtered using 0.2 μm filters). Unfortunately, the precautions taken proved to be insufficient, for control experiments revealed that the DNA sample solutions were contaminated with deoxyribonuclease, which "chops up" the 40-base polythymine molecules into multiple fragments. The control experiments consisted of auto-correlation experiments conducted to determine the diffusion constant of the DNA at various concentrations of magnesium. Calculation of the diffusion constant at 0 kV was done by analysing the τ_d parameter obtained from auto-correlation analysis fit to the equation:

$$G_A(\tau)-1=a\left(\frac{1}{1+\tau/\tau_d}\right)\left(\frac{1}{1+\kappa_0^2\,\tau/\tau_d}\right)^{1/2}\left(1+T_{eq}e^{-\tau/\tau_T}\right) \qquad (5.8)$$

where a, τ_d, and κ_0 are the same parameters appearing in equation 5.7 described earlier. The last term in equation 5.8 takes into account the kinetics of the nonfluorescent triplet state, whose characteristic timescale effects the analysis of auto-correlation data, but not cross-correlation data. T_{eq} is defined as $T_{eq}=T/(1-T)$, where T is the quantum yield, and τ_T is a time constant for population and depopulation of the triplet state.

Figure 5.3 shows the diffusion constants determined for the polythymine at various concentrations of magnesium. Note that there are two sets of data, one corresponding to DNA samples that were not boiled prior to correlation analysis, and the other set referring to DNA samples that were boiled prior to analysis. Inspection of the graph reveals two trends; boiled samples have smaller diffusion constants than unboiled samples, and the diffusion constant of the unboiled samples is much more dependent on relatively small concentrations of magnesium than the diffusion constant of boiled samples. Boiling of samples denatures any deoxyribonuclease enzymes present in the samples, preventing them from "chopping up" polythymine molecules. The unboiled samples exhibited much higher rates of diffusion, indicating that the enzyme was "digesting" molecules of polythymine, and so the diffusion constants measured are not for the 40-base polythymine, but rather the cleaved 1 or 2 bases at the end of the polythymine that are fluorescently labeled. The boiled samples of polythymine exhibited much lower rates of diffusion because the

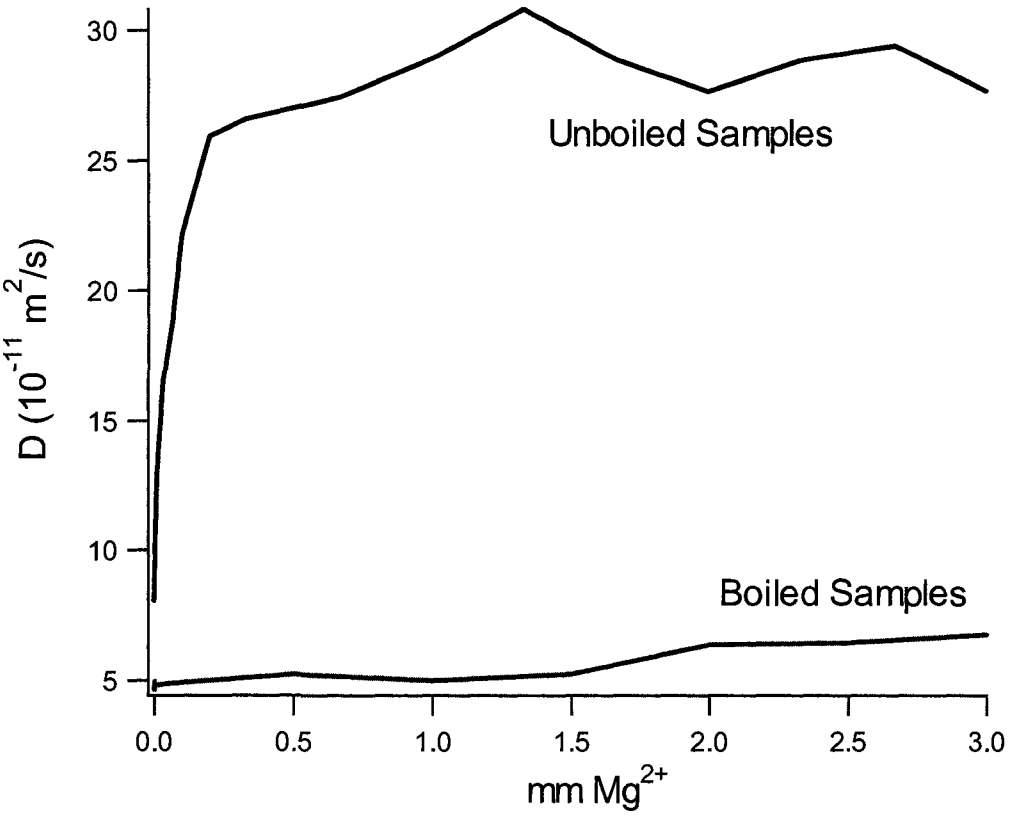

Figure 5.3: Comparison of the diffusion constants obtained by auto-correlation analyis of polythymine samples at various concentrations of magnesium. Unboiled samples show markedly faster rates of diffusion than boiled samples. This is indicative of deoxyribonuclease contamination.

deoxyribonuclease was denatured, and so the diffusion constants measured were for the whole, 40-base polythymine molecules. The extreme magnesium dependence of the unboiled samples' diffusion constants is easily explained in that magnesium serves as a cofactor for deoxyribonuclease[53-55].

The unfortunate action of the deoxyribonuclease enzymes on polythymine molecules was deduced from the fact that at high concentrations of magnesium, polythymine molecules were exhibiting diffusion rates similar to the diffusion rates of individual fluorophores such as free TAMRA. A 40-base nucleotide will never adopt a compact enough structure to diffuse at the same rate as a small organic dye! The control experiments confirmed my fears, and so it became necessary to account for the deoxyribonuclease contamination during sample preparation. Samples were not only boiled, but all lab equipment that touched sample solutions was autoclaved at 250°C to destroy deoxyribonuclease. Buffer solutions were also autoclaved prior to the fabrication of samples.

5.6 Analysis of Cross-Correlation Functions:

Figure 5.4 shows representative cross-correlation functions taken under three different conditions: polythymine with 0 mM Mg at 15 kV/24.2 cm (red), polythymine with 1.5 mM Mg at 15 kV/23.3 cm (green), and polythymine with 3 mM Mg at 15 kV/23.3 cm (blue). In figure 5.4, the experimentally determined data is represented by diamonds, and their theoretical fits determined from

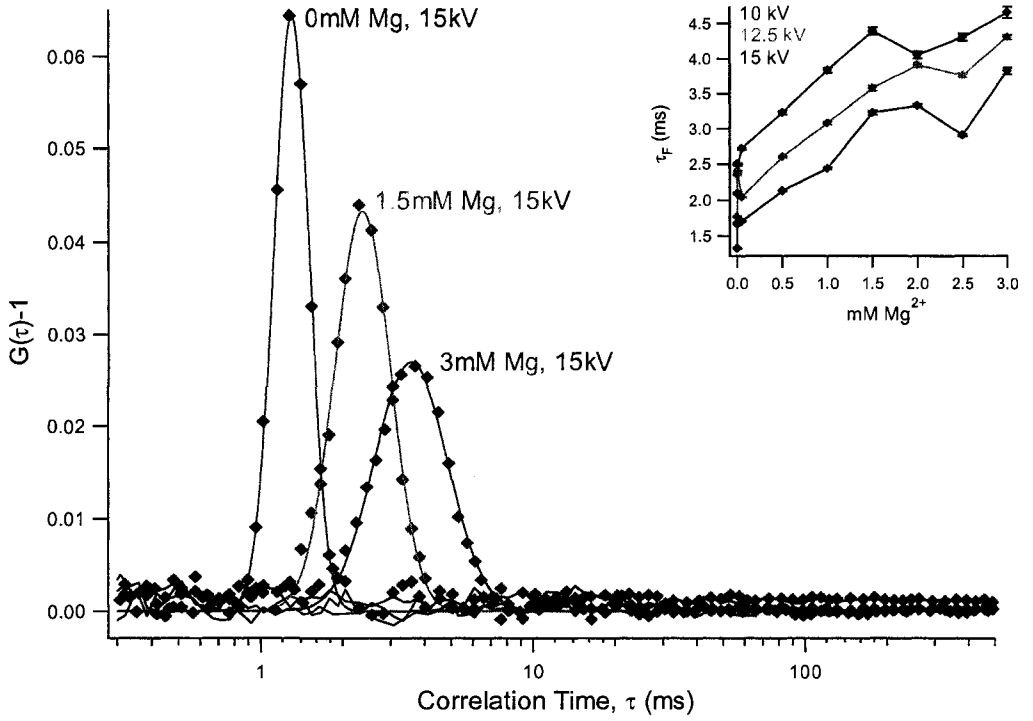

Figure 5.4: Representative "forward" channel cross-correlation experimental data (diamonds) and corresponding fitting curves (solid lines) from polythymine samples at three conditions; 0 mM Mg, 15 kV (red), 1.5 mM Mg, 15 kV (green), and 3 mM Mg, 15 kV (blue). "Blank" cross-correlation from the "reverse" channel can be seen as solid black baselines. The inset is a graph of the τ_F parameter versus magnesium obtained from fitting of cross-correlation data to equation 5.7. The data was taken at 3 different voltages; 10 kV (blue), 12.5 kV (green), and 15 kV (red).

Table 5.1: Parameters Determined from Cross-Correlation Analysis of Representative Data[a,b]

	polythymine		
	0 mM Mg, 15kV	1.5 mM Mg, 15 kV	3 mM Mg, 15 kV
τ_F (ms)	1.3257(82)	3.396(40)	3.935(58)
r	11.94(36)	11.75(36)	10.96(31)
a	0.420(27)	0.634(47)	0.647(47)
τ_d (ms)	0.245(22)	0.215(18)	0.180(15)
standard error[c]	8.81×10^{-5}	4.95×10^{-5}	4.18×10^{-5}

[a] Parameters correspond to the fitting analysis in Figure 3. [b] Values in parentheses are the 95% confidence intervals for the last digits. [c] Standard errors from each curve fitting are estimated using residual sum-of-squares

equation 5.7 are the solid lines. As stated above, all experimentally determined cross-correlation functions appeared in the "forward" channel, indicating that polythymine migrated towards the anode. The "blank" cross-correlation data in the "reverse" channel can be seen as black baselines. The parameters determined from the fits of the three cross-correlation functions depicted in figure 5.4 according to equation 5.7 can be seen in table 5.1. The inset of figure 5.4 depicts the trends in the τ_F parameter determined from the fitting over a range of magnesium concentrations and voltages.

As stated above, τ_F is inversely proportional to the electrophoretic migration velocity of the polythymine. As can be seen in both figure 5.4 and the inset, the rate of polythymine migration decreases with higher magnesium concentration and lower applied electric fields. This is exactly what's expected; at higher concentrations of magnesium, more counterions are expected to associate with polythymine, lowering the effective negative charge and the rate of migration towards the anode. In addition, as can be inferred from equation 5.4, the electrophoretic migration velocity of the polythymine is directly proportional to the electric field strength. Another aspect of figure 5.4 that stands out is that at higher values of τ_F, the cross-correlation functions become "shorter and wider." This is to due to the fact that as the migration time from one laser focus to another grows the polythymine molecules have more time to diffuse away from the direct path in between foci, resulting in fewer molecules being detected in both foci (lowering the height of the peak), and more variability in the transit time due to an increased number of indirect paths taken by the molecules (resulting in

a wider peak). It should be noted that the height of the peak actually depends on two aspects of equation 5.7; the amplitude, a, and the first diffusion term, $(1+\tau/\tau_d)^{-1}$. Thus, while the amplitude values presented in table 5.1 appear to be counterintuitively following the opposite trend expected, differences can be explained as a combination of day to day variation in the focal geometry, concentration, and the importance of the diffusion term.

5.7 Analysis of Diffusion:

Figure 5.5 depicts diffusion constants calculated from parameters determined by cross-correlation and auto-correlation analysis of polythymine samples at a range of magnesium concentrations and electric field strengths. The main graph depicts the diffusion constants versus magnesium on a logarithmic scale, while the inset shows the same graph on a linear scale. Polythymine's diffusion behavior was determined at every concentration of magnesium using four different applied voltages: 0 kV (black), 10 kV (blue), 12.5 kV (green), and 15 kV (red). Calculation of the diffusion constant at 0 kV was done by analysing the τ_d parameter obtained from auto-correlation analysis (Figure 5.6) fit to equation 5.8. Representative experimental auto-correlation data taken at 0 mM Mg and 0 kV can be seen in figure 5.6 (black diamonds) with the theoretical fit calculated from equation 5.8 (red solid line). Calculation of the diffusion constant at non-zero electric fields was done by the analysis of the τ_d

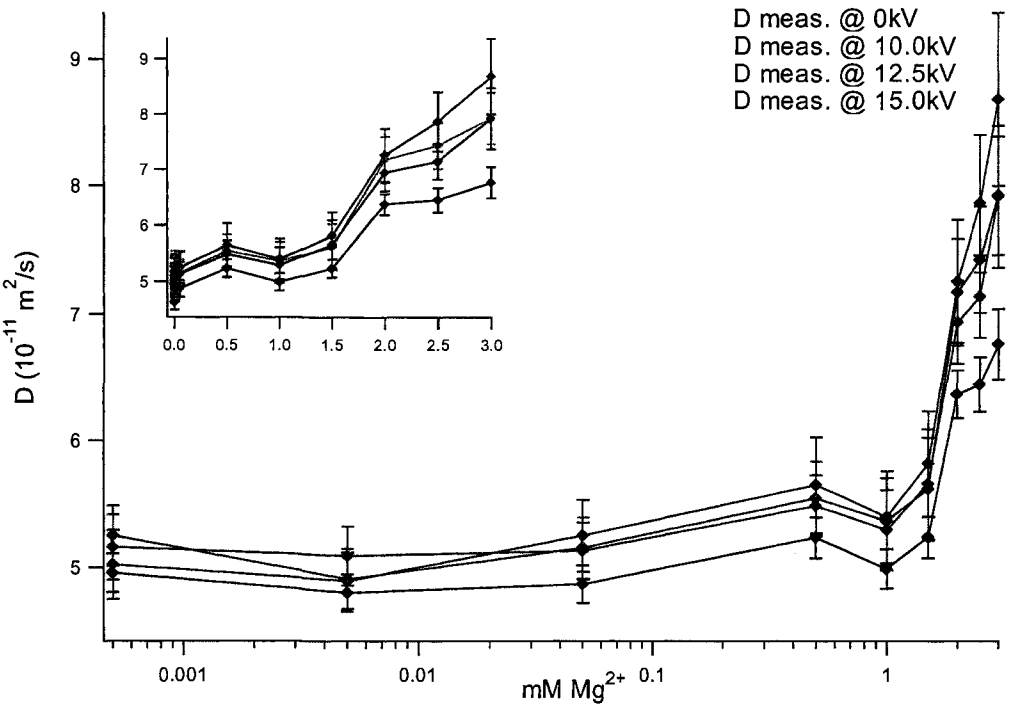

Figure 5.5: Diffusion data versus magnesium concentration at different applied voltages; 0 kV (black), 10 kV (blue), 12.5 kV (green), and 15 kV(red). All diffusion constants were calculated from parameters determined from fitting of auto and cross-correlation data. The main graph depicts the diffusion constant versus magnesium concentration on a logarithmic scale, while the inset depicts the same information on a linear scale.

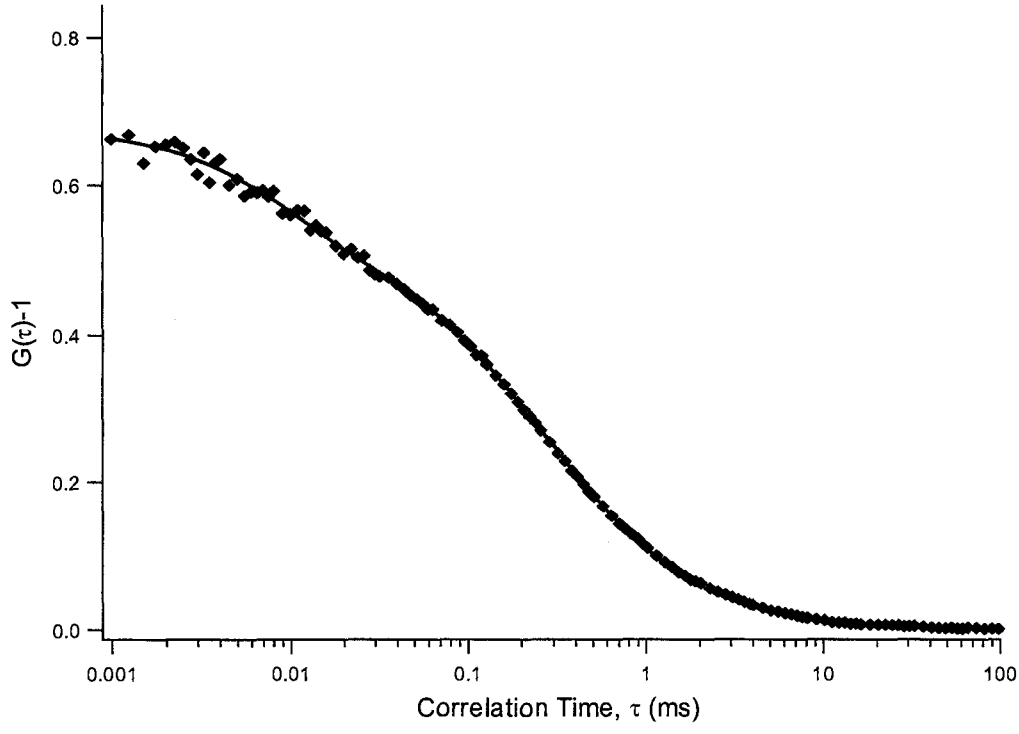

Figure 5.6: Experimental autocorrelation data (black diamonds) and corresponding fitting curve (red solid line) taken from a sample of polythymine at 0 mM Mg and 0 kV. Data was fit to equation 5.8.

Table 5.2: Diffusion Constants and Relevant Parameters[a]

	polythymine		
	0 mM Mg, 15kV	1.5 mM Mg, 15 kV	3 mM Mg, 15 kV
ω_0 (μm)[b]	0.2197(33)	0.2197(33)	0.2384(48)
D (10^{-7} cm^2/s)[c]	4.94(31)	5.66(43)	7.92(55)
V_{EOF} (10^{-5} m/s)[d]	6.68(14)	5.66(12)	6.31(14)
E (10^5 V/m)[e]	6.20(57)	6.44(63)	6.44(63)
μ_{DNA} (10^{-8} $m^2/V \cdot s$)[f]	3.04(29)	1.10(11)	0.935(95)
q_{eff} (e-)[g]	15.5(17)	4.90(62)	2.99(37)

[a]Values in parentheses are the 95% confidence intervals for the last digits. [c]Obtained from auto-correlation analysis of standard TAMRA solutions. [d]Calculated according to the equation, $D = \omega_0^2/(4\tau_d)$. [e]Obtained from EOF control experiments. [f]Obtained from applied voltage divided by length of capillary. [g]Calculated using equation 5.9. [h]Calculated using equation 3.

parameters obtained from cross-correlation fitting according to equation 5.7. Recall that the diffusion constant is related to τ_d by the expression, $D = \omega_0^2/(4\tau_d)$. The value for the focal radius, ω_0, used in the calculation was obtained from analysis of a standard TAMRA solution. Table 5.2 shows representative values for ω_0, and D.

Upon quick inspection of figure 5.5, one notices two trends; higher magnesium concentrations yield higher rates of diffusion for polythymine, and an apparent voltage dependence of the diffusion constant, which is more pronounced at higher concentrations of magnesium. Magnesium appears to have relatively little effect on the diffusion of polythymine at lower concentrations (<1 mM Mg), but at higher concentrations, the rate of diffusion of polythymine rapidly increases. Previous studies have shown that as small counterion concentration increases, negative charges on the backbone of the single-stranded DNA are neutralized, lowering its self repulsion, which allows it to adopt more compact structures with higher diffusion constants[9, 56-59].

The other trend that is visible in figure 5.5 is the dependence of the diffusion constant on electric field strength, which becomes more pronounced at higher concentrations of magnesium. This trend seems to contradict several studies which have indicated that DNA diffusion is independent of electric field strength[23, 27, 44]. One possibility is that the electric fields used in this experiment caused significant joule heating, which would raise the magnitude of the diffusion constants. While this is a possibility, control experiments were performed (data not shown) which monitored the molecular brightness of the R6G dye attached to

the polythymine at the range of field strengths used in the experiment. Studies have shown that the molecular brightness of fluorescent dyes decrease with increasing temperature, and can be used to monitor the temperature inside of capillaries during electrophoresis[60, 61]. These control experiments indicated no significant decreases or trends in the molecular brightness of the dye label at different field strengths.

Additional temperature-based control experiments performed on a steady-state fluorometer confirmed that the R6G label's brightness is sensitive to temperature, further corroborating the evidence that joule heating did not have a significant impact on the calculation of the diffusion constants. Finally, the diffusion data presented in figure 5.5 shows the most pronounced increase in diffusion constant for the lowest electric field strength used in the experiments, while the highest field strengths yielded diffusion data closest to the values obtained at zero electric field strength. If the differences in diffusion were due to increases in temperature, one would expect to see the highest electric field strengths yield the highest rates of diffusion.

This is not to say the joule heating was not a possible cause for the electric field dependence of the diffusion constant. While R6G's brightness has been shown to be dependent on temperature, it is possible that the temperature of the samples did not vary enough to significantly impact the R6G brightness. In addition, the diffusion constant is related to the temperature according to the equation, $D = k_B T / 6\pi\eta R_H$, where k_B is the Boltzmann constant, T is the temperature, η is the solvent viscosity, and R_H is the hydrodynamic radius. In this

equation, both the solvent viscosity and hydrodynamic radius (or equivalent volume the polythymine occupies in solution) are also affected by the temperature. This means that the effect of temperature on diffusion at different field strengths is much more complicated than a simple directly proportional relationship. More work will have to be done to determine the possible impact of joule heating on the diffusion information found for polythymine. For the purposes of data analysis throughout the rest of the chapter, it will be assumed that the joule heating was negligible.

Our experimentally determined diffusion constants for 40-base polythymine were found to range from $4.63 \pm 0.14 \times 10^{-7}$ cm^2/s to $8.68 \pm 0.68 \times 10^{-7}$ cm^2/s, which agreed well with previous studies of similar sized single-stranded DNA[9, 23, 28, 62].

5.8 Analysis of Effective Charge:

Figure 5.7 shows the relationship between the effective charge of the polythymine and the concentration of magnesium counterions present in the sample buffer. The main graph shows the impact of magnesium on effective charge on a logarithmic scale, while the inset is the same graph on a linear scale. All of the information used to calculate effective charge was determined from cross-correlation analysis and control experiments. As stated previously, the two key parameters needed to calculate the effective charge of polythymine are the

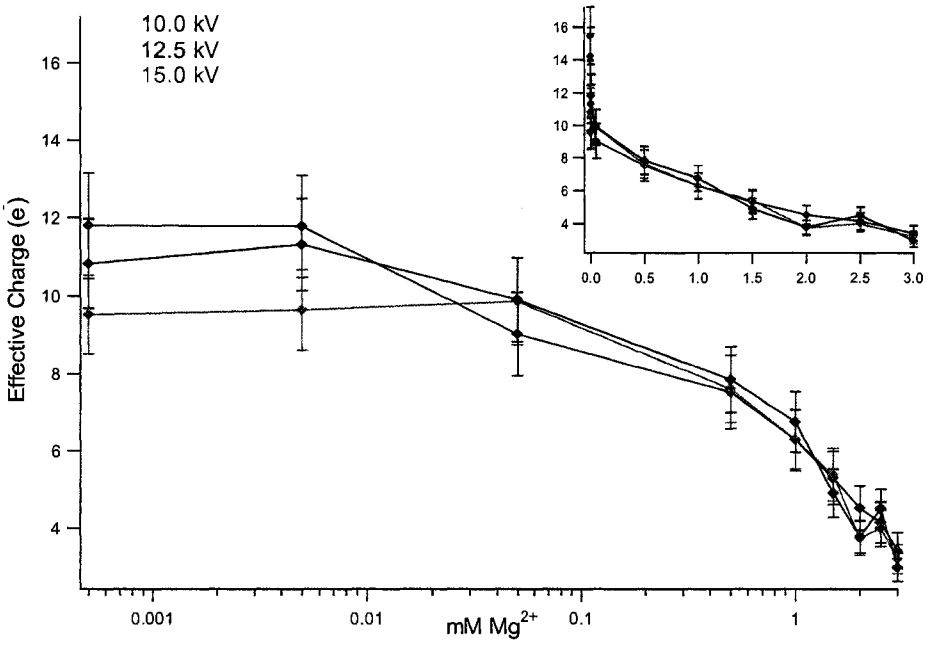

Figure 5.7: Effective charge in units of elementary charge versus magnesium concentration. Effective charge information was calculated from parameters obtained from fitting cross-correlation data and from control experiments at three different voltages; 10 kV (blue), 12.5 kV (green), and 15 kV (red). The main graph depicts effective charge versus magnesium on a logarithmic scale, and the inset depicts the same information on a linear scale.

diffusion constant and the electrophoretic mobility. The electrophoretic mobility of the polythymine was determined using the equation:

$$\mu_{DNA} = \frac{(\tau_F \omega_0 / r) - V_{EOF}}{E} \tag{5.9}$$

The parameters τ_F and r were determined from fitting the cross-correlation data to equation 5.7, ω_0 and V_{EOF} were determined from control experiments described previously, and E was determined from the potential applied across the capillary and the length of the capillary. It should be noted that $V_x = \tau_F \omega_0 / r$, and that polythymine migrated against EOF. Once the electrophoretic mobility of the polythymine is known, the effective charge can be calculated using equation 5.3. Representative data used to obtain the effective charge information in figure 5.7 can be seen in table 5.2. Upon first glance, figure 5.7 appears to be an almost mirror image of figure 5.5, with the effective charge becoming smaller as the diffusion constant grows larger. Closer inspection reveals a subtle difference; while the diffusion constant starts to significantly change at magnesium concentrations over 1 mM, it appears that the effective charge starts significantly dropping before that, at about 0.5 mM Mg. This would seem to indicate that, as theorized, magnesium counterions associate with and neutralize polythymine's negatively charged backbone, which allows it to overcome self-repulsion and adopt more compact configurations. Another interesting observation is that the effective charge seems intuitively to be quite low for a polythymine with 40 negative charges along its backbone. Even at zero magnesium concentration, the background electrolytes of 3 mM Tris and glycine present in the sample

buffer effectively neutralize about half of the charge on the polythymine backbone. Ideally, experiments could have been performed without the background electrolytes. Unfortunately, it was found that the fluorescent signal was too unstable at extremely low ionic strengths, which was assumed to be due to increased wall interactions of polythymine under such conditions. Electrophoretic mobilities calculated using equation 5.9 varied from 0.935 ± 0.095 X 10^{-4} cm^2/Vs to 3.04 ± 0.29 cm^2/Vs, which agreed well with results obtained from previous studies[23, 44, 63]. The agreement between our experimentally determined diffusion constants and electrophoretic mobilities and those found elsewhere bodes well for the accuracy of our effective charge data.

5.9 Conclusions:

In summary, it has been demonstrated that 2bFCCS-CFCE can be used to determine the effective charge of single-stranded DNA in the presence of magnesium. Knowledge concerning the effective charge of biological macromolecules yields important insight into the important role that small counterions play in their structure and function. The advantage that 2bFCCS-CFCE has over other electrophoresis techniques in this area is its ability to simultaneously monitor diffusion and electrophoretic migration. It was found that the diffusion of the single-stranded DNA varied with electric field strength, possibly due to fluctuations in the DNA's ionic atmosphere. In addition, it was

found that increasing magnesium concentration increased the rate of DNA diffusion while also lowering the effective charge. This result indicates that neutralization of the negative charges on the single-stranded DNA's backbone allow it to overcome self-repulsion to adopt more compact conformations.

Future work includes using simultaneous analysis of auto-correlation, photon counting histogram[64], and cross-correlation, and extending the temporal resolution of the techniques into the nanosecond regime. Accomplishing this would allow for the simultaneous measurement of temperature and cross-correlation data, which might explain the diffusion constant's dependence on electric field strength. Another topic of continued interest is more thorough interrogation of the ionic atmosphere at lower timescales, potentially leading to a comprehensive study of DNA-counterion kinetics. Investigation of dye-quencher interactions on specifically labeled biological macromolecules can also provide a potential window into the impact of ionic atmosphere on the active conformations of proteins, DNA, and RNA.

1. Warshel, A.; Sharma, P. K.; Kato, M.; Parson, W. W., Modeling electrostatic effects in proteins. *Biochimica et Biophysica Acta, Proteins and Proteomics* **2006,** 1764, (11), 1647-1676.

2. Honig, B.; Sharp, K.; Yang, A. S., Macroscopic models of aqueous solutions: biological and chemical applications. *Journal of Physical Chemistry* **1993,** 97, (6), 1101-9.

3. Orozco, M.; Luque, F. J., Theoretical Methods for the Description of the Solvent Effect in Biomolecular Systems. *Chemical Reviews (Washington, D. C.)* **2000,** 100, (11), 4187-4225.

4. Misra, V. K.; Draper, D. E., On the role of magnesium ions in RNA stability. *Biopolymers* **1998,** 48, (2-3), 113-135.

5. Misra, V. K.; Draper, D. E., Mg2+ Binding to tRNA Revisited: The Nonlinear Poisson-Boltzmann Model. *Journal of Molecular Biology* **2000,** 299, (3), 813-825.

6. Draper, D. E., A guide to ions and RNA structure. *Rna* **2004,** 10, (3), 335-343.

7. Nakamura, H., Roles of electrostatic interaction in proteins. *Quarterly Reviews of Biophysics* **1996,** 29, (1), 1-90.

8. Anderson, C. F.; Record, M. T., Jr., Salt-nucleic acid interactions. *Annual Review of Physical Chemistry* **1995,** 46, 657-700.

9. Doose, S.; Barsch, H.; Sauer, M., Polymer properties of polythymine as revealed by translational diffusion. *Biophysical Journal* **2007,** 93, (4), 1224-1234.

10. Zhang, Y.; Huang, K. X., On the interactions of hydrated metal cations (Mg2+, Mn2+, Ni2+, Zn2+) with guanine-cytosine Watson-Crick and guanine-guanine reverse-Hoogsteen DNA base pairs. *Journal Of Molecular Structure-Theochem* **2007,** 812, (1-3), 51-62.

11. Petrov, A. S.; Pack, G. R.; Lamm, G., Calculations of Magnesium-Nucleic Acid Site Binding in Solution. *Journal of Physical Chemistry B* **2004,** 108, (19), 6072-6081.

12. Sundaresan, N.; Pillai, C. K. S.; Suresh, C. H., Role of Mg2+ and Ca2+ in DNA bending: Evidence from an ONIOM-based QM-MM study of a DNA fragment. *Journal Of Physical Chemistry A* **2006,** 110, (28), 8826-8831.

13. Munoz, J.; Sponer, J.; Hobza, P.; Orozco, M.; Luque, F. J., Interactions of hydrated Mg2+ cation with bases, base pairs, and nucleotides. Electron topology,

natural bond orbital, electrostatic, and vibrational study. *Journal Of Physical Chemistry B* **2001,** 105, (25), 6051-6060.

14. Subirana, J. A.; Soler-Lopez, M., Cations as hydrogen bond donors: A view of electrostatic interactions in DNA. *Annual Review Of Biophysics And Biomolecular Structure* **2003,** 32, 27-45.

15. Landers, J. P., Ed., *Handbook of Capillary Electrophoresis*. 2nd ed.; CRC Press: Boca Raton, 1997; p 894.

16. Foret, F.; Deml, M.; Bocek, P., Capillary zone electrophoresis. Quantitative study of the effects of some dispersive processes on the separation efficiency. *Journal of Chromatography* **1988,** 452, 601-13.

17. Ali, I.; Aboul-Enein, H. Y.; Gupta, V. K., Precision in capillary electrophoresis. *Analytical Letters* **2006,** 39, (11), 2345-2357.

18. Huang, X.; Coleman, W. F.; Zare, R. N., Analysis of factors causing peak broadening in capillary zone electrophoresis. *Journal of Chromatography* **1989,** 480, 95-110.

19. Roberts, G. O.; Rhodes, P. H.; Synder, R. S., Dispersion effects in capillary zone electrophoresis. *Journal of Chromatography* **1989,** 480, 35-67.

20. Mayer, B. X., How to increase precision in capillary electrophoresis. *Journal of Chromatography, A* **2001,** 907, (1-2), 21-37.

21. Schaeper, J. P.; Sepaniak, M. J., Parameters affecting reproducibility in capillary electrophoresis. *Electrophoresis* **2000,** 21, (7), 1421-1429.

22. Walbroehl, Y.; Jorgenson, J. W., Capillary zone electrophoresis for the determination of electrophoretic mobilities and diffusion coefficients of proteins. *Journal of Microcolumn Separations* **1989,** 1, (1), 41-5.

23. Nkodo, A. E.; Garnier, J. M.; Tinland, B.; Ren, H.; Desruisseaux, C.; McCormick, L. C.; Drouin, G.; Slater, G. W., Diffusion coefficient of DNA molecules during free solution electrophoresis. *Electrophoresis* **2001,** 22, (12), 2424-2432.

24. Yao, Y. J.; Li, S. F. Y., Determination of diffusion coefficients by capillary zone electrophoresis. *Journal of Chromatographic Science* **1994,** 32, (4), 117-20.

25. Kenndler, E.; Schwer, C., Nondependence of diffusion-controlled peak dispersion on diffusion coefficient and ionic mobility in capillary zone electrophoresis without electroosmotic flow. *Analytical Chemistry* **1991,** 63, (21), 2499-502.

26. Maichel, B.; Gas, B.; Kenndler, E., Diffusion coefficient and capacity factor in capillary electrokinetic chromatography with replaceable charged polymeric pseudophase. *Electrophoresis* **2000,** 21, (8), 1505-1512.

27. Stellwagen, N. C.; Magnusdottir, S.; Gelfi, C.; Righetti, P. G., Measuring the translational diffusion coefficients of small DNA molecules by capillary electrophoresis. *Biopolymers* **2001,** 58, (4), 390-397.

28. Stellwagen, E.; Stellwagen, N. C., Determining the electrophoretic mobility and translational diffusion coefficients of DNA molecules in free solution. *Electrophoresis* **2002,** 23, (16), 2794-2803.

29. Stellwagen, N.; Gelfi, C.; Righetti, P. G., The use of gel and capillary electrophoresis to investigate some of the fundamental physical properties of DNA. *Electrophoresis* **2002,** 23, (2), 167-175.

30. Muijselaar, P. G.; van Straten, M. A.; Claessens, H. A.; Cramers, C. A., Determination of diffusion coefficients and separation numbers in micellar electrokinetic chromatography. *Journal of Chromatography, A* **1997,** 766, (1 + 2), 187-195.

31. Ware, B. R.; Flygare, W. H., Simultaneous measurement of the electrophoretic mobility and diffusion coefficient in bovine serum albumin solutions by light scattering. *Chem. Phys. Letters* **1971,** 12, (1), 81-5.

32. Ware, B. R.; Flygare, W. H., Light scattering in mixtures of BSA [bovine serum albumin], BSA dimers, and fibrinogen under the influence of electric fields. *J. Coll. Interf. Sci.* **1972,** 39, (3), 670-5.

33. Semenov, S. N., Correlation analysis of fluctuations in continuous observation of electrophoresis. *Zhurnal Fizicheskoi Khimii* **1995,** 69, (11), 2070-3.

34. Castro, A.; Shera, E. B., Single-Molecule electrophoresis. *Analytical Chemistry* **1995,** 67, (18), 3181-6.

35. Shortreed, M. R.; Li, H.; Huang, W.-H.; Yeung, E. S., High-Throughput Single-Molecule DNA Screening Based on Electrophoresis. *Analytical Chemistry* **2000,** 72, (13), 2879-2885.

36. Anazawa, T.; Matsunaga, H.; Yeung, E. S., Electrophoretic quantitation of nucleic acids without amplification by single-molecule imaging. *Analytical Chemistry* **2002,** 74, (19), 5033-5038.

37. Lee, J.-y.; Li, H.-W.; Yeung, E. S., Single-molecule spectroscopy for molecular identification in capillary electrophoresis. *Journal of Chromatography, A* **2004,** 1053, (1-2), 173-179.

38. Van Orden, A.; Keller, R. A., Fluorescence Correlation Spectroscopy for Rapid Multicomponent Analysis in a Capillary Electrophoresis System. *Analytical Chemistry* **1998,** 70, (21), 4463-4471.

39. Brinkmeier, M.; Doerre, K.; Stephan, J.; Eigen, M., Two-beam cross-correlation. A method to characterize transport phenomena in micrometer-sized structures. *Analytical Chemistry* **1999,** 71, (3), 609-616.

40. LeCaptain, D. J.; Michel, M. A.; Van Orden, A., Characterization of DNA-protein complexes by capillary electrophoresis-single molecule fluorescence correlation spectroscopy. *Analyst* **2001,** 126, (8), 1279-1284.

41. LeCaptain, D. J.; Van Orden, A., Two-beam fluorescence cross-correlation spectroscopy in an electrophoretic mobility shift assay. *Analytical Chemistry* **2002,** 74, (5), 1171-1176.

42. Fogarty, K.; Van Orden, A., Two-beam fluorescence cross-correlation spectroscopy for simultaneous analysis of positive and negative ions in continuous-flow capillary electrophoresis. *Analytical Chemistry* **2003,** 75, (23), 6634-6641.

43. Sonehara, T.; Kojima, K.; Irie, T., Fluorescence Correlation Spectroscopy Excited with a Stationary Interference Pattern for Capillary Electrophoresis. *Analytical Chemistry* **2002,** 74, (19), 5121-5131.

44. Bayer, J.; Raedler, J. O., DNA microelectrophoresis using double focus fluorescence correlation spectroscopy. *Electrophoresis* **2006,** 27, (20), 3952-3963.

45. Schiro, P. G.; Kuyper, C. L.; Chiu, D. T., Continuous-flow single-molecule CE with high detection efficiency. *Electrophoresis* **2007,** 28, (14), 2430-2438.

46. Brister, P. C.; Weston, K. D., Evaluation of two-beam fluorescence cross correlation spectroscopy for electrophoretic analysis of protein digests. *Analyst (Cambridge, United Kingdom)* **2006,** 131, (2), 303-310.

47. Brinkmeier, M.; Rigler, R., Flow analysis by means of fluorescence correlation spectroscopy. *Exp. Techn. Phys.* **1995,** 41, (2), 205-210.

48. Gao, Q.; Yeung, E. S., A matrix for DNA separation: genotyping and sequencing using poly(vinylpyrrolidone) solution in uncoated capillaries. *Analytical Chemistry* **1998,** 70, (7), 1382-1388.

49. Belder, D.; Deege, A.; Husmann, H.; Koehler, F.; Ludwig, M., Cross-linked poly(vinyl alcohol) as permanent hydrophilic column coating for capillary electrophoresis. *Electrophoresis* **2001,** 22, (17), 3813-3818.

50. Huang, X.; Gordon, M. J.; Zare, R. N., Current-monitoring method for measuring the electroosmotic flow rate in capillary zone electrophoresis. *Analytical Chemistry* **1988,** 60, (17), 1837-8.

51. Brinkmeier, M., Cross-correlated flow analysis in microstructures. In *Fluorescence Correlation Spectroscopy: Theory and Applications*; Elson, E. S., Ed. Springer: Berlin, 2001; Vol. 65, pp 379-395.

52. Jung, J.; Van Orden, A., Folding and Unfolding Kinetics of DNA Hairpins in Flowing Solution by Multiparameter Fluorescence Correlation Spectroscopy. *Journal of Physical Chemistry B* **2005,** 109, (8), 3648-3657.

53. Shack, J.; Bynum, B. S., Interdependence Of Variables In Activation Of Deoxyribonuclease 1. *Journal Of Biological Chemistry* **1964,** 239, (11), 3843-&.

54. Shack, J.; Bynum, B. S., Determination Of The Interaction Of Deoxyribonucleate And Magnesium Ions By Means Of A Metal Ion Indicator. *Nature* **1959,** 184, (4686), 635-636.

55. Shack, J., Influence Of Sodium And Magnesium Ions On The Action Of Deoxyribonuclease-Ii. *Journal Of Biological Chemistry* **1959,** 234, (11), 3003-3006.

56. Murphy, M. C.; Rasnik, I.; Cheng, W.; Lohman, T. M.; Ha, T. J., Probing single-stranded DNA conformational flexibility using fluorescence spectroscopy. *Biophysical Journal* **2004,** 86, (4), 2530-2537.

57. Tinland, B.; Pluen, A.; Sturm, J.; Weill, G., Persistence length of single-stranded DNA. *Macromolecules* **1997,** 30, (19), 5763-5765.

58. Caliskan, G.; Hyeon, C.; Perez-Salas, U.; Briber, R. M.; Woodson, S. A.; Thirumalai, D., Persistence length changes dramatically as RNA folds. *Physical Review Letters* **2005,** 95, (26).

59. Mills, J. B.; Vacano, E.; Hagerman, P. J., Flexibility of single-stranded DNA: Use of gapped duplex helices to determine the persistence lengths of poly(dT) and poly(dA). *Journal Of Molecular Biology* **1999,** 285, (1), 245-257.

60. Xuan, X. C.; Xu, B.; Sinton, D.; Li, D. Q., Electroosmotic flow with Joule heating effects. *Lab On A Chip* **2004,** 4, (3), 230-236.

61. Ross, D.; Gaitan, M.; Locascio, L. E., Temperature measurement in microfluidic systems using a temperature-dependent fluorescent dye. *Analytical Chemistry* **2001,** 73, (17), 4117-4123.

62. Stellwagen, E.; Lu, Y.; Stellwagen, N. C., Unified Description of Electrophoresis and Diffusion for DNA and Other Polyions. *Biochemistry* **2003,** 42, (40), 11745-11750.

63. Dong, Q.; Stellwagen, E.; Dagle, J. M.; Stellwagen, N. C., Free solution mobility of small single-stranded oligonucleotides with variable charge densities. *Electrophoresis* **2003,** 24, (19-20), 3323-3329.

64. Chen, Y.; Muller, J. D.; So, P. T. C.; Gratton, E., The photon counting histogram in fluorescence fluctuation spectroscopy. *Biophysical Journal* **1999,** 77, (1), 553-567.

Chapter 6: Conclusion and Future Directions

In this dissertation, work towards the development of two-beam fluorescence cross-correlation spectroscopy coupled with continuous-flow capillary electrophoresis (2bFCCS-CFCE) was presented. The technique of 2bFCCS-CFCE has the potential to be a powerful addition to capillary electrophoresis analytical techniques. The work presented here demonstrated three applications of 2bFCCS-CFCE that illustrate the advantages this technique has over conventional electrophoresis techniques. All of the techniques showed promise for future development and application of 2bFCCS-CFCE in a variety of fields.

The first demonstration of 2bFCCS-CFCE elucidated the technique's ability to monitor ions migrating in opposite directions in continuous electrophoretic flow. This was a measurement incapable of being made on conventional capillary electrophoresis (CE) instrumentation. Conventional CE requires macroscopic separation of analytes in order to perform analysis. The technique of 2bFCCS-CFCE overcomes the requirement for macroscopic separation by monitoring the migration of fluorescently labeled analyte species

between two spatially separated laser focal regions. The cross-correlation data generated by this technique is conceptually similar to the electrophoretic peaks of conventional CE data, in that the migration time of analytes between two points is monitored. The ability of 2bFCCS-CFCE to perform electrophoretic analysis without the requirement of macroscopic separation eliminates the complex buffer conditions and sample injection steps required for conventional CE.

Another advantage is that cross-correlation analysis can operate in two modes simultaneously. Fluorescent molecules migrating from the first to the second laser beam, or migrating in a forward direction, contribute to cross-correlation data found in the "forward channel." The forward channel is only sensitive species which migrate in the forward direction. Conversely, if the molecules are migrating in the reverse direction, or from laser beam two to laser beam one, they contribute to cross-correlation data in the "reverse channel." The reverse channel is only sensitive species which migrate in the reverse direction. The two channels of cross-correlation analysis are capable of monitoring the migration of analytes in opposite directions, independently of one another. Conventional CE is not capable of making this measurement, because the requirement of macroscopic separation necessitates the placement of a detection region downstream of the sample injection point. Conventional CE, therefore, is only capable of detecting analytes flowing in one direction.

The ability of 2bFCCS-CFCE to continuously monitor ions migrating in opposite directions was successfully demonstrated. The analysis was performed on a three-component mixture containing the cation Rhodamine 6G (R6G) and

the anions tetramethyl-6-carboxyrhodamine (TAMRA) and TAMRA labeled poly(dT)$_{39}$ single stranded DNA (TAMRA-ssDNA) in aqueous buffer solution. The TAMRA and TAMRA-ssDNA contributed to two cross-correlation peaks in the forward channel of the cross-correlation analysis. The R6G contributed to cross-correlation data in the reverse channel of the cross-correlation analysis. Besides being able to determine the individual migration velocities of the three components, 2bFCCS-CFCE analysis was able to determine relative concentrations and diffusion coefficients for the three respective species. The ability of 2bFCCS-CFCE to discern the diffusion information of the species illustrates another advantage of the technique relative to conventional CE analysis. Conventional CE is not able to determine diffusion information due to sample dispersion effects caused by different experimental features such as sample injection, analyte-wall interactions, joule heating, and variable electroosmotic flow (EOF). Thus the technique of 2bFCCS-CFCE was not only able to perform analysis under conditions not accessible to conventional CE analysis, it was also able to discern information about the sample molecules inaccessible to conventional CE.

The work presented in chapter three illustrated the analytical advantages that 2bFCCS-CFCE has relative to traditional CE techniques, in the next chapter work was demonstrated that illustrated the possible design advantages 2bFCCS-CFCE has over conventional microchip capillary electrophoresis (MCCE) techniques. As was demonstrated in chapter three, 2bFCCS-CFCE is capable of performing electrophoretic analysis on ions migrating in multiple directions, in

continuous solution, over the distance of a few microns. These advantages led to the development of 2bFCCS-CFMCCE, or two-beam cross-correlation analysis performed on electrophoresis microchips. The development of electrophoresis on microchips is driven by two concepts; miniaturization, or the ability to perform analysis on smaller sample sizes, and device integration, or the ability to incorporate MCCE into more complex devices. While there has been much promising work on the development of MCCE, the technique ultimately suffers from the need for macroscopic separation of sample components. The need for macroscopic separation necessitates the use of multiple different buffers in order to perform analysis, which adds to the complexity of fluid-handling requirements on-chip. In addition, the requirement of macroscopic separation limits the miniaturization capabilities of MCCE in that a minimum separation distance is required. Because 2bFCCS-CFMCCE can perform analysis in homogeneous solution, over the distance of a few microns, it has the potential to be a much more flexible microchip analysis technique than conventional MCCE.

The first 2bFCCS-CFMCCE analysis was performed on polydimethylsiloxane (PDMS) microchips. This material was chosen due to the relative ease of fabrication of microchips from this material. 2bFCCS-CFMCCE was demonstrated on two different PDMS microchip designs. One design was the "T-chip" design format used for the majority of conventional MCCE applications. This proof-of-concept experiment demonstrated the analysis of the same three-component mixture used in chapter three. While the migration velocities and relative concentrations of the three components were measured

effectively, the diffusion information obtained was anomalously slow. This was thought to be due to wall interactions between the analyte molecules and the PDMS substrate.

The second microchip format studied illustrated the design advantages available to 2bFCCS-CFMCCE in comparison with conventional MCCE. The single channel, 1 cm separation channel format was both simpler and smaller than the prototypical MCCE microchip. The analysis of a two-component TAMRA/R6G mixture was demonstrated on this second chip. A different coating (polybrene) was used in this second microchip to try to alleviate the problems with wall-interactions experienced in the first chip. These experiments successfully demonstrated the measurement of relative concentration, migration velocity, and diffusion on a microchip format unamenable to conventional MCCE analysis. Unfortunately it was found in future experiments on PDMS microchips that it was difficult to obtain reproducible results with low background noise. This was thought to be due to the material used to make the microchip, PDMS, which does not illustrate surface properties as uniform as glass. For this reason, future 2bFCCS-CFMCCE experiments were performed on glass microchips.

The glass microchips used consisted of two formats. One format was a 44 microchannel chip with 1 mm length channels, while the other was of the same dimensions as the single-channel PDMS chip. The 44 microchannel chip was fabricated in a 1X1 in^2 area, which demonstrated even further the design benefits afforded by 2bFCCS-CFMCCE. Unfortunately, the design features of the chip that took advantage of flexibility of 2bFCCS-CFMCCE also added a

degree of difficulty to the fluid handling necessary for use of the chip. While brief glimpses of cross-correlation data were seen on this chip, ultimately artifacts related to the fluid handling, such as bubbles and sample evaporation, limited our ability to use this chip. In addition, the fabrication of the 44 microchannel chip was particularly laborious, and so it was deemed wise to switch to simpler glass microchip formats to both ease fluid handling requirements and speed fabrication of chips. Experiments performed on the single-channel glass microchips were much more promising than those performed on the 44-channel chips. Cross-correlation data was obtained that exhibited expected trends. Unfortunately, theoretical analysis of the cross-correlations peaks obtained on the glass microchip proved to yield nonsensical values for various parameters. This was thought to be due to an artifact of the glass microchip fabrication process. The coverslips through which the two-laser beams were focused had been subjected to thermal bonding at high temperature. The thermal bonding process often produced distortions in the coverslip surfaces that negatively impacted the geometry of the laser foci, rendering inapplicable the theoretical models used for data-fitting.

The results of the 2bFCCS-CFMCCE experiments were ultimately a mixed bag. Results were obtained that illustrated the promise of the technique for expanding the design and analysis capabilities of MCCE, but it proved difficult to produce such results reproducibly. In addition, more elegant approaches to fabrication of and fluid handling in microchips would have made further development of 2bFCCS-CFMCCE much more practical. It was ultimately

decided to switch focus back to 2bFCCS-CFCE on fused silica capillaries due to ease-of-use. In the ensuing experiments, the ability of 2bFCCS-CFCE to measure the effective charge of 40-oligo poly(dT) single-stranded DNA (polythymine) labeled at the 5' end with Rhodamine 6G (R6G-ssDNA) was demonstrated.

In CE-based techniques, the electrophoretic mobility of species is related to their size and charge. 2bFCCS-CFCE, unlike conventional CE, is capable of simultaneously measuring both a species' electrophoretic mobility and its size. This allows for the possibility of measuring the charge of an analyte molecule in solution. The charge measured in such a manner is not the chemical charge of the molecule (40^- for the R6G-ssDNA), but rather an "effective" charge that is dependent on the number of oppositely-charged ions, or counterions, closely associated with the analyte species in solution. Determination of effective charge, therefore, can elucidate the quantity of counterions associated with the analyte molecule in solution. Monitoring both the size and effective charge can also illuminate the effects counterions have on the conformation of polyelectrolytes such as DNA. 2bFCCS-CFCE's unique capabilities make it the only CE technique of performing such a measurement.

The model system chosen for study was the magnesium-ssDNA interaction. This system was chosen because magnesium has been shown to have an important role in the conformation and behavior of DNA in biological systems. Our goal was to measure the diffusion and migration velocity of DNA at various concentrations of magnesium and at a variety of electric field strengths.

From this information and the temperature the electrophoretic mobility and effective charge information could be calculated. An experimental determination of the effective charge of DNA in relation to magnesium concentration has never been previously demonstrated, and it was hoped our technique could shed some valuable light on the magnesium-DNA interaction. It was also hoped that the concentration and electric field dependence of the interaction might shed some light on the strength of magnesium-DNA interactions.

Chapter five reports the results of the magnesium-DNA study by 2bFCCS-CFCE analysis. The measured change in DNA diffusion and effective charge with magnesium concentration showed some interesting trends. The effective charge of the R6G-ssDNA appeared to be more susceptible to low concentrations of magnesium than the diffusion constant. This led to a hypothesis that a certain "charge threshold" exists at which the R6G-ssDNA is able to begin adopting more compact conformations. In other words, a minimum number of magnesium counterions must associate closely with the ssDNA before it can fold into compact structures. Below this threshold, the negative charges on the DNA backbone are too self-repulsive to allow the DNA to fold, and the DNA is much more likely to be in a long drawn-out conformation with minimal contortions. As stated before, this was the first time that such a measurement has been demonstrated, and it was a measurement uniquely suited to 2bFCCS-CFCE.

Although the results were very promising, there remains one experimental hurdle to leap before the results are ready for publication in scientific journals.

Measurements of the diffusion of R6G-ssDNA in an electric field showed a voltage dependence. This was thought to be due to joule heating of the sample solution during electrophoresis. Control experiments that attempted to determine the higher temperature caused by joule heating were inconclusive. In order to calculate the effective charge accurately, the temperature of the solutions must be found.

The work presented in this dissertation shows the immense potential of 2bFCCS-CFCE as electrophoresis analysis technique. Much progress was made in the development of new applications of 2bFCCS-CFCE, but ultimately the technique is still in its infancy. There are multiple possible future directions for 2bFCCS-CFCE in the work presented in this dissertation as well as in areas outside the scope of this dissertation.

The development of 2bFCCS-CFMCCE, or 2bFCCS-CFCE on microchips, showed much promise, but ultimately was abandoned due to logistical difficulties in the implementation. The relative inexperience of our group in the field of microchip fabrication meant that finding the optimal conditions for microchip fabrication and use was a laborious and time-consuming process. In addition, methodologies for fluid handling and application of polymer treatments to microchips were primitive at best. Our emphasis was on performing the measurements rather than on designing the microchip platforms. If, on the other hand, the focus was shifted towards microchip platform design, fabrication and fluid handling, perhaps conditions could be found where the full analytical power of 2bFCCS-CFMCCE could be realized. In addition, only microchips constructed

of glass and PDMS were used. Perhaps other materials, such as poly(methyl methacrylate) (PMMA), would be better suited for 2bFCCS-CFMCCE.

Another route for the improvement of the 2bFCCS-CFCE technique is to expand the data analysis options of the technique by simultaneous measurement of auto-correlation, cross-correlation, photon counting histogram (PCH) and fast-timescale correlation. While the only measurements presented in this dissertation are the two-beam cross-correlation or single-beam auto-correlation analyses performed individually, it is possible to perform simultaneous single-beam auto-correlation analysis on each of the two beams while cross-correlation analysis is also performed. In addition, it is also possible to simultaneously perform photon counting histogram analysis on the fluorescent time traces of the two individual beams. Auto-correlation analysis can also be used to investigate processes occurring on much shorter timescales than available to cross-correlation analysis, processes occuring on timescales as low as nanoseconds[1]. Development of methodologies which use all of these methods in concert increase the analytical power of the 2bFCCS-CFCE technique. Not only would we be able to simultaneously measure migration velocity and diffusion using 2bFCCS, but PCH analysis gives much more accurate information on molecular brightness and fluorophore concentration, and the fast-timescale auto-correlation analysis could supply interesting information on the rotational diffusion and fluorescence lifetime of fluorophores. Molecular brightness information could be used to simultaneously monitor the temperature and possible dye-quencher interactions of analyte systems of interest. In addition, rotational diffusion and

fluorescence lifetime information would elucidate information on the environment of the fluorophore[1]. Clearly, the field of 2bFCCS-CFCE is ripe for development.

This dissertation has demonstrated the development of a technique, 2bFCCS-CFCE, that expands the frontiers of capillary electrophoresis analysis. Hopefully the three areas in which the work was performed have illustrated for the reader the promise that 2bFCCS-CFCE has as an analytical technique.

1. Elson, E. S.; Rigler, R., Eds., *Fluorescence Correlation Spectroscopy: Theory and Applications*. 1 ed.; Springer-Verlag: Berlin, 2001; Vol. 65, p 487.